GEOSCIENCE CANADA
JOURNAL OF THE GEOLOGICAL ASSOCIATION OF CANADA
JOURNAL DE L'ASSOCIATION GÉOLOGIQUE DU CANADA

Nuancing the Stone: The Delicate Ordovician World of the Tyndall

Magmatic Magnetitite Morsels in the Mountains of Alaska

2023 VOLUME 50

Publisher/Éditeur
Geological Association of Canada
Alexander Murray Bld., Rm ER4063
Memorial University of Newfoundland
St. John's, NL, Canada, A1B 3X5
Tel: (709) 864-7660
Fax: (709) 864-2532
gac@mun.ca
www.gac.ca

Print Edition: ISSN 0315-0941
Online Edition: ISSN 1911-4850

Volume 50

A journal published quarterly by the Geological Association of Canada, incorporating the Proceedings.
Une revue trimestrielle publiée par l'Association géologique du Canada et qui en diffuse les actes.

Subscriptions: Receiving four issues of Geoscience Canada per year for $50 is one of the benefits of being a GAC member. To obtain institutional subscriptions, please contact Érudit: www.erudit.org

Abonnement: Recevoir quatre numéros par année pour 50,00 $ du magazine Geoscience est l'un des avantages réservés aux membres de l'AGC. Pour les abonnements institutionnels, s'il vous plaît contacter Érudit: www.erudit.org

Those wishing to submit material for publication in Geoscience Canada should refer to the Instructions to Authors on the journal's website, www.geosciencecanada.ca

AUTHORS PLEASE NOTE:
Please use the web address http://journals.hil.unb.ca/index.php/GC/index for submissions; please do not submit articles directly to the editor.

The Mission of the Geological Association of Canada is to facilitate the scientific well-being and professional development of its members, the learned discussion of geoscience in Canada, and the advancement, dissemination and wise use of geosciences in public, professional and academic life. Articles in Geoscience Canada are freely available one year after their publication date, unless authors have arranged for immediate open access. Opinions expressed and interpretations presented are those of the authors and do not necessarily reflect those of the editors, publishers and other contributors. Your comments are welcome.

Cover Image: A diorama reconstructing the Late Ordovician seafloor that may have produced Tyndall Stone limestone and below, a sketch of the abundant marine fossils and mottling that make Tyndall Stone one of Canada's most attractive building stone. Artwork: Peter Russell.

SERIES

Heritage Stone 9. Tyndall Stone, Canada's First Global Heritage Stone Resource: Geology, Paleontology, Ichnology and Architecture

Brian R. Pratt[1] and Graham A. Young[2]

[1]Department of Geological Sciences, University of Saskatchewan Saskatoon, Saskatchewan, S7N 5E2, Canada
E-mail: brian.pratt@usask.ca

[2]Manitoba Museum, 190 Rupert Avenue, Winnipeg Manitoba, R3B 0N2, Canada

SUMMARY

Tyndall Stone is a distinctively mottled and strikingly fossiliferous dolomitic limestone that has been widely used for over a century in Canada, especially in the Prairie Provinces. It comprises 6–8 m within the lower part of the 43 m thick Selkirk Member of the Red River Formation, of Late Ordovician (Katian) age. It has been quarried exclusively at Garson, Manitoba, 37 km northeast of Winnipeg, since about 1895, and for the past half-century extraction has been carried out solely by Gillis Quarries Ltd. The upper beds tend to be more buff-coloured than the grey lower beds, as a result of groundwater weathering. Tyndall Stone, mostly with a smooth or sawn finish, has been put to a wide variety of uses, including exterior and interior cladding with coursed and random ashlar, and window casements and doorways. Split face finish and random ashlar using varicoloured blocks split along stylolites have become popular for commercial and residential buildings, respectively. Tyndall Stone lends itself to carving as well, being used in columns, coats of arms and sculptures. Many prominent buildings have been constructed using Tyndall Stone, including the provincial legislative buildings of Saskatchewan and Manitoba, the interior of the Centre Block of the House of Commons in Ottawa, courthouses, land titles buildings, post offices and other public buildings, along with train stations, banks, churches, department stores, museums, office buildings and university buildings. These exhibit a variety of architectural styles, from Beaux Arts to Art Deco, Châteauesque to Brutalist. The Canadian Museum of History and the Canadian Museum for Human Rights are two notable Expressionist buildings.

The lower Selkirk Member is massive and consists of bioturbated, bioclastic wackestone to packstone, rich in crinoid ossicles. It was deposited in a low-energy marine environment within the photic zone, on the present-day eastern side of the shallow Williston Basin, which was part of the vast equatorial epicontinental sea that covered much of Laurentia at the time. Scattered thin bioclastic grainstone lenses record episodic, higher energy events. Tyndall Stone is spectacularly fossiliferous, and slabs bearing fossils have become increasingly popular. The most common macrofossils are receptaculitids, followed by corals, stromatoporoid sponges, nautiloid cephalopods, and gastropods. The relative abundance of the macrofossils varies stratigraphically, suggesting that subtle environmental changes took place over time.

The distinctive mottles — 'tapestry' in the trade — have been regarded as dolomitized burrows assigned to *Thalassinoides* and long thought to have been networks of galleries likely made by arthropods. In detail, however, the bioclastic muddy sediment underwent a protracted history of bioturbation, and the large burrows were mostly horizontal backfilled features that were never empty. They can be assigned to *Planolites*. The matrix and the sediment filling them were overprinted by several generations of smaller tubular burrows mostly referrable to *Palaeophycus* due to their distinctive laminated wall linings. Dolomite replaced the interiors of the larger burrows as well as smaller burrows and surrounding matrix during burial, which is why the mottling is so variable in shape.

RÉSUMÉ

Tyndall Stone est un calcaire dolomitique distinctement marbré et remarquablement fossilifère qui a été largement utilisé

pendant plus d'un siècle au Canada, en particulier dans les provinces des Prairies. Ce calcaire s'étend sur 6 à 8 m dans la partie inférieure du membre de Selkirk de la formation de Red River, d'une épaisseur de 43 m et d'âge Ordovicien supérieur (Katien). Il est exploité exclusivement à Garson (Manitoba), à 37 km au nord-est de Winnipeg, depuis environ 1895 et, depuis un demi-siècle, l'extraction est assurée exclusivement par Gillis Quarries Ltd. En raison de l'altération par les eaux souterraines, les couches supérieures ont tendance à être brun clair alors que les couches inférieures sont grises. Le calcaire Tyndall Stone, dont la finition est le plus souvent adoucie ou sciée, a été utilisé à des fins très diverses, notamment pour le revêtement extérieur et intérieur avec des pierres de taille à assises irrégulières, ainsi que pour les encadrements de fenêtres et les embrasures de portes. Le fini éclaté et la pierre de taille de dimension aléatoire utilisant des blocs polychromes fendus le long de stylolites sont devenus populaires pour les bâtiments commerciaux et résidentiels, respectivement. Tyndall Stone se prête également à la taille de colonnes et à la réalisation d'armoiries et de sculptures. De nombreux bâtiments importants ont été construits en Tyndall Stone, notamment les édifices législatifs provinciaux de la Saskatchewan et du Manitoba, l'intérieur de l'édifice du Centre de la Chambre des communes à Ottawa, des palais de justice, des bureaux de titres fonciers, des bureaux de poste et d'autres édifices publics, ainsi que des gares, des banques, des églises, des grands magasins, des musées, des immeubles de bureaux et des bâtiments universitaires. Ces bâtiments présentent une grande variété de styles architecturaux, des Beaux-Arts à l'Art déco, en passant par le style Château et le Brutalisme. Le Musée canadien de l'histoire et le Musée canadien pour les droits de la personne sont deux bâtiments expressionnistes remarquables.

Le membre inférieur de Selkirk est massif et se compose de roche sédimentaire carbonatée wackestone à packstone bioturbée et bioclastique, riche en ossicules de crinoïdes. Il s'est déposé dans un environnement marin à faible énergie dans la zone photique, sur l'actuel versant oriental du bassin de Williston peu profond, qui faisait partie de la vaste mer épicontinentale équatoriale couvrant la majeure partie de la Laurentia à l'époque. De minces lentilles éparses de grès bioclastique témoignent d'événements épisodiques à haute énergie. Tyndall Stone est spectaculairement fossilifère et les dalles contenant des fossiles sont de plus en plus populaires. Les macrofossiles les plus courants sont les réceptaculitides, suivis des coraux, des éponges stromatoporoïdes, des céphalopodes nautiloïdes et des gastéropodes. L'abondance relative des macrofossiles varie en fonction de la stratigraphie, ce qui suggère que des changements environnementaux subtils ont eu lieu au fil du temps.

Les marbrures distinctives – appelées "tapisserie" dans le commerce – ont été perçues comme des terriers dolomitisés attribués aux *Thalassinoides* et longtemps considérées comme des réseaux de galeries vraisemblablement creusés par des arthropodes. Dans le détail, cependant, le sédiment vaseux bioclastique a subi une longue histoire de bioturbation, et les grands terriers étaient principalement des éléments horizontaux remblayés qui n'étaient jamais vides. Ils peuvent être attribués à des *Planolites*. La matrice et les sédiments qui les remplissent sont surchargés par plusieurs générations de terriers tubulaires plus petits, principalement attribuables à des *Palaeophycus* en raison de leurs revêtements muraux stratifiés distinctifs. La dolomite a remplacé l'intérieur des plus grands terriers ainsi que des plus petits terriers et la matrice environnante pendant l'enfouissement, ce qui explique la forme variable de la marbrure.

INTRODUCTION

Tyndall Stone is a highly fossiliferous dolomitic limestone quarried northeast of Winnipeg, in southern Manitoba. It is arguably Canada's best recognized building stone, thanks to its unique composition and appearance, and widespread use in prominent buildings across the country. Its distinctive 'tapestry' is due to a striking colour mottling that is not exhibited by other building stones in Canada, and indeed elsewhere in the world. Tyndall Stone is a trade name that has been in use since the early 1900s, soon after numerous quarries were opened in the village of Garson beginning in 1895, because it was shipped by rail from nearby Tyndall. The name is now trademarked by Gillis Quarries Ltd., which is the sole remaining quarry operator.

Tyndall Stone belongs to the Selkirk Member of the Upper Ordovician (Katian) Red River Formation. It was deposited on the northeastern side of the Williston Basin, part of a shallow, tropical epicontinental sea that covered most of North America some 450 million years ago. It has been studied in detail owing to its conspicuously fossiliferous nature and the distinctive diagenetic dolomitization that was related to burrows made by infaunal invertebrates.

Stone from the Selkirk Member that is similar to Tyndall Stone was first used for masonry purposes in the construction of Lower Fort Garry, near Selkirk, which began in 1832. Subsequently, Tyndall Stone was used extensively in western Canada, notably for the Saskatchewan and Manitoba legislative buildings, completed in 1912 and 1920, respectively (Fig. 1A, B), but also in many other government buildings such as courthouses, town and city halls, and post offices, as well as banks, department stores, train stations, hotels and so forth in a variety of architectural styles. It was used to spectacular effect in the interior of the rotunda of Confederation Hall in the House of Commons, Ottawa, completed in 1922 (Fig. 2A–D). In recent decades, its use has expanded to other commercial buildings, museums, hospitals, universities and churches, as well as in residential applications, both exterior and interior. Tyndall Stone has been used for several public buildings in the USA and for Canada House (Kanada Haus) in Berlin, which houses the Embassy of Canada to Germany, completed in 2005. Upon our nomination, Tyndall Stone was formally designated as a Global Heritage Stone Resource by the International Union of the Geological Sciences in November 2022.

This paper aims to bridge geology and architecture. It reviews the geological attributes and use of the Tyndall Stone and explores in detail the nature and origin of the mottling and the burrow fabrics that were overprinted by dolomitization during burial diagenesis.

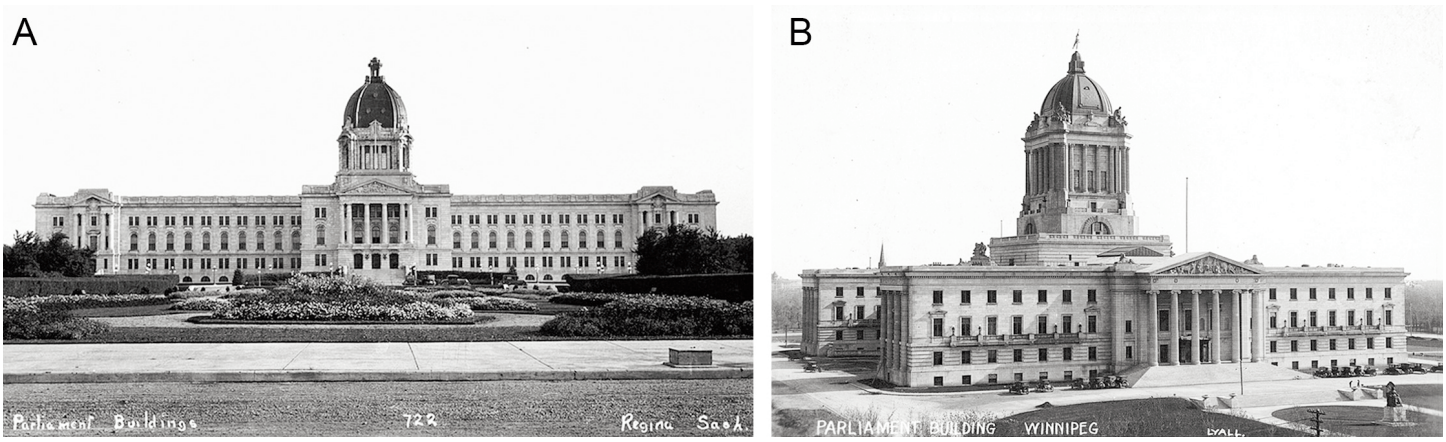

Figure 1. A. Saskatchewan Legislative Building, Regina, from a postcard of unknown origin, ca. 1925. B. Manitoba Legislative Building, Winnipeg, from a postcard by Lyall Commercial Photo Co. Ltd., ca. 1925. Images credit: PC013073 and PC013424, respectively, Prairie Postcards Collection, courtesy of Peel's Prairie Provinces (peel.library.ualberta.ca), a digital archive of University of Alberta Libraries.

BUILDING STONES

Heritage Stones

Building stone has long been the purview of quarry workers, architects, masons, tilers and interior designers, especially in North America, but in recent years there has developed increased recognition amongst geoscientists and the lay public that building stones and dimension stones are noteworthy components of both historical and modern constructions, and that they have considerable cultural, historical, archaeological, educational and scientific significance. Some stones, such as the Carrara Marble of Tuscany, have been extracted for thousands of years. For certain stratigraphic units, whose quarries have been exhausted, existing dimension stones represent a critical geological and historical record. The desire to enhance recognition of the importance of building stones led to the establishment of the Heritage Stone Subcommission of the International Commission on Geoheritage of the International Union of Geological Sciences (Pereira and Page 2017; Kaur 2022). The focus of the companion Heritage Sites and Collections Subcommission is on 'geodiversity', especially via the designation of key 'geosites'. The task of the Heritage Stone Subcommission is to encourage nominations for formal designation as Global Heritage Stone Resources.

To date, 22 stones belonging to a wide range of lithologies have been formally recognized, such as Carrara Marble (Primavori 2015), Tennessee Marble from the United States (Byerly and Knowles 2017), Larvikite from Norway (Heldal et al. 2014) and Makrana Marble from India (Garg et al. 2019), the last having been used to build the Taj Mahal. In turn, there has been media coverage of heritage stone recognition, for example, the Makrana Marble. Many others have been documented and await formal nomination and approval (e.g. Hannibal et al. 2020). We submitted a formal nomination of Tyndall Stone for heritage status in July 2022 and the proposal was ratified by the Executive Committee of the International Union of Geological Sciences in October 2022. It is the first and only Canadian stone to be nominated and receive this recognition.

Building Stone in Canada

Canada, being a comparatively young country and originally heavily forested in proximity to sites of early colonization, does not have a long tradition of building with stone, and Indigenous groups in southern Canada did not employ it for permanent structures before the arrival of Europeans. Some of the earliest stone buildings include a number of windmills, houses, towers, mills and forts in Quebec City and in the Montreal area, from the late 1600s and early 1700s. Notre-Dame de Québec church in Quebec City dates from 1647, and a stone chapel was built in Montreal in 1675. The early 1700s saw construction of the Fortress of Louisbourg in Nova Scotia and the striking Prince of Wales Fort on the shore of Hudson Bay by Churchill, Manitoba. With population growth in the 1800s, stone was used more frequently, especially in expanding urban areas like Montreal, Kingston, Ottawa and Hamilton, where there was ready access to nearby strata, mostly Middle Ordovician limestone units in eastern Ontario and adjacent Quebec, and Silurian dolostone and sandstone beds in the Niagara region (for examples of different building stone use, visit https://raisethehammer.org/authors/197/gerard_v_middleton). As the means of transportation evolved, stones were imported from further afield.

The situation was somewhat different after Canada became a dominion in 1867 and Manitoba joined the Canadian Confederation in 1870, followed later by the Northwest Territories, which included the areas that would become the provinces of Saskatchewan and Alberta. Aided by the completion of the Canadian Pacific Railway in 1885, the late 1800s saw a large influx of settlers arriving on the Prairies, and the corresponding growth of several cities, especially Winnipeg, Manitoba, which in 1911 was the third largest city by population in Canada. Like southern Ontario and Quebec, but unlike many other places on the Prairies, suitable building stone was at hand near Winnipeg, primarily Upper Ordovician dolostone and dolomitic limestone belonging to the Selkirk Member of the Red River Formation. This stone, quarried along the Red River north of Winnipeg at Saint Andrews and East Selkirk, was first

https://doi.org/10.12789/geocanj.2023.50.196

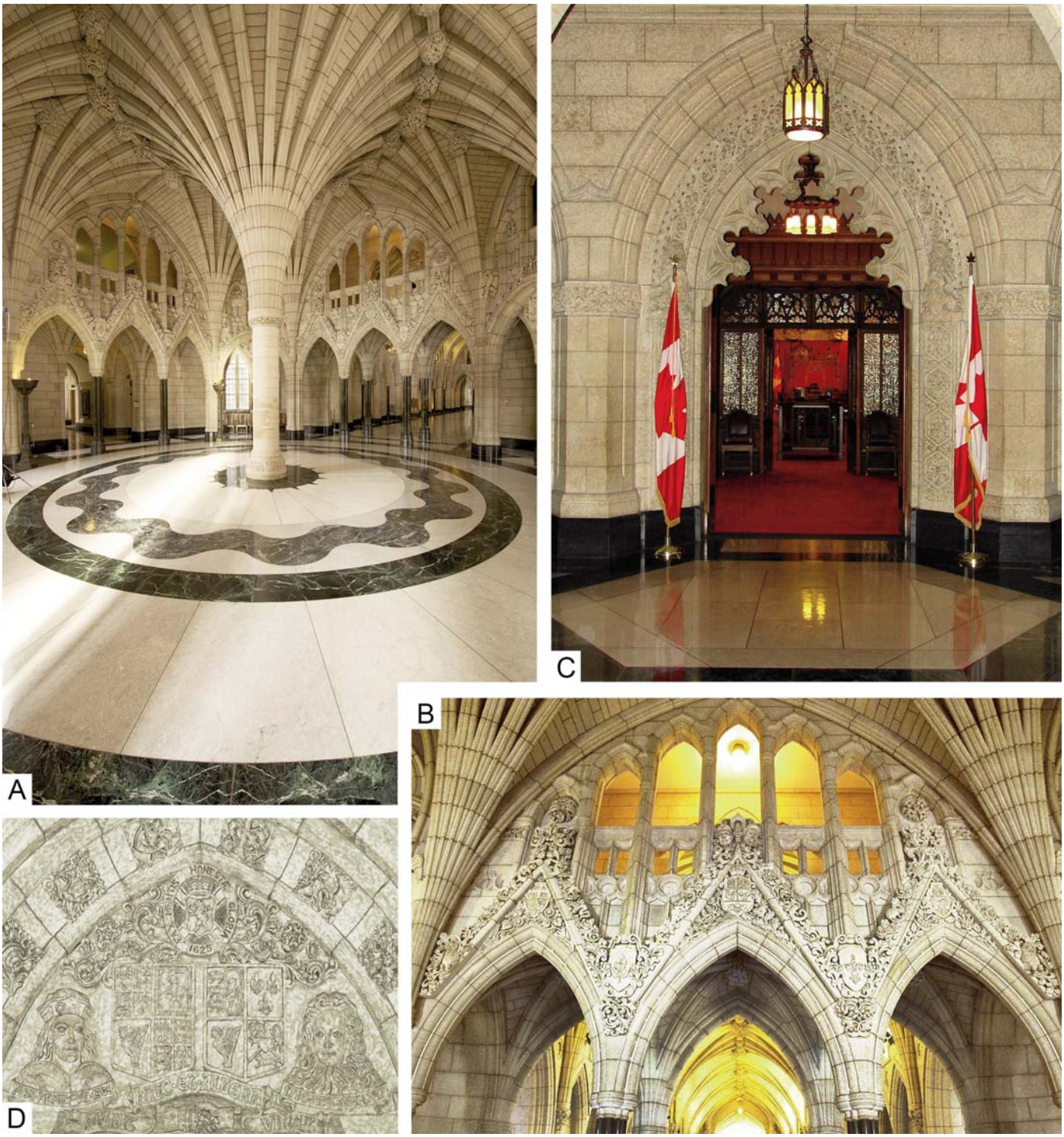

Figure 2. Elaborately carved Tyndall Stone used in Centre Block, House of Commons, Parliament Hill, Ottawa. A. The rotunda of Confederation Hall, the formal entrance to the Centre Block. It consists of a central fluted column, high-vaulted ceiling, arches, coats of arms of each province and territory, and various vegetal symbols. The floor consists of polished Missisquoi Marble from Philipsburg, Quebec, and serpentinites from Roxbury, Vermont and Tinos, Greece. The wavy pattern symbolizes the importance of water to Canada. Image credit: Canada Public Services and Procurement Canada (https://www.tpsgc-pwgsc.gc.ca/citeparlementaire-parliamentaryprecinct/decouvrez-discover/centre-eng.html). B. Detail of the Gothic arches and tympana in the rotunda above the entrance to the Hall of Honour. The two carved heads at the central gable apex show a miner (left) and a lumberjack (right) above the escutcheon of Canada. The left gable springer has an escutcheon with a trillium representing Ontario and the right one shows a fleur-de-lis representing Quebec. Image credit: Wikimedia Commons, Concierge. 2C (https://commons.wikimedia.org/wiki/File:Ottawa_-_Parliament_Hill_-_Centre_Block_10.JPG). C. Entrance to the Senate Chamber showing the carved arch and tympanum. Image credit: Canada Public Services and Procurement Canada (https://www.tpsgc-pwgsc.gc.ca/citeparlementaire-parliamentaryprecinct/decouvrez-discover/centre-eng.html). D. Tympanum at the Government Entrance to the House of Commons Chamber, showing figureheads of Henry VII (left) and George I (right) with escutcheons bearing the coats of arms of the two English kings. Image credit: courtesy of William Stewart.

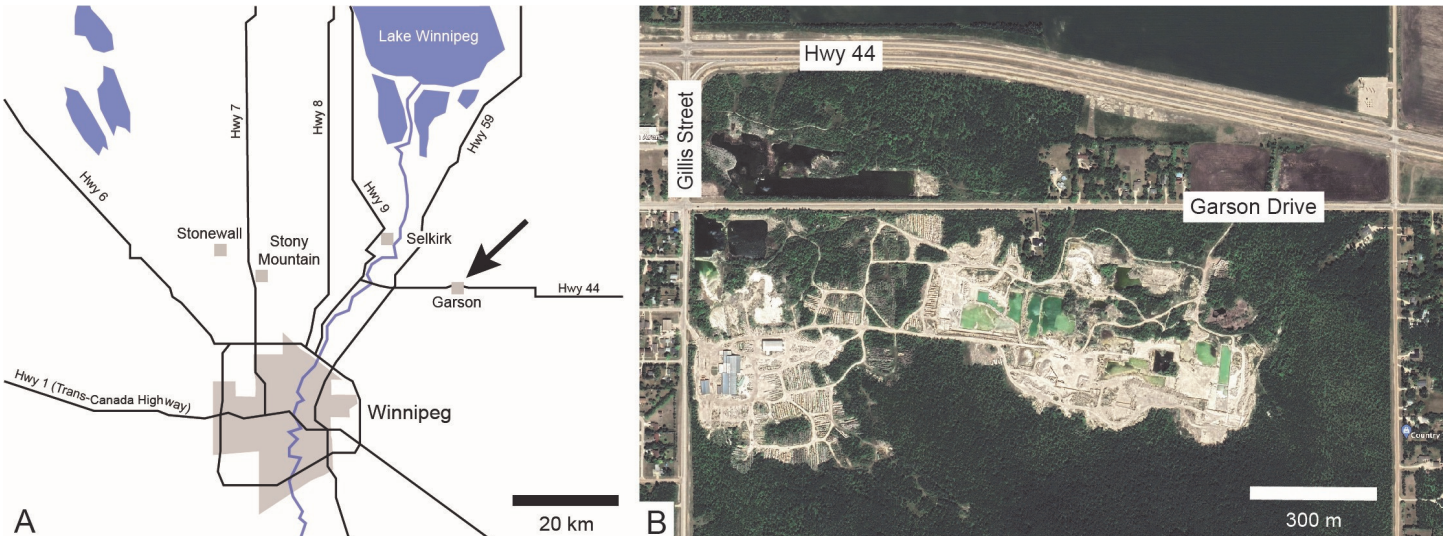

Figure 3. A. Map of the Winnipeg area of southern Manitoba, showing selected highways, the Red River and the southern end of Lake Winnipeg, the city of Selkirk, and the villages of Stonewall, Stony Mountain, and Garson (arrowed), where the Gillis Quarry is located. B. Google Earth view of Gillis Quarry in Garson.

used for the walls of Lower Fort Garry in the 1840s. It was later used as blocks for foundations in Winnipeg and elsewhere, and as finished stone in structures such as the Stony Mountain Penitentiary (1877) and Holy Trinity Church, Winnipeg (1884). By contrast, overlying dolostone units from the Stony Mountain and Stonewall formations were used for some foundations and walls (Young et al. 2008), but this was limited due to the difficulty of shaping these tough stones. As public and commercial building increased in the 1890s, the Tyndall Stone quarries at Garson were opened. Stone from the Selkirk Member, and Tyndall Stone in particular, was used in numerous other buildings especially as exterior cladding, and often carved for ornamentation.

Relatively few other Canadian limestone and dolostone units have been extracted for similar purposes. Light grey Mississquoi Marble was quarried during the first half of the 20th century at Philipsburg, Quebec, by Lake Champlain. It belongs to the Strites Pond Formation of late Cambrian age (Salad Hersi et al. 2002). It has been used for cladding, but it takes a good polish so it was mostly used as an indoor dimension stone, including in the Centre Block of the House of Commons, and several provincial legislature buildings (Lawrence 2001; Burwash et al. 2002; Ledoux and Jacob 2003; Brisbin et al. 2005). The light grey to buff Adair limestone (actually dolostone) and the strikingly laminated, grey to brown Eramosa Formation are two Silurian dolostone units extracted from southern Bruce Peninsula, Ontario.

TYNDALL STONE EXTRACTION

Quarry Location

Tyndall Stone proper was first quarried at the village of Garson in about 1895. Garson is the only place where the distinctive stone is extracted, and it has been quarried there for over a century (Fig. 3A, B). At the end of the 1800s it was known as Garson stone, from the name of the person who opened the first quarry and whose name lent itself to the village. It was also called Manitoba limestone, Manitoba Tapestry limestone and Winnipeg limestone. In the early days the stone was transported on spur lines using small steam locomotives to the village of Tyndall, about 2 km east of the quarries, where there was a freight depot on the Canadian Pacific Railway. Thus, it became better known as 'Tyndall Stone', i.e. stone shipped from Tyndall (https://www.tyndallstone.com). Tyndall Stone was extracted from several adjacent quarries owned by a number of companies in the early years (Goudge 1933, fig. 7), but most notably since 1925 by family-owned Gillis Quarries Ltd., which was incorporated in 1922. Gillis Quarries Ltd. has been the exclusive producer since 1969. Exposures of equivalent strata to the north, beyond Grand Rapids and The Pas and into adjacent east-central Saskatchewan (Nicolas et al. 2010), while containing similar fossils and burrows, lack the visually contrasting mottling against a limestone matrix because they are fully dolomitized. These rocks are utilized only for aggregate.

Quarry Operation

Tyndall Stone is extracted using standard methods for stratified limestone (Fig. 4A–D). The stone is cut vertically, using either an eight-foot (2.44 m) diameter saw or a nine-foot (2.74 m) long belt saw mounted on one hundred-foot (30.5 m) tracks. It is then split into 6–8 tonne blocks using a jackhammer and wedges inserted by hand parallel to bedding; the blocks are then moved using front-end loaders. Gillis Quarries Ltd. operates a large finishing plant with an area of about 4000 m^2. Stone is processed along advanced cutting lines that feature three primary saws and three gantry saw/line stations, four saw/profiler stations, as well as a tile line and lathe, allowing it to be cut into a variety of sizes, shapes and finishes (Fig. 4E, F) as specified by the architects (https://www.tyndallstone.com). These finished pieces are delivered to the customer and no further fabrication is required. Even though Tyndall Stone is extracted from just a single, privately owned and operated quarry, the property is large and the Selkirk Member is widely distributed in the Garson area. Thus, there

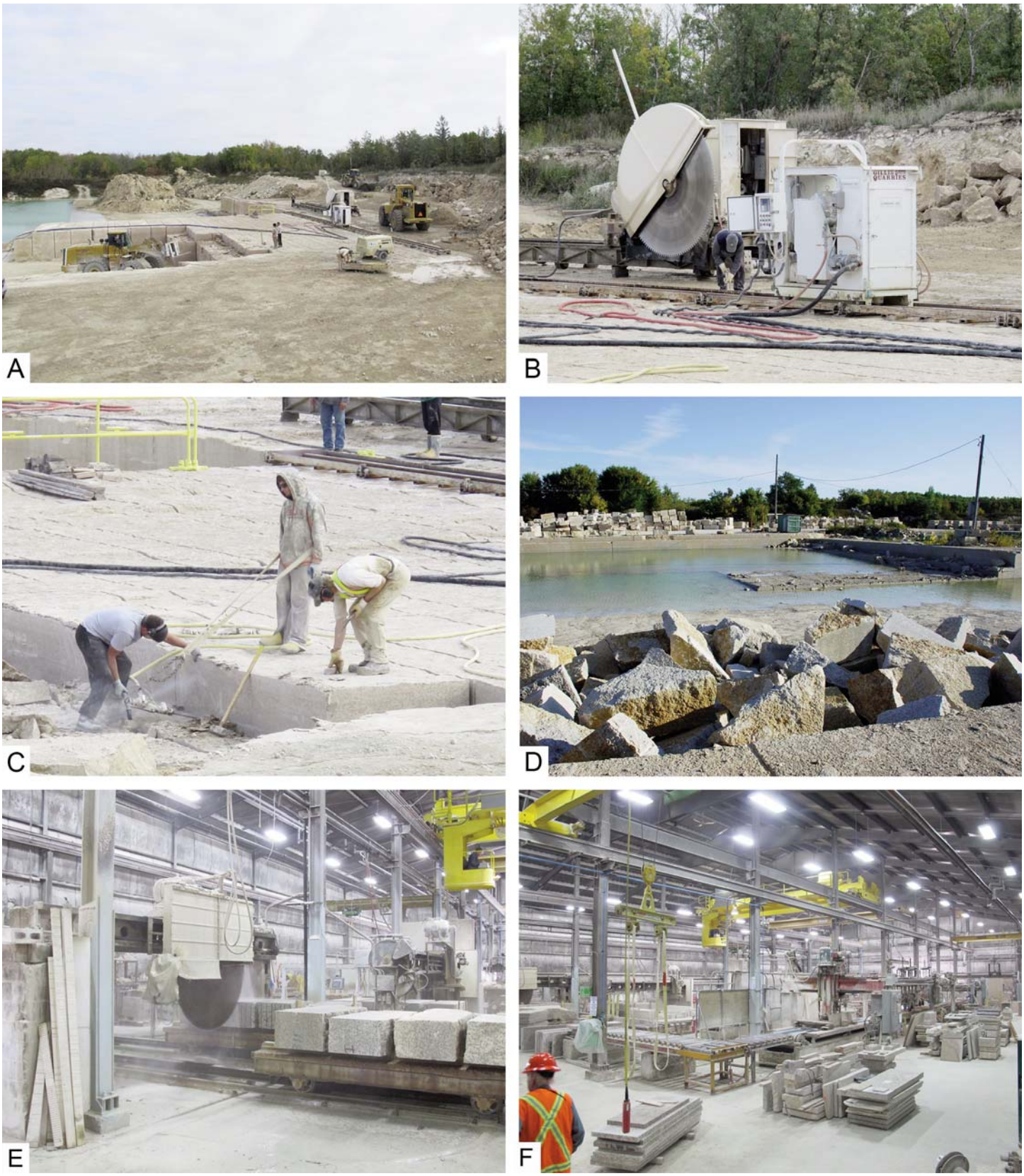

Figure 4. Gillis Quarry in operation at Garson. A. Extracting blocks from the middle zone. B. Circular saw and belt saw (white box) on movable tracks. C. Jackhammering cut blocks so that they split apart along stylolitic horizons. D. Flooded lower zone with stacked blocks behind; blocks are aged prior to cutting into slabs. E. Sawing blocks into slabs in the finishing plant. F. Various sawn slabs and pieces prepared according to customer specifications.

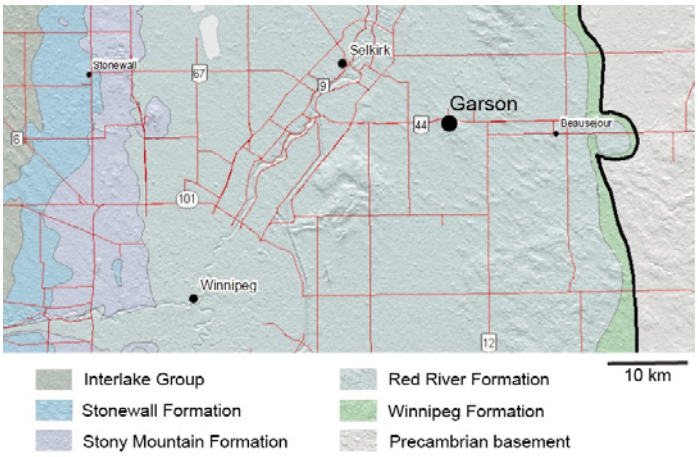

Figure 5. Geological map of the Winnipeg area, southern Manitoba. Adapted from Nicolas et al. (2010).

is no prospect of stone supplies running out in the foreseeable future.

TYNDALL STONE GEOLOGY

Stratigraphy

The Upper Ordovician to lower Silurian succession cropping out in west-central to southeastern Manitoba consists of nearly flat-lying limestone and dolostone beds dipping imperceptibly to the west (Fig. 5). These strata originated as carbonate sediment deposited on the eastern side of the Williston Basin, a shallow epeiric (epicontinental) sea in the centre of Laurentia, the early Paleozoic North American craton (Fig. 6A, B). Tyndall Stone is formally part of the Selkirk Member of the Red River Formation (Fig. 7). In the early 20th century before modern stratigraphic nomenclature was established, it was called the Upper Mottled Limestone (Dowling 1900). Tyndall Stone occurs within the lower half of the 43 m thick member; the lowest horizon in the Garson quarries is about 10 m above

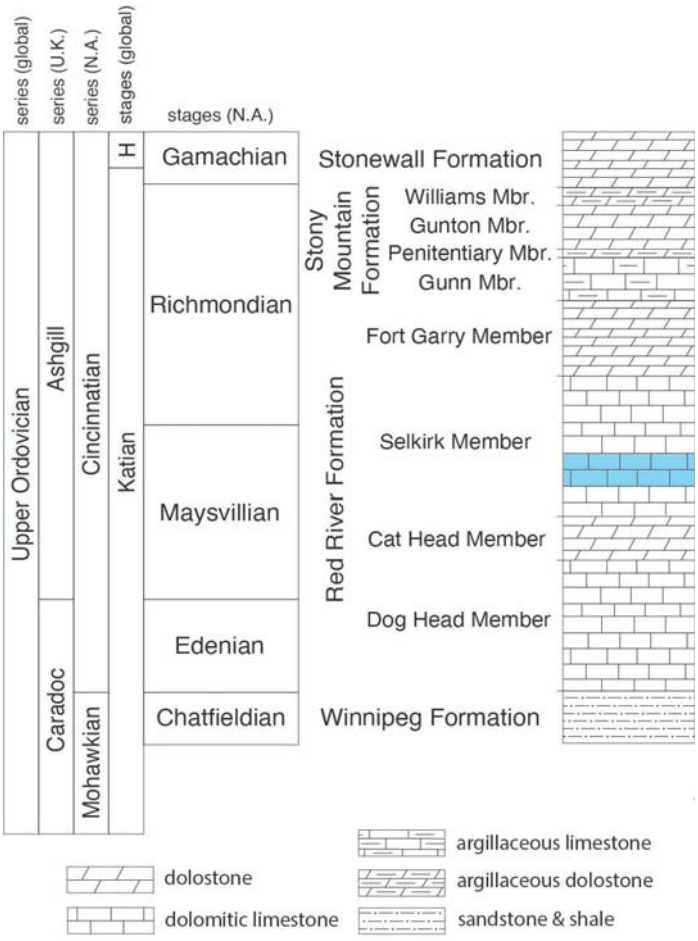

Figure 7. Stratigraphic framework of the Tyndall Stone (Selkirk Member of the Red River Formation) in the Williston Basin, southern Manitoba. The interval from which Tyndall Stone is extracted is highlighted. Adapted from Elias et al. (2013, fig. 6).

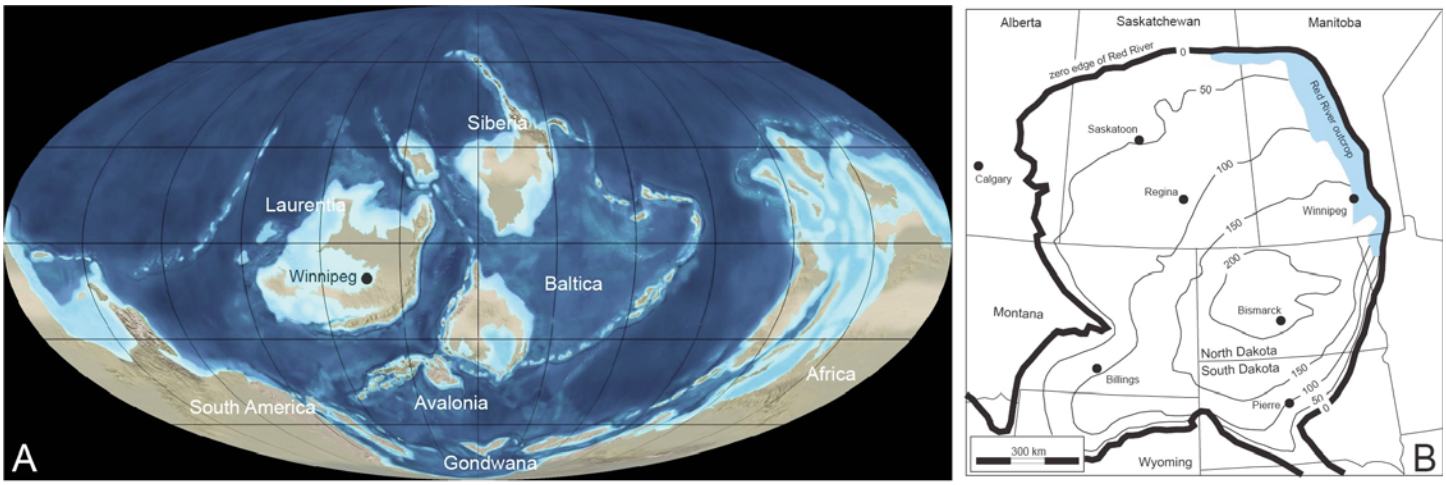

Figure 6. Global and regional context of Upper Ordovician strata in central North America. A. Paleogeography of Laurentia and other cratons with shallow epicontinental seas shown in light blue, and the location of Winnipeg, Manitoba. Map courtesy of R. Blakey and DeepTimeMaps™, Colorado Plateau Geosystems Inc. B. Isopach map of the Red River Formation in the Williston Basin. From Pratt and Haidl (2008), based on sources cited therein (see also El Taki and Pratt 2012, fig. 4A). Contour interval is 50 m.

https://doi.org/10.12789/geocanj.2023.50.196

the top of the underlying Cat Head Member (Goudge 1944; Cowan 1971; Young et al. 2008). In terms of North American Late Ordovician chronostratigraphy, the Selkirk Member is Maysvillian to early Richmondian (~ 450 Ma) in the Cincinnatian Series (Young et al. 2008), which is equivalent to the middle part the global Katian Stage. The Red River Formation correlates with the Surprise Creek Formation of the upper part of the Bad Cache Rapids Group across the Severn Arch in the Hudson Bay Basin (Jin et al. 1997; Lavoie et al. 2022). Tropical, shallow-water conditions were present across much of Laurentia at this time and correlative strata are widely distributed, from west Texas and New Mexico to the Arctic Islands and northwest Greenland (e.g. Sweet and Bergström 1984; Holland and Patzkowsky 2009; Jin et al. 2012, 2013; Cocks and Torsvik 2021). The invertebrate biota defines the Red River–Stony Mountain Faunal Province due to its similarity over the whole region, which contrasts with that of parts of eastern North America (Elias 1981, 1991; Young et al. 2008). Broadly similar limestone units of Middle and Late Ordovician age were deposited in other areas of the world, notably in the Baltic Basin, exposed in southern Sweden, southern Finland, Estonia and the St. Petersburg area of western Russia (e.g. Nestor et al. 2007). These strata bear some similarity to fabrics present in the Upper Ordovician units in Manitoba.

Tyndall Stone is dolomitic limestone. Dolomite is secondary, having replaced limestone during burial. Most of it is concentrated in and around burrows; this gives the rock its characteristic mottled appearance. The relative proportion of dolomite to calcite is therefore variable. According to Goudge (1933, 1944), chemically it is 83.21–89.26% $CaCO_3$ and 9.43–14.91% $MgCO_3$. According to Parks (1916), the light-coloured matrix averages 94% calcite and the darker coloured mottles average 71% $CaCO_3$, the rest being $MgCO_3$. Silica makes up 1.5% in both. There is a slight increase in iron oxide and clay in the burrows. The former could be due to a small amount of pyrite or iron enrichment in the dolomite, or both; it may also reflect contamination from iron-bearing groundwaters. The cream to light-buff colour of much of the Tyndall Stone is likely due to the effects of groundwater flow during Quaternary interglacial episodes, which affected the surface deposits by oxidizing trace amounts of iron in both the matrix and the dolomitic mottles. Some beds, particularly those lower in the quarries, retain a greyish colouration.

Lithology

Tyndall Stone is a massive dolomitic limestone; a pseudo-bedding is locally imparted by horizontal stylolites. It is an abundantly fossiliferous, bioclastic packstone and locally wackestone (in Dunham terminology). Intraclasts are rare, confined to the bases of some grainstone lenses. Stylo-bedding surfaces exposed by splitting and removal of overlying rock are lumpy due to the differences between the limestone matrix and the dolomite and may show the scattered areal distribution of robust fossils such as large stromatoporoid demosponges (Fig. 8A). Sawn quarry walls show that the stromatoporoids and colonial corals are typically concentrated at certain horizons (Fig. 8B) but other macrofossils seem to be more sporadically distributed (Fig. 8C–F), except where they have been collected together by redeposition during high-energy events (Fig. 8C, D).

In thin section, the matrix around the macrofossils is a biomicrite (in Folk terminology). Bioclasts, as whole and fragmented shells and skeletons of a wide range of sizes, occur in variable amounts and are surrounded by a microcrystalline calcite matrix (Fig. 9A–D). These small fossils are mostly not visible on rock surfaces and include a variety of taxonomic groups, such as crinoid ossicles, trepostome bryozoan skeletons, gastropods, brachiopods, dasycladalean calcareous algae, tetradiids, small solitary rugose corals and problematical skeletons of unknown but possible algal affinity. The variable orientation of the bioclasts within the matrix indicates that the sediment was mostly completely mixed due to bioturbation.

Some preferential alignment of nautiloid conchs and solitary rugose corals is apparent (Wong 2002), which suggests the presence of comparatively weak, west–east oscillatory currents. There is an upward increase in the presence of planar-laminated, normally graded, fossiliferous bioclastic grainstone lenses and remnants of lenses that escaped complete bioturbation (Fig. 8C, D), which have been interpreted as sediment deposited by occasional storms (Westrop and Ludvigsen 1983; Wong 2002). If so, this suggests a gentle shallowing such that the seafloor came within ambient storm wave base, or that storms became more frequent and/or stronger. Alternatively, if these record weak tsunami effects (cf. Pratt and Bordonaro 2007), then they may reflect episodic faulting, likely in the basin centre where syndepositional fault movements are recorded in overlying laminated facies by synsedimentary deformation structures (El Taki and Pratt 2012).

Paleontology

Fossils are commonly visible on sawn surfaces of Tyndall Stone. There is no comprehensive taxonomic listing, but the most complete one is in Young et al. (2008). Among the most conspicuous of the macrofossil biota are the molluscs. They include hyperstrophic gastropods belonging to *Maclurina* (Fig. 10A; also Fig. 11E) and turbinate gastropods probably belonging to *Hormotoma* (Fig. 10B). These are commonly preserved as shell moulds filled with dolomite microspar from replacement of microcrystalline calcite that records lime mud that infiltrated the cavities. Nautiloids are represented by a diverse assemblage that includes the straight-shelled actinocerid *Armenoceras* (Fig. 10B, E), straight-shelled endocerids possibly belonging to *Cameroceras* (Fig. 10C) and cyrtoconic nautiloids with curving conches such as the discosorid *Winnipegoceras* (Fig. 10D, F). Often the septa and conch walls have been either abraded or dissolved, or both, with partially preserved moulds filled with dolomitized microcrystalline calcite, and all the primary shell material that remains is the heavily calcified axial siphuncle. The segmented, beaded siphuncles of the actinocerids, whether exposed on glacially transported boulders or in the walls of buildings, are commonly misidentified by casual observers as vertebrate backbones. The dolomite that fills shell moulds points to dissolution of aragonite at and just under the sediment surface.

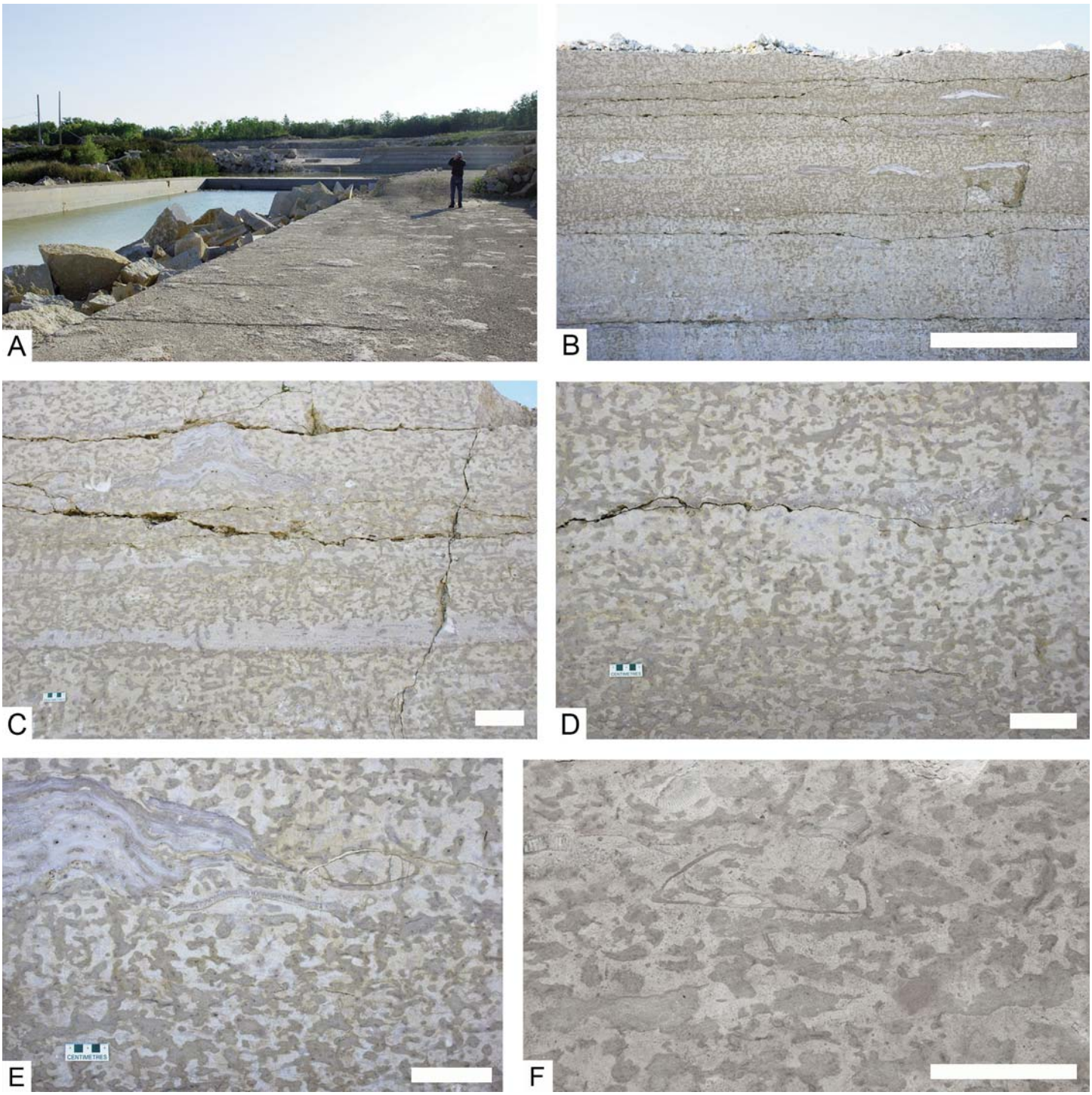

Figure 8. Exposures of Tyndall Stone in Gillis Quarry. A. Bedding plane with scattered domical stromatoporoids and colonial corals, partially flooded lower interval to the left, and upper interval in the background. Person for scale. B. Sawn wall in the upper interval with numerous stromatoporoids and colonial corals visible as thin lenses. Scale bar is 1 m. C. Sawn wall showing dolomite-mottled limestone with two thin layers of bioclastic grainstone (lighter coloured layers across and below middle; also Figure 15E), and cross-section of a high-relief domical stromatoporoid with intercalated sediment (upper left of centre). Scale bar is 10 cm. D. Sawn wall showing dolomite-mottled limestone, with burrowed grainstone (upper right). Scale bar is 10 cm. E. Sawn wall showing dolomite-mottled limestone with cross-sections of a receptaculitid (above centre), domical stromatoporoid (upper left), and a curving nautiloid (upper right). Scale bar is 10 cm. F. Sawn wall showing dolomite-mottled limestone and cross-section of large gastropod belonging to *Maclurina*. Scale bar is 10 cm.

Corals include horn-shaped solitary rugose corals, most of which belong to *Grewingkia* (Fig. 11A), colonial rugose corals belonging to *Crenulites* (Fig. 11C, D) and tabulate corals, which are colonial, belonging to the chain corals *Catenipora* (Fig. 10C) and *Manipora* (Fig. 11B), the honeycomb corals such as *Safforddophyllum,* and the common, domical *Calapoecia* (Fig. 11F). Dis-

https://doi.org/10.12789/geocanj.2023.50.196

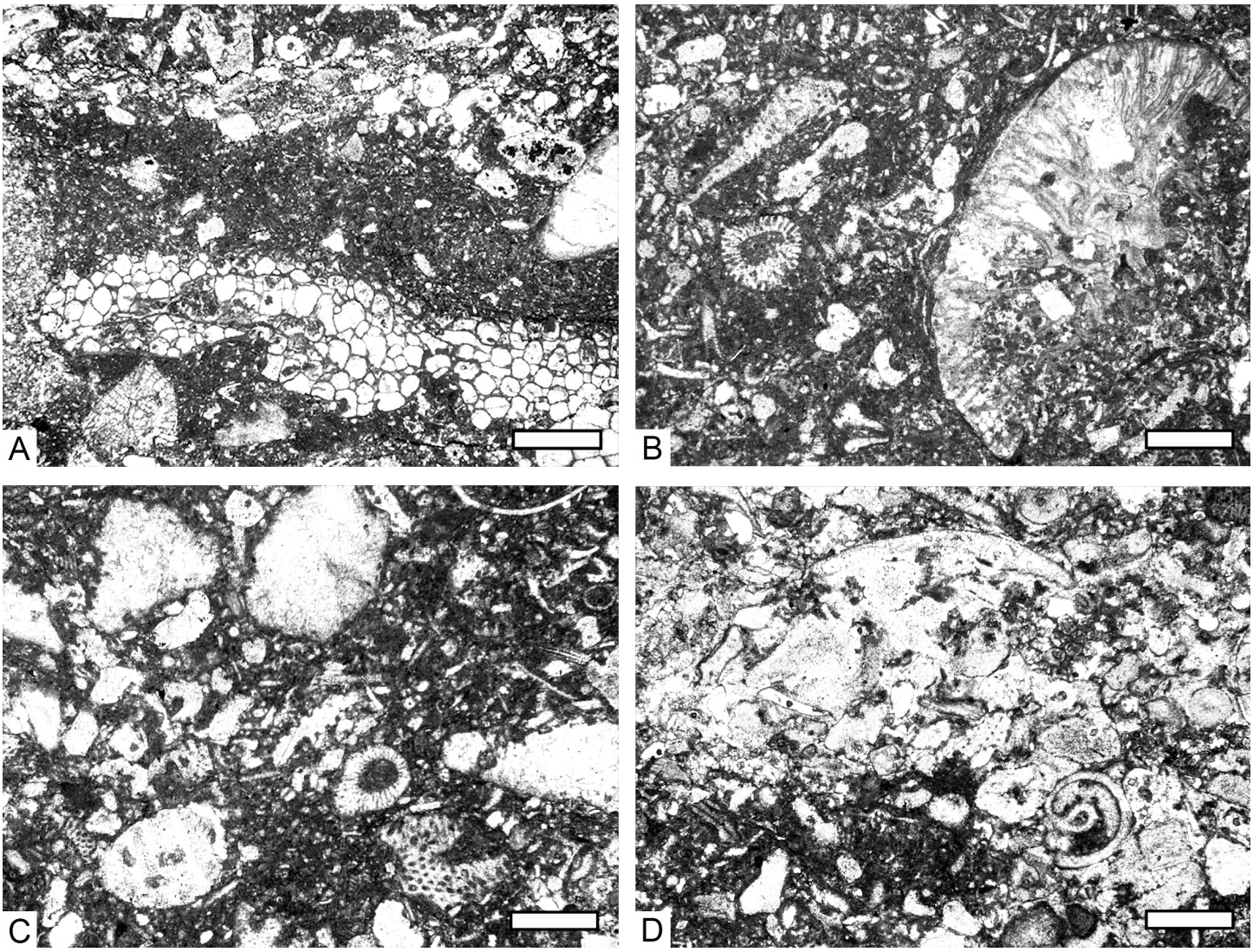

Figure 9. Thin section photomicrographs of biomicrite matrix of Tyndall Stone. Plane-polarized light, greyscale; oriented perpendicular to bedding. A. Possible calcareous alga (lower) overlain in turn by wackestone (middle) and packstone (upper) consisting mostly of crinoid ossicles plus lime mud, with a trepostome bryozoan (lower left). Scale bar is 2 mm. B. Wackestone to packstone matrix with abraded solitary rugose coral (right), dasycladalean green alga (centre left), and smaller bioclasts many of which are crinoid ossicles. Scale bar is 2 mm. C. Wackestone to packstone containing common crinoid ossicles, dasycladalean algae (lower right) and other bioclasts. Scale bar is 1 mm. D. Wackestone overlain by crinoidal packstone with a small gastropod (lower right) and abraded fragment of gastropod shell (upper centre). Scale bar is 1 mm.

tinctive on many Tyndall Stone surfaces are white laminar fossils with a dense microstructure that cannot be discerned even with a hand lens. These are the tabulate corals *Ellisites* and *Protrochiscolithus,* which were obligate encrusters, especially on stromatoporoids (Fig. 11E), but are difficult to distinguish on sawn surfaces. They often preferentially exhibit vertical borings termed *Trypanites,* which are absent in other shells and skeletons, apart from generally lesser numbers in solitary rugose corals and stromatoporoids (Elias 1980; Stewart et al. 2010).

Labechiid stromatoporoids are also common, forming tabular to dome-shaped masses of varying diameter and height, with internal growth lamination and ragged margins reflecting episodic lateral expansion and contraction (Figs. 8C, E, 11E). Siliceous sponges are rare.

Receptaculitids assigned to *Fisherites* are distinctive fossils in both plan and vertical views of Tyndall Stone (Fig. 12A–C). They are circular in plan view, but in vertical view are tabular to undulating to gently domical, and they may appear variable depending on the plane of horizontal section. Receptaculitids are composed of individual, interlocking skeletal elements termed meroms with a spiral orientation, which is why they have been called 'sunflower corals'. Specimens with the meroms partially disaggregated are also observed. They are replaced mostly by blocky calcite which is suggestive of a primary aragonite composition, yet they do not appear to have been leached and infiltrated with lime mud like the molluscs. The affinity of receptaculitids is unknown but they are commonly regarded to have been a form of calcareous algae (Nitecki et al. 1999). This is supported by their absence in deeper water deposits in the Saskatchewan subsurface (Kendall 1976).

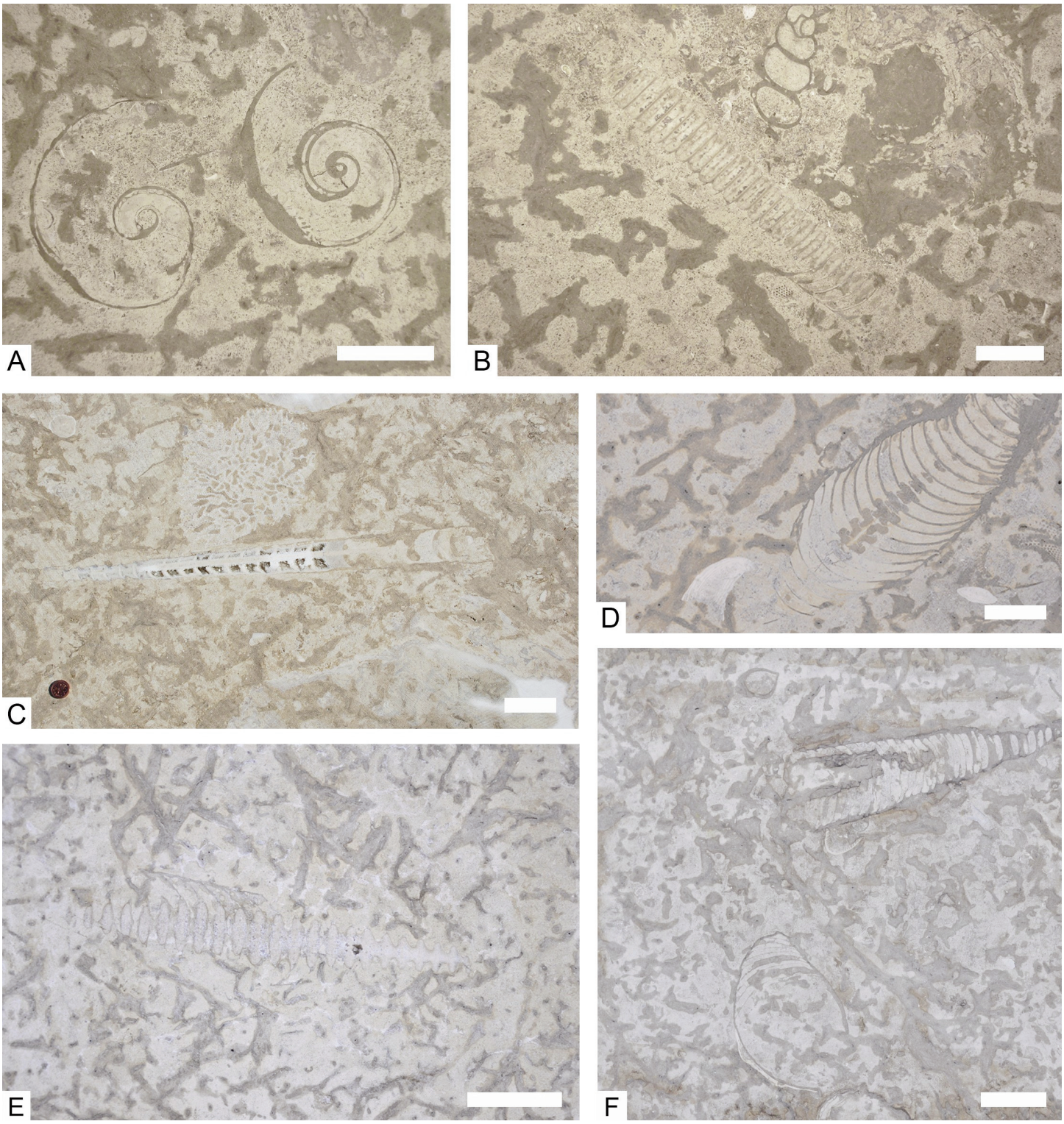

Figure 10. Fossil molluscs in Tyndall Stone, sawn parallel to bedding. Apart from calcitic siphuncles, shells were dissolved and the moulds are filled with dolomudstone. Scale bars are 5 cm. A. Two large hyperstrophic gastropods with a flattened base belonging to *Maclurina*. Polished, memorial wall to students who fell in the Second World War, Department of Geological Sciences, University of Saskatchewan. B. Large high-spired gastropod belonging to *Hormotoma* (upper centre) and part of actinoceratid nautiloid cephalopod, belonging to *Armenoceras*, preserving mostly the beaded siphuncle, with some septa (lower right). Same location as A. C. Endoceratid nautiloid (middle) preserving septa and siphuncle (left) but dissolved towards the aperture (right), with chain coral belonging to *Catenipora* (upper centre). Sawn surface, Gillis Quarry. D. Cyrtoconic nautiloid with dolomudstone-filled siphuncle, with rugose coral probably belonging to *Grewingkia* (lower left). Honed finish, exterior of TCU Financial Group building, Saskatoon. E. Siphuncle of actinoceratid nautiloid belonging to *Armenoceras*, preserving a few septa (left of centre). Honed finish, interior presentation wall, same location as D. F. Partially burrowed endoceratid nautiloid (upper centre) and possible cyrtoconic nautiloid (lower left) encrusted with a thin *Prototrochiscolithus* coral (white lamina). Same location as D.

https://doi.org/10.12789/geocanj.2023.50.196

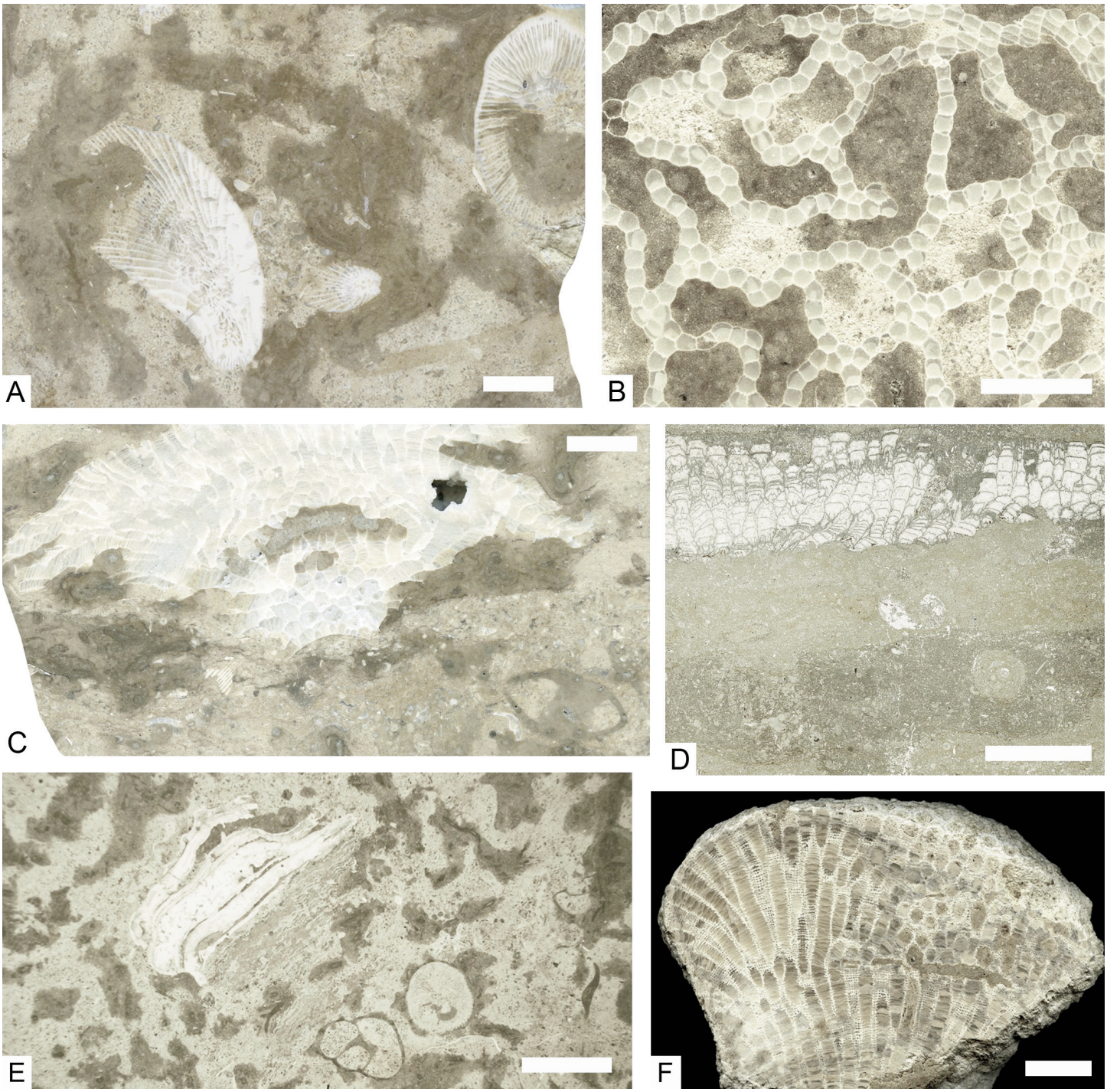

Figure 11. Corals in Tyndall Stone. All polished surfaces except D, which is a scanned, vertically oriented thin section. A, C, D = rugose corals; B, E, F = tabulate corals. A. Two large and one small solitary corals belonging to *Grewingkia*. Skeleton at left is perforated by numerous borings. Surface cut perpendicular to bedding. Scale bar is 2 cm. B. Close-up of chain coral belonging to *Manipora*. Surface cut parallel to bedding. Scale bar is 10 mm. C. Domical honeycomb coral belonging to *Crenulites*, with gastropod (lower right). Surface cut perpendicular to bedding. Scale bar is 2 cm. D. Bioclastic packstone with horizontal burrow conforming to *Planolites* (lower right) overlain in turn by wackestone and tabular honeycomb coral belonging to *Crenulites*. Vertical section. Scale bar is 2 mm. E. Stromatoporoid (indistinct laminae in centre) encrusted by several generations of dense, white-coloured skeletons belonging to tabulate corals *Protrochiscolithus* and/or *Ellisites*, with two gastropods probably belonging to *Hormotoma* (lower right). Surface sawn parallel to bedding. Second World War memorial wall. Scale bar is 5 cm. F. Tabulate coral belonging to *Calapoecia*. Surface cut vertical to bedding. Scale bar is 10 mm.

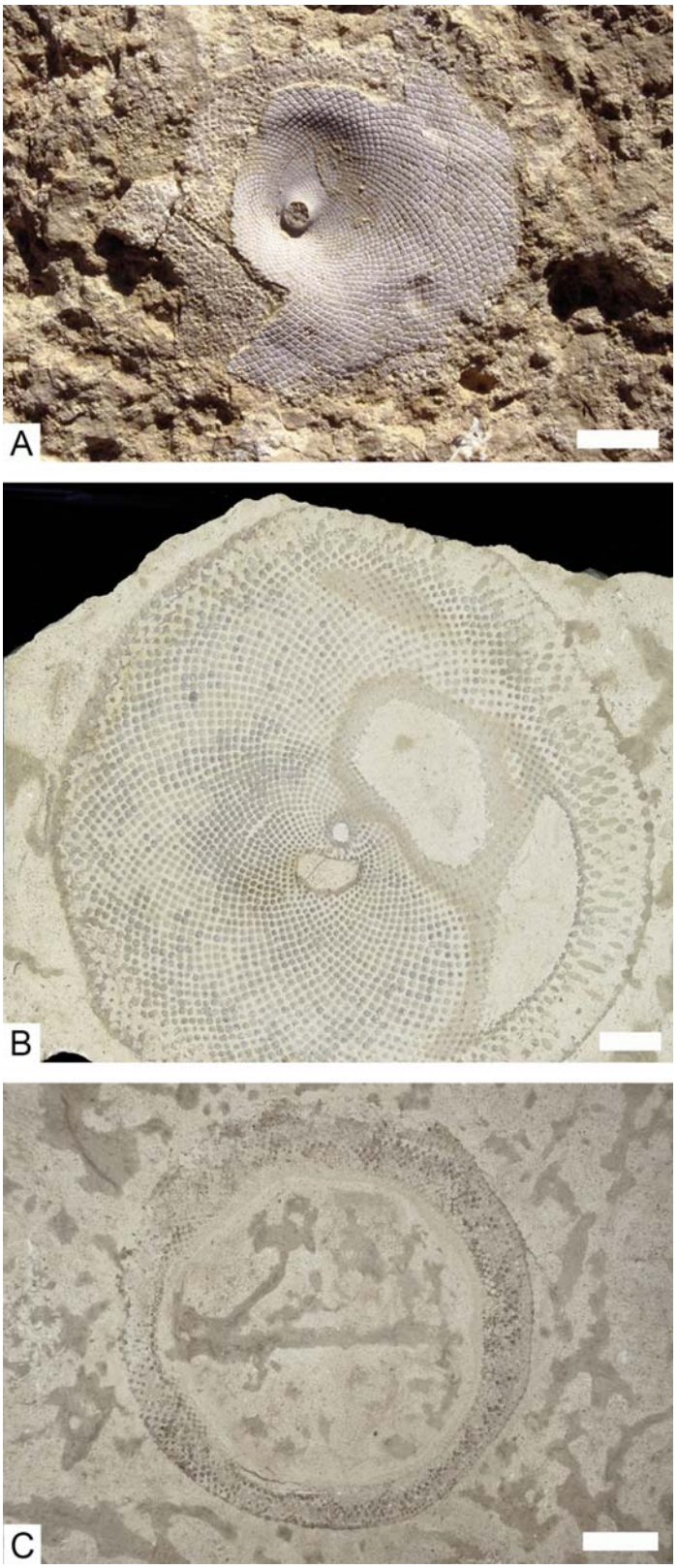

Figure 12. Plan views of tabular to gently domical receptaculitids belonging to *Fisherites*. A. Split surface at Gillis Quarry, Garson. Scale bar is 2 cm. B. Honed finish, surface sawn parallel to bedding. Scale bar is 2 cm. C. Polished, surface sawn parallel to bedding, Second World War memorial wall. Scale bar is 5 cm.

Paleoecology

Receptaculitids are the most common macrofossil type (Wong 2002; Brisbin et al. 2005; Young et al. 2008). Collectively the corals rival the receptaculitids in abundance, but in terms of individual groups the next most common fossil is solitary rugose corals. Cephalopods, stromatoporoids and gastropods are the next most common groups. Trilobites and brachiopods are present (Westrop and Ludvigsen 1983; Jin and Zhan 2001) but are difficult to identify on sawn surfaces. A striking feature of the biota is that many groups tend to be large in comparison with the same or related taxa in correlative strata elsewhere, such as in eastern Ontario (Young et al. 2008; Jin et al. 2012). The reason for this 'gigantism' is uncertain but may reflect abundant food resources at the base of the food chain, which was passed onto some of the higher trophic groups. Alternatively, some aspect of seawater temperature may have been conducive to enhanced growth rate or longevity. Stable environmental conditions also would have permitted organisms such as corals to grow to larger size, in comparison with environments with frequent disturbance of the seafloor.

In the Gillis Quarry, there is an overall upward increase in the abundance of stromatoporoids, receptaculitids, *Protrochiscolithus*, and colonial rugose corals, and increased abrasion of the solitary rugose corals, which suggests a gradual shallowing (Wong 2002). On the other hand, the relative abundances of solitary rugose corals and nautiloids decrease upward (Wong 2002). Other elements like tabulate corals show no obvious trends. Both *Maclurina* and *Hormotoma* appear to show an upward increase in size, whereas average nautiloid size remains more or less constant (Wong 2002). The relative proportion of tabular to domical coral and stromatoporoid growth forms is similar throughout (Wong 2002).

Near the base of the quarry section, more than half the solitary rugose coral skeletons are abraded, the proportion rising to more than 80 percent in the overlying strata. This interval shows a decrease in the number of stromatoporoids and receptaculitids, and the proportion of solitary rugose corals, and is thought to record a slight deepening (Wong 2002) and a small increase in sedimentation rate (Young et al. 2008). Other skeletons and shells, however, do not exhibit a similar degree of abrasion, although tabulate corals may also be broken and some actinocerid siphuncles are broken transversely. Breakage of small bioclasts is evident. It seems that physical reworking does not explain all these observations, and thus the cause is unclear.

The seafloor substrate was apparently soft, as indicated by the distribution of the skeletons of large benthic fossils, the abundance of lime mud and absence of evidence for distinct firmground or hardground surfaces. At the same time, it was somewhat consolidated, being able to support large skeletons, the visible burrows retained their shape, and moulds of dissolved molluscs did not collapse before they were infilled with lime mud. Shells and skeletons comprised the only hard substrates, and as a result they were encrusted by a variety of organisms (Young et al. 2008). Common examples included obligate encrusters such as the corals *Protrochiscolithus* and *Ellisites,* and also stromatoporoids, the coral *Calapoecia* and bry-

https://doi.org/10.12789/geocanj.2023.50.196

ozoans. The occurrence of 'stacks', consisting of the skeletons of several different organisms that grew sequentially on top of one another, demonstrates that hard substrates were sporadically developed, and some of them were exposed on the seafloor for considerable lengths of time (Young et al. 2008). Many of these hard substrates also exhibit macroborings (Elias 1980; Stewart et al. 2010), a further indication of long-term exposure on the seafloor. Calcite cementation began under relatively shallow burial. This may have been below ~ 20 cm, as suggested by the vertical extent of burrows and the presence of intraclasts only in some grainstone lenses, eroded and redeposited during the stronger scouring events.

Combining the macrofossil biota with petrographic observations, the muddy seafloor had large quantities of small shells, skeletons and fragments mixed in, on which grew meadows of crinoids, representing the upper-tier suspension feeders. Lower-tier suspension feeders were tabulate corals, stromatoporoids, bryozoans, siliceous sponges, brachiopods, as well as *Maclurina* (Novack-Gottshall and Burton 2014). Rugose corals may have been microcarnivores. The trilobites were mobile detritus feeders and suspension feeders and/or scavengers. The turbinate gastropods were mobile deposit-feeders or herbivores. Delicate photosynthetic dasycladalean calcareous algae were rooted in the muddy sediment. Receptaculitids may have been sessile photosynthesizers. The nautiloids were likely nektobenthic predators. A variety of infaunal organisms burrowed the sediment. Undoubtedly there were soft-bodied animals and possibly green algae that are not preserved. An important point is that, despite the presence of common corals and stromatoporoids, and the propensity of some corals and stromatoporoids to encrust one another, there are no framework reefs or bioherms in the Tyndall Stone, or anywhere in the outcrop belt of the Red River Formation, although there are some small patch reefs at the top of the Selkirk Member equivalent in the Saskatchewan subsurface (Pratt and Haidl 2008).

Tyndall Stone's abundantly fossiliferous nature has inspired museum reconstructions of the paleoecological setting of the Late Ordovician tropical seafloor, such as the exhibit at the Manitoba Museum which blends the Selkirk Member and Stony Mountain Formation (Fig. 13A; Young et al. 2008, fig. 5). The display in the Stonewall Quarry Park, Stonewall (Fig. 13B, C) is supposed to reflect the biota in the Selkirk Member rather than the younger, less fossiliferous Stonewall Formation, which is the interval exposed in the quarry. Nevertheless, as is usual with such reconstructions, there is some artistic license taken, especially in the unrealistic crowding of the various biotic elements and the seafloor topography. In older dioramas receptaculitids were portrayed as globular (Fig. 13A), but a lower domical shape is more likely (Fig. 13C). Reconstructions in the USA are based on approximately correlative strata from the Cincinnati, Ohio area which consist of a different facies (e.g. https://www.priweb.org/blog-post/vanished-worlds; https://lsa.umich.edu/paleontology/resources/beyond-exhibits/life-through-the-ages.html), and that in the Redpath Museum, McGill University, Montreal, Quebec, reflects the Upper Ordovician of the Saint Lawrence Lowlands which also consists of different facies (https://www.mcgill.ca/redpath/article/ordovician-diorama).

TYNDALL STONE MOTTLING

Bioturbation

Description

The limestone exhibits brownish mottling due to the presence of dolomite that has incompletely replaced the original limestone. This unique and aesthetically desirable 'tapestry' of Tyndall Stone comes alive with its appearance on surfaces sawn parallel to bedding (Fig. 14A–D). From a distance the margins of the mottles appear sharp, but in detail they may be somewhat diffuse; in no case do they exhibit a distinct wall that comprises their margins. Locally the sharpness has been enhanced in vertical view by pressure solution and subhorizontal stylolite formation (Fig. 15A).

In horizontal view, the dolomitic mottles range from irregular to roughly circular and lobate patches, to elongate and seemingly branching to commonly crudely reticulate. Occasionally there are strikingly long, straight to curvilinear, sinuous features up to ~ 50 cm in length (Fig. 14C). Width of these domains is variable, up to ~ 4 cm wide. Where linear mottles are well defined, they are typically ~ 1–2 cm and occasionally up to 3 cm wide. In vertical view, the dolomitic domains are also variable in shape, from similarly circular to lobate to branching both vertically and horizontally (Fig. 15A–E).

Where grainstone lenses are interbedded, mottles are typically concentrated in the matrix just under them (Figs. 8C, 15E). Larger mottles intersect these lenses subvertically from the top, and they range from cylindrical to irregularly lenticular in shape and some penetrate the whole layer. Narrow, horizontally oriented, cylindrical mottles are also present.

The interiors of the mottles exhibit a swirly aspect imparted by various shades of brown and greyish brown; multiple generations of cross-cutting, cylindrical to tubular burrows can be discerned (Fig. 16A–F). These darker coloured, more distinctly defined curvilinear to irregularly sinuous burrows, are dominantly roughly horizontal (Fig. 16A–D) but also locally oblique and rarely vertically oriented (Figs. 15D, 16F). These burrows possess darker coloured linings. Their diameter is 5–13 mm. Many have a core 2–10 mm wide, cemented by dolomitic blocky microcrystalline calcite that is often leached leaving linear pores (burrow porosity); in some cases, there is geopetal dolomite on the bottoms of these pores. In addition, the dolomite that fills mollusc shell moulds commonly contains similar curvilinear burrows. Branching burrows 1 mm in width are locally preserved in the matrix inside nautiloids. Packstone-filled burrows that are not dolomitized are also locally visible in the limestone matrix.

In thin section, the mottles are seen to consist of brownish, variably dolomitized biomicrite in which bioclasts are still typically evident in the dolomicrite (Fig. 17A, B), although fewer in number than in the matrix; the larger, mostly robust particles like crinoid ossicles have escaped replacement (Fig. 17C). The interiors of the mottles typically show one or more horizontal burrows exhibiting the same features as those visible on sawn surfaces, that is, dolomitic calcite-cemented tunnels sur-

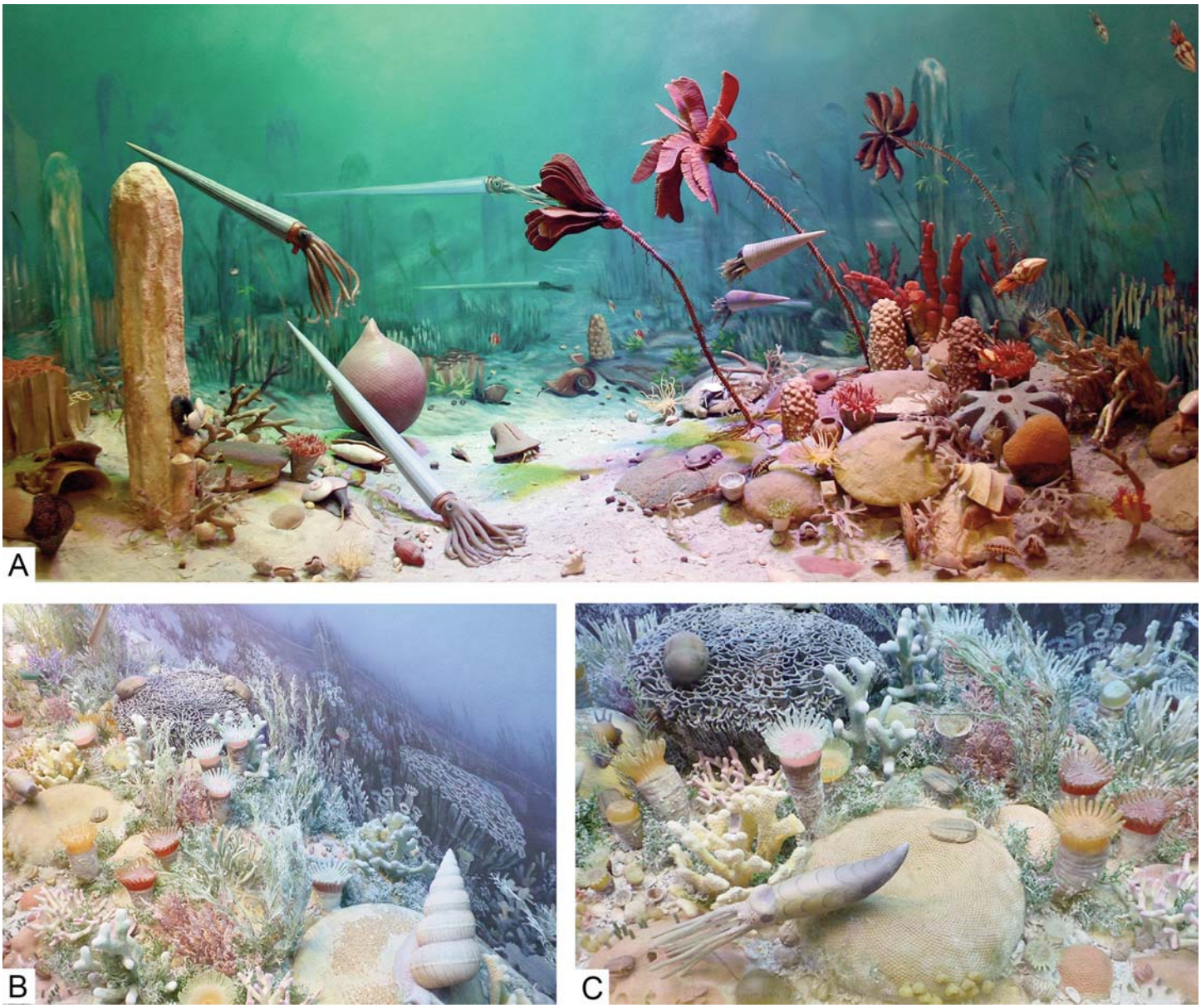

Figure 13. Museum dioramas showing reconstructions of the seafloor during deposition of Ordovician sedimentary rocks, including the Tyndall Stone (Selkirk Member). A. Manitoba Museum, Winnipeg, dating from the 1970s, composite of Ordovician biotas from Red River and Stony Mountain formations showing columnar aulacerid sponge, elongate orthocone nautiloids, globular receptaculitid, gastropods (snails) and other benthic invertebrates at left, and crinoids (sea lilies), short nautiloids, rugose and tabulate corals and other invertebrates at right. Copyright Manitoba Museum. B and C. Stonewall Quarry Park, Stonewall, dating from the early 2000s, showing rugose and tabulate corals including chain corals, domical receptaculitids, gastropods, trilobites, brachiopods and other invertebrates. These dioramas take some artistic license, such as crowding the organisms and exaggerating the seafloor topography in B and C. Used with permission from the Town of Stonewall Quarry Park Heritage Centre, 166 Main Street, Stonewall, Manitoba.

rounded by brownish, crudely concentric laminae and haloes. The margins of the dolomite mottles are not confined to these burrows and, rather, extend beyond them. Whereas the biomicrite matrix is clearly churned, in that bioclasts are variably oriented, in places straight to curvilinear burrows are recognizable. In cross-section some of these also have concentric linings and are filled with biomicrite in which the bioclasts range from variably to crudely concentrically oriented (Fig. 17D).

Comparable Facies

While the distinctive colouration and dolomitic mottling selectively overprinting limestone are unique to Garson, comparable burrow types are common to other Ordovician limestone and dolostone occurrences deposited in a similar low-energy, subtidal setting, including in equivalent dolostone beds of the Red River Formation nearby and far to the north on the northeastern side of the basin (Fig. 18A), and in broadly correlative limestone units in the Hudson Bay Basin across the Severn Arch (Fig. 18B). The former show well-defined, cross-cutting burrows that are 1–1.5 cm wide. More detailed fabrics are not visible, however, due to the complete dolomitization. The Gunton Member of the Stony Mountain Formation, which is

https://doi.org/10.12789/geocanj.2023.50.196

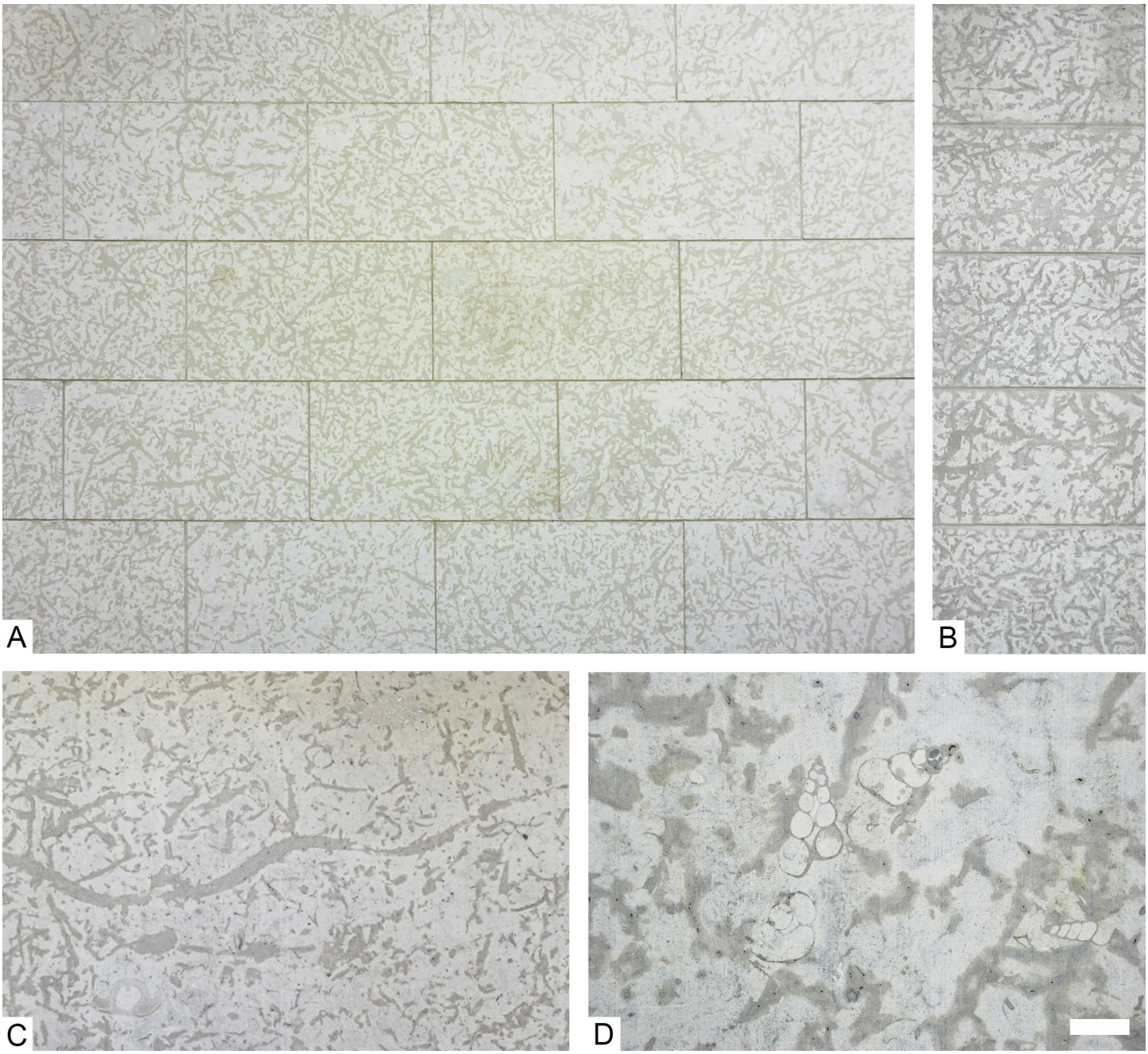

Figure 14. Walls sawn parallel to bedding with honed finish, showing the variation of shapes of dolomite mottling ('tapestry'). A. Exterior wall. Old bank building, Prince Albert, Saskatchewan. Slabs are 15 x 36 inches (~ 38 x 91 cm) in size. B. Exterior wall showing linear, elongate, irregular, branching, reticulate and circular shapes. Surfaces are 43 cm x 53 cm in size. Health Sciences Building, University of Saskatchewan. C. Interior wall with large sinuous mottle (across middle) overprinting curvilinear burrow. Mottle is 1 m in length. Health Sciences Building. D. Exterior wall showing relatively narrow mottles, with cluster (centre) of gastropods probably belonging to *Hormotoma*. Health Sciences Building. Scale bar is 3 cm.

younger than the Selkirk Member, also shows dense burrow patterns including long and reticulate features (Elias et al. 2013, fig. 29). In limestone of the Chasm Creek Formation of the Hudson Bay Basin, dolomite mottles are slightly narrower but well delineated, indicating a close morphological relationship with the original burrow fabrics (Fig. 18B). Besides some vertically oriented burrows, the networks may exhibit primary branching, unlike those in Tyndall Stone, suggesting a somewhat different behaviour, although this is not certain. Middle Ordovician limestone units of the Baltic Basin show comparable features but dolomitization of burrows is patchier, so only parts of burrows are replaced (Fig. 18C). Many younger fine-grained limestone beds deposited in low-energy subtidal conditions exhibit similar fabrics of backfilled branching and intersecting burrows (Fig. 18D).

Local iron staining in the Stony Mountain Formation, while in a different facies than the Selkirk Member, shows the bioturbation fabrics in striking detail, suggesting that burrowing in

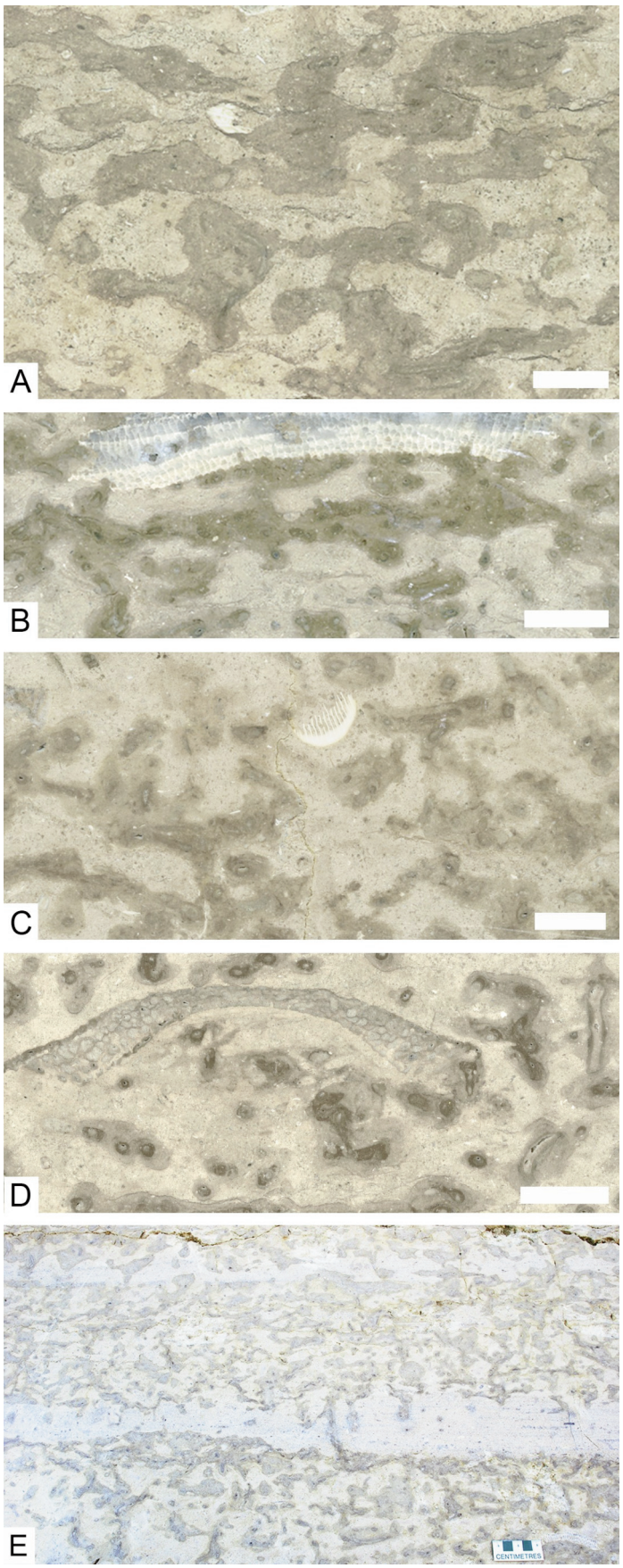

Figure 15. *(opposite)* Tyndall Stone cut perpendicular to bedding, showing details of dolomitic mottles (darker brown). A–D are polished surfaces; E is close-up of Gillis Quarry wall (shown in Figure 8C). A. Relatively large lobate mottles, with stylolites common near top. Scale bar is 3 cm. B. Elongate and variably shaped mottles, with some sharply abutting colonial rugose coral belonging to *Crenulites* (at top). Scale bar is 3 cm. C. Branching mottles with the edge of a solitary rugose coral calice possibly belonging to *Grewingkia* (upper centre). Scale bar is 3 cm. D. Small mottles including one with a vertical orientation (at right), with oblique cut through receptaculitid (also Figure 16F). Scale bar is 3 cm. E. Massive packstone with two lenticular, planar laminated grainstone beds that were burrowed from above. Lower bed shows mostly vertical and subvertical dolomitized burrows, ~ 1 cm wide. Upper bed is mostly burrowed away but exhibits some horizontal burrows (at left). Scale is in centimetres.

Tyndall Stone was likely much more complex than is readily apparent. Short curvilinear burrows with concentric linings, 0.2–0.3 cm in diameter, overprint the churned matrix which exhibits some narrower, seemingly mostly vertical burrows with curvilinear parts lacking linings (Fig. 19A, B). Some of these might be U-shaped. The lined burrows include many circular cross-sections as seen on surfaces cut parallel to bedding, and they only locally cross-cut each other. Brachiopod valves and trilobite sclerites are unoriented in the matrix. Larger burrows, 0.5 cm wide, have a lining and meniscate backfilling (Fig. 19B). Longer horizontal burrows 0.5–1 cm wide without linings are present and are cross-cut by many smaller burrows (Fig. 19C). Also present are indistinct horizontal burrows lacking walls but exhibiting a poorly defined meniscate backfilling. These are cross-cut by the smaller unlined and lined burrows.

Interpretation

Although they were initially regarded as plant and algal fossils and termed 'fucoids' (Wallace 1913) due to their vague resemblance to shoreline-inhabiting seaweed belonging to *Fucus* (which was a common view of such features at the time), it was later recognized that the mottles in Tyndall Stone reflected bioturbation by infaunal invertebrates, especially worms (Birse 1928). The apparent burrow networks were compared to gallery systems belonging to *Spongeliomorpha* (Kendall 1977), which in much younger rocks (and modern sediments) are ascribed to excavating crustaceans (e.g. Gibert and Ekdale 2010). Later, these kinds of burrows in Ordovician limestone were referred to *Thalassinoides,* which also consists of galleries (Sheehan and Schiefelbein 1984; Myrow 1995; Eltom and Goldstein 2023), and this identification has persisted for the mottles in Tyndall Stone and in subsurface equivalents and correlative units (Pak and Pemberton 2003; Cherns et al. 2006; Young et al. 2008; Jin et al. 2012, 2013). Sheehan and Schiefelbein (1984) suggested that these burrow systems reached a depth of one metre, although this is not apparent in the Gillis Quarry and in rock samples where the vertical expression seems to be no more than ~ 10 cm. The presence of trilobites associated with burrows led Cherns et al. (2006) to suggest that they had created the galleries which later became filled with biomicrite. No such relationship with dolomite mottles has been observed in Tyndall Stone.

Kendall (1977) reconstructed the burrows as empty galleries made by arthropods that excavated before, during and

https://doi.org/10.12789/geocanj.2023.50.196

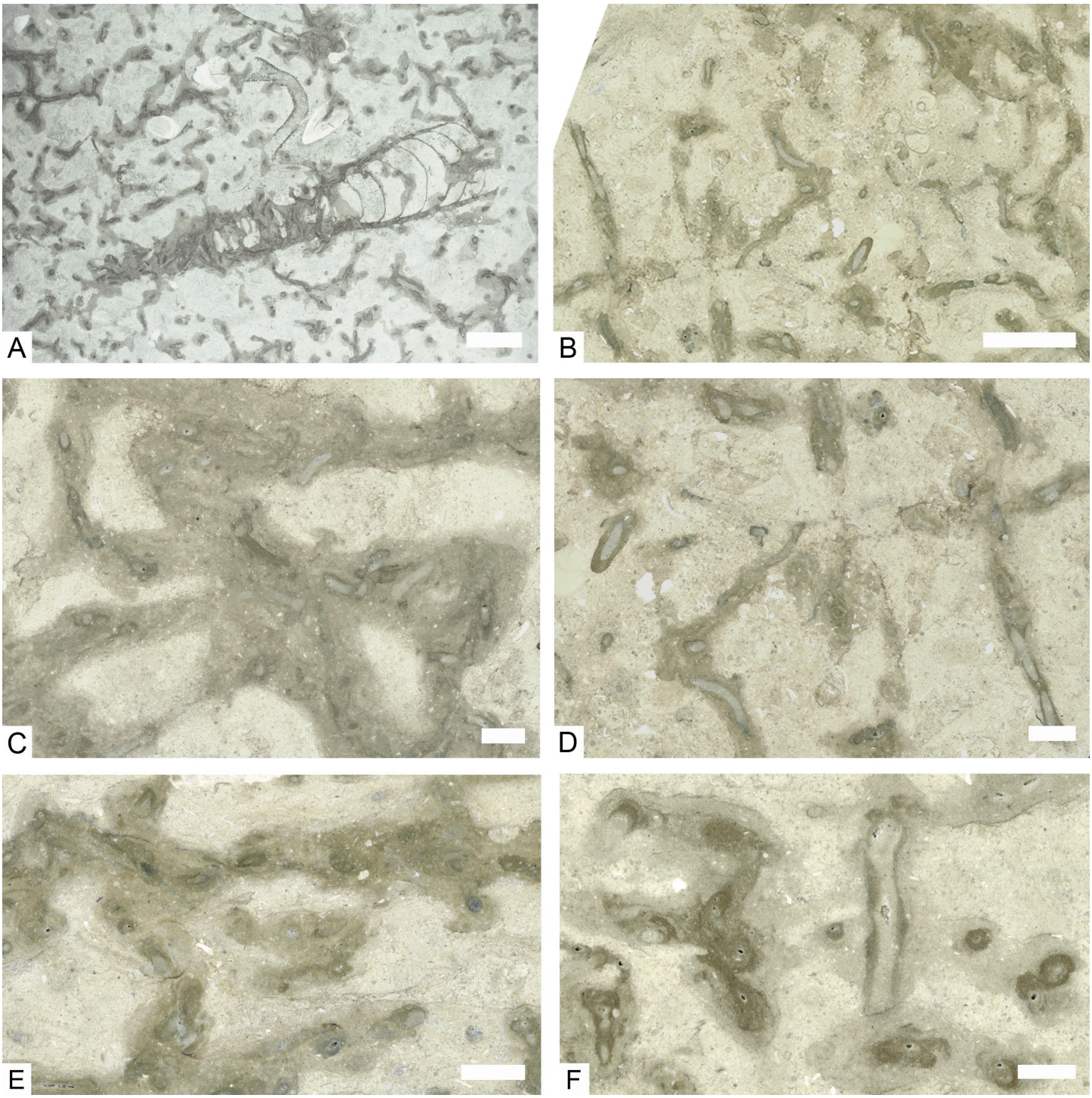

Figure 16. Close-up photographs showing details of dolomitic mottles (darker brown). A–D are surfaces sawn parallel to bedding; E and F are surfaces sawn perpendicular to bedding. A is honed finish; B–F are polished surfaces. A. Narrow linear and small circular mottles, densely cross-cutting each other around the posterior end of mould of orthoconic nautiloid (centre), with three solitary rugose corals probably belonging to *Grewingkia* and a receptaculitid (upper centre). Agriculture Building, University of Saskatchewan. Scale bar is 5 cm. B. Narrow, mostly linear mottles conforming to *Palaeophycus*, including some with calcite microspar-filled tubes, with gastropods (upper right of centre). Scale bar is 3 cm. C. Wide mottles with numerous burrows conforming to *Palaeophycus*. Scale bar is 2 cm. D. Narrow mottles with numerous burrows. Scale bar is 2 cm. E. Horizontally and vertically oriented mottles containing horizontally oriented burrows conforming to *Palaeophycus*. Close-up of left side of Figure 15B. Scale bar is 2 cm. F. Horizontally and vertically oriented mottles containing horizontally and vertically oriented burrows, the former corresponding to *Palaeophycus* and the latter to a vertically oriented *Palaeophycus* or possibly *Skolithos*. Close-up of right side of Figure 15D. Scale bar is 2 cm.

after sediment cementation, such that these burrows as well as aragonite shell moulds were filled after lithification and below the depth of active tunnelling, by lime mud that was then available to be burrowed by worms. The pervasive presence of

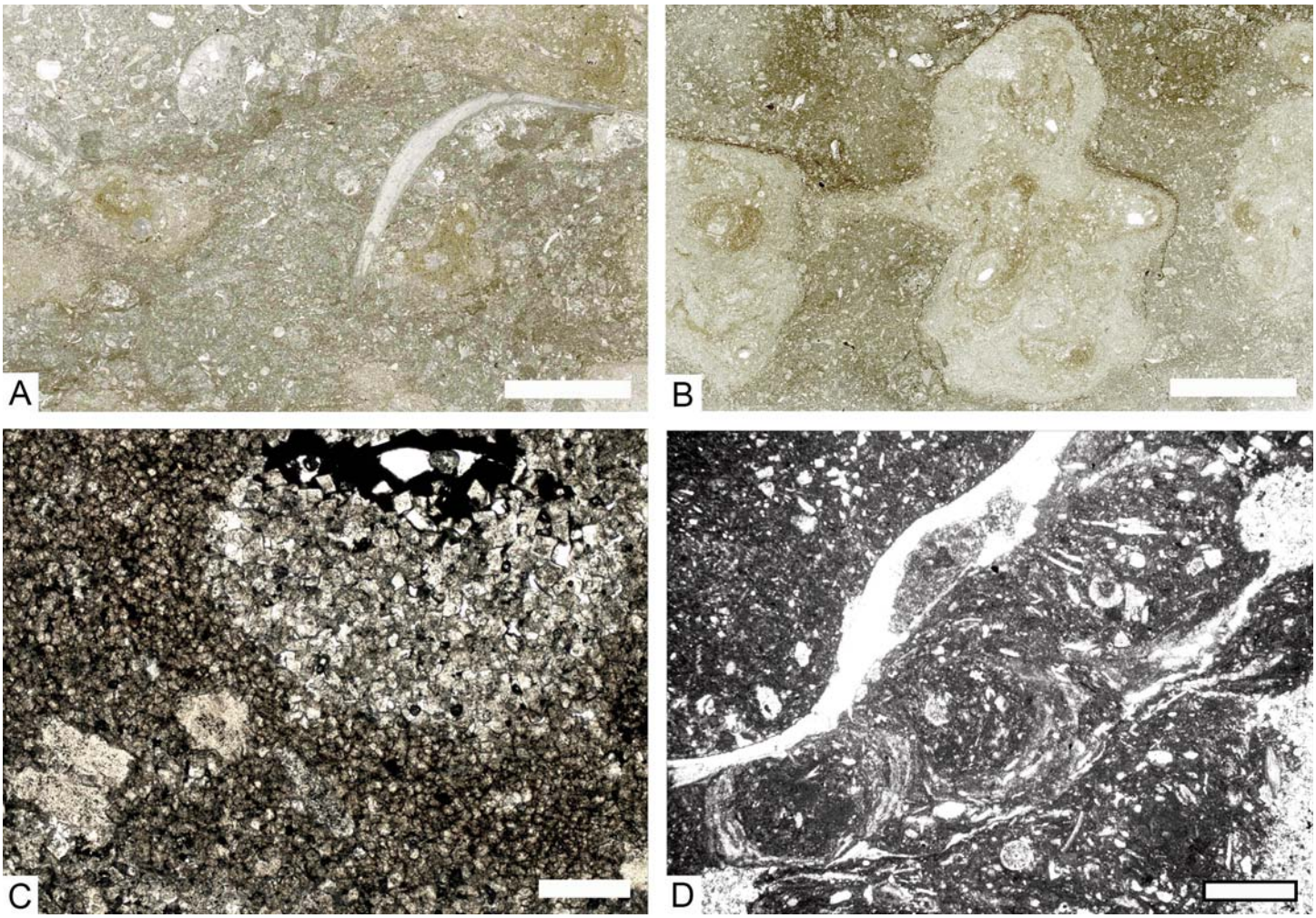

Figure 17. Petrographic detail of dolomitic mottles in biomicrite (packstone). Vertically oriented thin sections. A. Scanned image, including brachiopod shell (centre right), showing dolomitic, brown-stained linings and haloes of horizontal burrows. Natural colour. Scale bar is 10 mm. B. Scanned image showing interconnected, lobate dolomitic domains containing brown-stained horizontal burrows some of which show linings and haloes and calcite microspar-filled cores. Stylolites are present between the upper margins of the mottles and the matrix. Natural colour. Scale bar is 10 mm. C. Photomicrograph of part of a horizontal burrow showing central portion consisting of microcrystalline dolomite surrounded by brown-stained microcrystalline dolomite with finer crystal size containing scattered crinoid ossicles. The dolomite in the central portion shows geopetal structure overlain by opaque material collected inside pore after calcite dissolution. Plane-polarized light; natural colour. Scale bar is 1 mm. D. Photomicrograph of interior of nautiloid shell with horizontal, backfilled burrows with lining defined by crude concentric laminae. Plane-polarized light; greyscale. Scale bar is 2 mm.

large, empty galleries in lithifying sediment, however, is contradicted by the absence of sharp boundaries of the large burrows, their variable width, the presence of smaller burrows cross-cutting the margins of the mottles, and the sparse biomicrite filling large burrows. The multiple generations of smaller burrows in the biomicrite matrix and rarity of biomicrite intraclasts, present only in some grainstone lenses, also argue against excavation of cementing or cemented matrix. Some burrows in the correlative Yeoman Formation in the Saskatchewan subsurface (Kendall 1976, plate VIIIB; Pak and Pemberton 2003, figs. 11, 15) may be an exception to this. In these cases, it is possible that the matrix may have been lightly cemented, because the smaller burrows within do not penetrate the margins. These burrows may have been empty due to winnowing, before being infiltrated with lime mud. Washed-out burrows are present in the Gunn Member. There, the upper surface of some grainstone interbeds is a scoured surface showing grooves ~ 2 cm wide with smoothed margins. Comparable surfaces seem to be absent in Tyndall Stone. Moreover, it is difficult to envisage a complex system of interconnected, three-dimensional galleries continually being created by winnowing followed by filling due to sediment infiltration.

The small, millimetre-sized, curvilinear burrows in the biomicrite matrix and the dolomitic mottles mostly correspond to the ichnogenus *Palaeophycus* (Pak and Pemberton 2003). This taxon is distinguished from *Planolites* due to the lining of the burrow walls (Pemberton and Frey 1982; Keighley and Pickerill 1995). *Palaeophycus* appears to be common in lower Paleozoic limestone units, but in some cases the lining may instead be a diagenetic halo (Pak and Pemberton 2003; Pratt and Bordonaro 2007). Small, unlined, backfilled burrows correspon-

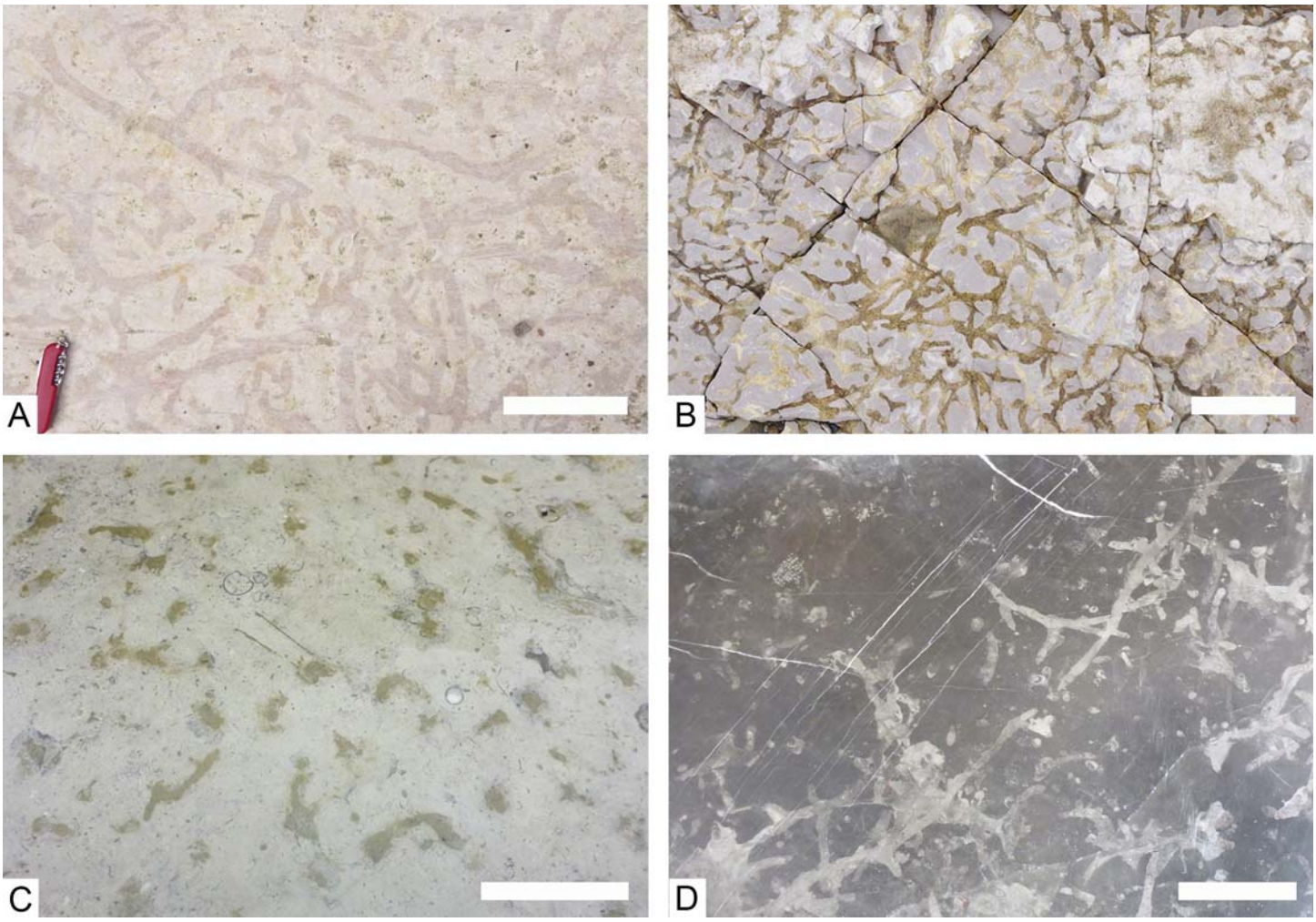

Figure 18. Comparable burrows in other limestones. A, B = Upper Ordovician; C = Middle Ordovician; D = mid-Cretaceous. A. Glacially polished, cream-coloured dolostone bedding plane showing well-defined large burrow networks. Red River Formation (undivided), Cranberry Portage quarry, 84 km north of The Pas, Manitoba. Scale bar is 10 cm. B. Limestone bedding surface with large burrow networks replaced by buff- to brown-coloured dolomite. Chasm Creek Formation, Churchill River Group, Churchill River, Churchill, Manitoba. This formation is correlative with the Stony Mountain Formation of southern Manitoba. Scale bar is 10 cm. C. Sawn block (capstone) of Reval, consisting of grey-coloured, bioclastic and fossiliferous packstone with portions of burrows replaced by brown-coloured dolomite. Tallinn, Estonia. Scale bar is 5 cm. D. Polished slab showing vertical and backfilled horizontal burrows. Hotel lobby floor, Mazatlán, Sinaloa (source is northeastern Mexico). Scale bar is 10 cm.

ding to *Planolites* are not prominent in the Tyndall Stone but are present in the correlative Yeoman Formation in the Saskatchewan subsurface (Pak and Pemberton 2003).

Pak and Pemberton (2003) identified a number of other ichnogenera in cores from the subsurface Yeoman Formation, including *Asterosoma*, *Rhizocorallium*, *Tricophycus*, *Skolithos* and *Chondrites*. However, *Asterosoma* is a radiating trace fossil and nothing resembling it is evident on horizontal surfaces of Tyndall Stone. *Rhizocorallium* consists of a looping horizontal burrow with curving spreiten in between, and it is also not apparent on horizontal surfaces. Burrows attributed to *Tricophycus* may be unusually wide mottles. Tyndall Stone exhibits rare vertical burrows that might be *Skolithos* but without a three-dimensional view it is also possible they are vertically oriented *Palaeophycus*. It is unlikely that they are *Arenicolites* as no U-shaped burrows have been identified in vertical section and pairs of circular burrow openings are not apparent on horizontal surfaces. Small branching burrows belonging to *Chondrites* are rare in Tyndall Stone. In the Stony Mountain Formation, Zheng et al. (2018) identified *Palaeophycus*, *Planolites*, *Nereites*, *Phycosiphon*, *Chondrites*, *Teichichnus*, *Rhizocorallium* and *Balanoglossites*. Parts of this unit exhibit a complex ichnofabric with seemingly abundant *Planolites* and small bioturbation features that are not readily discernible in Tyndall Stone.

Knaust (2021, p. 18) identified the dolomitic mottles in Tyndall Stone as *Balanoglossites,* which are empty galleries associated with firmgrounds. However, no firmground surfaces were observed in the Selkirk Member and in correlative dolostones farther north. Other, more sharply defined burrow systems in Ordovician limestones have also been assigned to *Balanoglossites*, including those in correlative Upper Ordovician units in Laurentia that lack evidence of seafloor cementation. *Balanoglossites* was identified in the Stony Mountain Formation (Zheng et al. 2018). While that unit does have evidence for early lithification in some beds, such as intraclasts in grainstone, and corroded or encrusted erosion surfaces that may

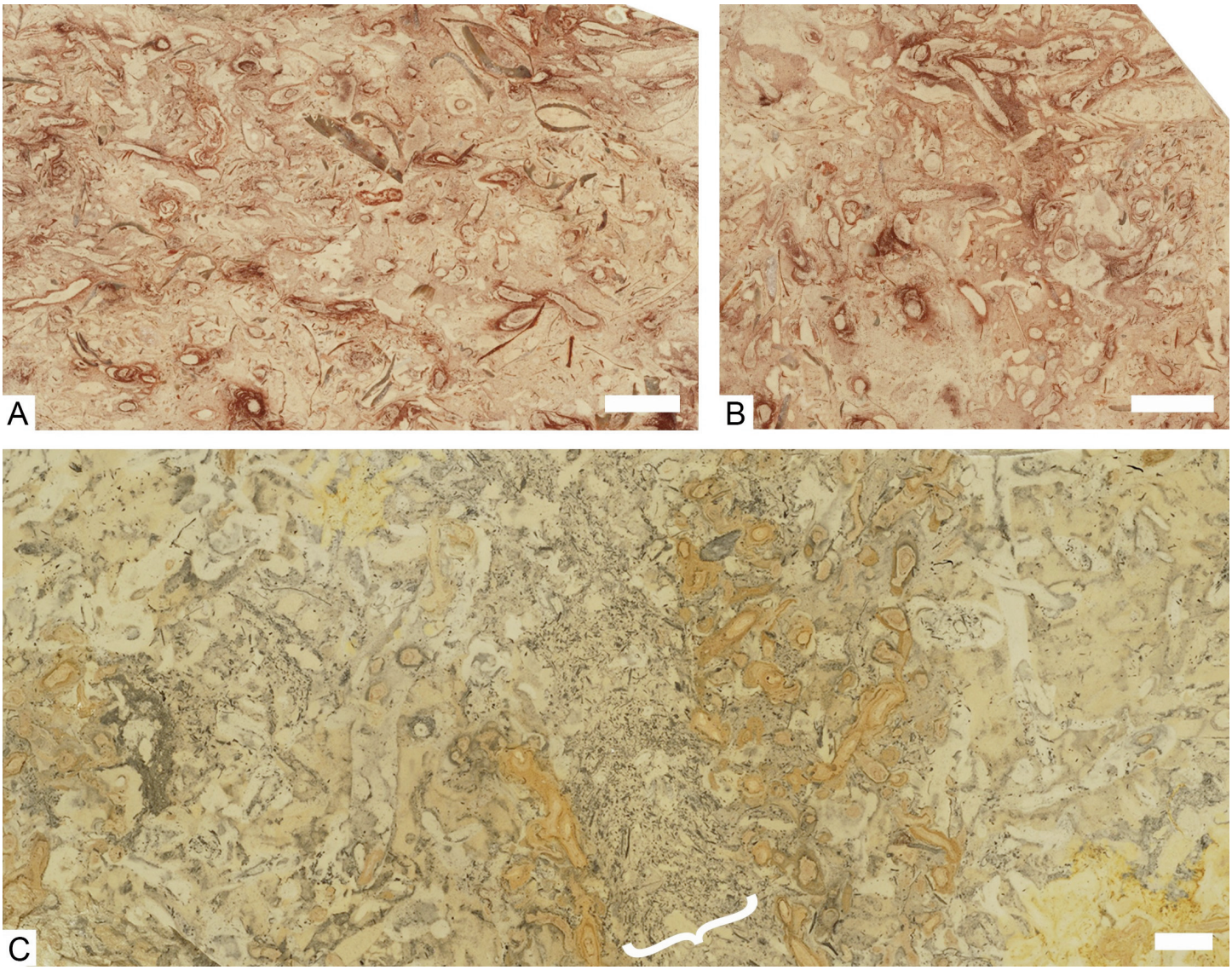

Figure 19. Comparable burrow fabrics in dolostone of the Stony Mountain Formation. A, B = Penitentiary Member, City of Winnipeg Quarry, Stony Mountain, Manitoba; C = Sturgeon Landing quarry, 56 km northwest of The Pas, Manitoba. Scale bars are 1 cm. A. Polished surface cut perpendicular to bedding, showing heavily bioturbated finely bioclastic carbonate mudstone overprinted by curvilinear burrows with linings conforming to *Palaeophycus*. The earlier bioturbation left a variegated appearance with locally discernible, short, narrow curvilinear burrows lacking linings, along with variably oriented brachiopod valves. B. Oblique and horizontal burrows with linings conforming to *Palaeophycus*, with wider burrow (upper right) exhibiting meniscate backfill. Polished surface cut parallel to bedding. C. Polished surface of buff-coloured dolostone sawn parallel to bedding showing wide, obliquely oriented, horizontal burrow (in middle) with meniscate backfill of micrite and tiny bioclasts (the width shown by white curly bracket), a narrower horizontal, mud-filled *Planolites* burrow (left of centre) that disturbs the part of the older portion of the larger burrow and is in turn cut by vertical burrows, and bioturbated matrix in which mud-filled *Planolites* burrows are discernible, with a final stage of backfilled *Palaeophycus* burrows with linings (mostly orange-coloured). *Planolites* burrows of the final stage do not penetrate the interior of the wide burrow, but the earlier generation of *Planolites* burrows disturbed the older portion of the large burrow (at top).

represent firm- or hardgrounds, the burrows appear to have been made before consolidation and erosion. Partially pyritized grooves ~ 1 cm wide on the surfaces were interpreted as tracks (Zheng et al. 2018), whereas similar grooves were named *Sulcolithos* by Knaust (2020) and interpreted as burrows or borings made on firmground and hardground surfaces. However, those in the Stony Mountain Formation represent relatively large burrows that were exhumed by the high-energy events that deposited the grainstone beds. Burrows attributed to *Balanoglossites* in the Stony Mountain Formation appear to be similar to the larger burrows in the Tyndall Stone and similarly have variable shapes. On the other hand, in dolomitic limestone of the Hudson Bay Basin, the larger burrows may be interconnected but it is unclear if they were ever empty gallery systems.

In Tyndall Stone, the variably well-defined, large curvilinear burrows containing biomicrite, oriented dominantly horizontally, were likely created by deposit-feeding worms ranging up to about 1 cm in diameter, that backfilled the burrows as they moved through the sediment. Examples of apparent branching represent mostly false branching due to crisscrossing burrows created by other worms active at the same time, as well as

multiple generations of worms. The fact that the reworked sediment in the burrows is still a mixture of lime mud and bioclasts, although containing fewer of the larger grains such as crinoid ossicles, means that it does not strongly contrast texturally from the matrix. The large burrows and matrix were reburrowed by generations of smaller worms that produced *Palaeophycus*. Calcite microspar cement commonly fills an empty tube or the upper part of a tube with a geopetal micrite floor. Thus, the wide curvilinear and unlined burrows belong to neither *Thalassinoides* nor *Balanoglossites*, but can be assigned to *Planolites*, albeit a very large form.

As is typical for shallow-marine carbonate rocks in shelf and epicontinental seas, dolomitization is a diagenetic phenomenon that post-dated microcrystalline and blocky calcite cementation and took place during burial, followed locally by crystal size increase due to neomorphism (Zenger 1996a, b), rather than by near-surface biogeochemical reactions as proposed by Gingras et al. (2004). In Tyndall Stone, the brown dolomite is only crudely selective, in that it is a replacement of mostly microcrystalline calcite and small bioclasts in the larger burrows as well as *Palaeophycus* and some of the surrounding matrix. Thus, the mottles are not confined to discrete burrows, which is part of the reason why the mottles range so widely in size and shape. By contrast, in completely dolomitized carbonate rocks of the Red River Formation to the north, the outlines of the larger burrows are more distinct.

TYNDALL STONE IN ARCHITECTURE

Aesthetics and Uses

Tyndall Stone is rarely used as a polished dimension stone, with notable exceptions including the lobby floor and staircases of the Banff Springs Hotel, a feature wall in the former Royal Alberta Museum and the memorial wall in the Geology Building, University of Saskatchewan, commemorating the geology students who fell in the Second World War. For the latter two, slabs particularly rich in macrofossils were selected.

Tyndall Stone used for cladding on both interior and exterior walls is usually sawn parallel to bedding (Fig. 20A, B) and a smooth finish (rubbed or honed) is most common. In some cases the original sawn surface is retained. Other surfaces can be prepared. In older buildings, surfaces that were bush-hammered to give the stone a texture were popular for stone at eye level. Uniformity in hue is selected for individual projects. Because large, conspicuous fossils are variably present, slabs with numerous fossils were typically discarded in earlier years when they were deemed visually undesirable because they interrupted the appearance. In recent years, slabs with fossils have more often been used for cladding. The unique paleontological content is increasingly being recognized as worth showcasing in some situations. For example, two bank buildings, one in Saskatoon and the other in Regina, have feature walls using eye-catching fossiliferous slabs. In the foyer of the Manitoba Museum are two walls with the fossils labelled and interpreted.

Split face finish (broken perpendicular to bedding) is increasingly being used for exterior walls (Fig. 20C). Ashlar (wall consisting of dressed stone) utilizing blocks with rustic ranch finish (split parallel to bedding) typically has hues that are mixed for a mosaic effect (Fig. 20D). This is popular especially for houses and other residential buildings. Machine-shaped decorative elements like string courses, window casements, doorways and buttresses are used, especially in collegiate gothic buildings at the University of Saskatchewan (Fig. 20E). There, Berea Sandstone was used before the First World War, then Indiana Limestone was employed, but in recent decades Tyndall Stone has been used exclusively. Tyndall Stone is also now used for indoor flooring and besides large slabs (Fig. 20F), roughly one foot x two foot (297 mm x 500 mm) rectangular tiles are manufactured with a honed or polished finish, and thin veneer products have been recently introduced.

Tyndall Stone also lends itself to carving, although it is a much harder stone than Indiana Limestone and some stones popular in other countries. In earlier years, government buildings like provincial legislatures and courthouses were especially well decorated (Figs. 2A–D; 21A–C, F–H). Numerous public and commercial buildings have been adorned with carved scenes (Figs. 20A, 21E). Hand-carved elements are still occasionally produced (Fig. 21D). There are sculptors who have utilized large blocks of Tyndall Stone.

While Tyndall Stone is a particularly durable material, it is still a carbonate rock with a hardness much less than that of granite, and it is soluble in acidic water. In rare situations where the stone is under some stress, such as in exterior staircases, cracks may develop in stone that has been in place for many years (Fig. 22A). Gradual etching of surfaces close to the ground may occur due to rain splash and from salt spread on sidewalks during winter (Fig. 22B). In a few cases, receptaculitids have popped out of blocks or cladding due to water infiltration and freeze–thaw cycles (Fig. 22C). Rare chalky-textured chert has also been a problem in external walls of some older buildings due to differential weathering, but slabs exhibiting this impurity have long been avoided. In locations where there is excess moisture, surfaces may by stained somewhat by black fungal or microbial growth (Fig. 22C). Probably the most visible 'damage' is done by repairs such as patching with cement or using stone with a different size or hue (Fig. 22D). On the other hand, Tyndall Stone cladding has been recovered from some demolished buildings and re-used.

Geotechnical Specifications

Comparison of the physical properties needs to take into account that some measurements conform to American Society for Testing and Materials (ASTM) standards, while others are based on other testing procedures, not to mention difficulties in comparing European (EN) standards. This makes comparisons with European dimension stones difficult. Tyndall Stone has properties similar to those of many other fairly hard limestone and marble examples, such as Tennessee Marble (a bioclastic limestone) and Georgia Marble (a true marble), but it is less dense and has greater water absorption due to the presence of minor porosity (Table 1; Parks 1916; Goudge 1933). The porosity is probably related to leaching by groundwater. Tyndall Stone is slightly denser than Indiana Limestone, which is a softer stone that is easier to work.

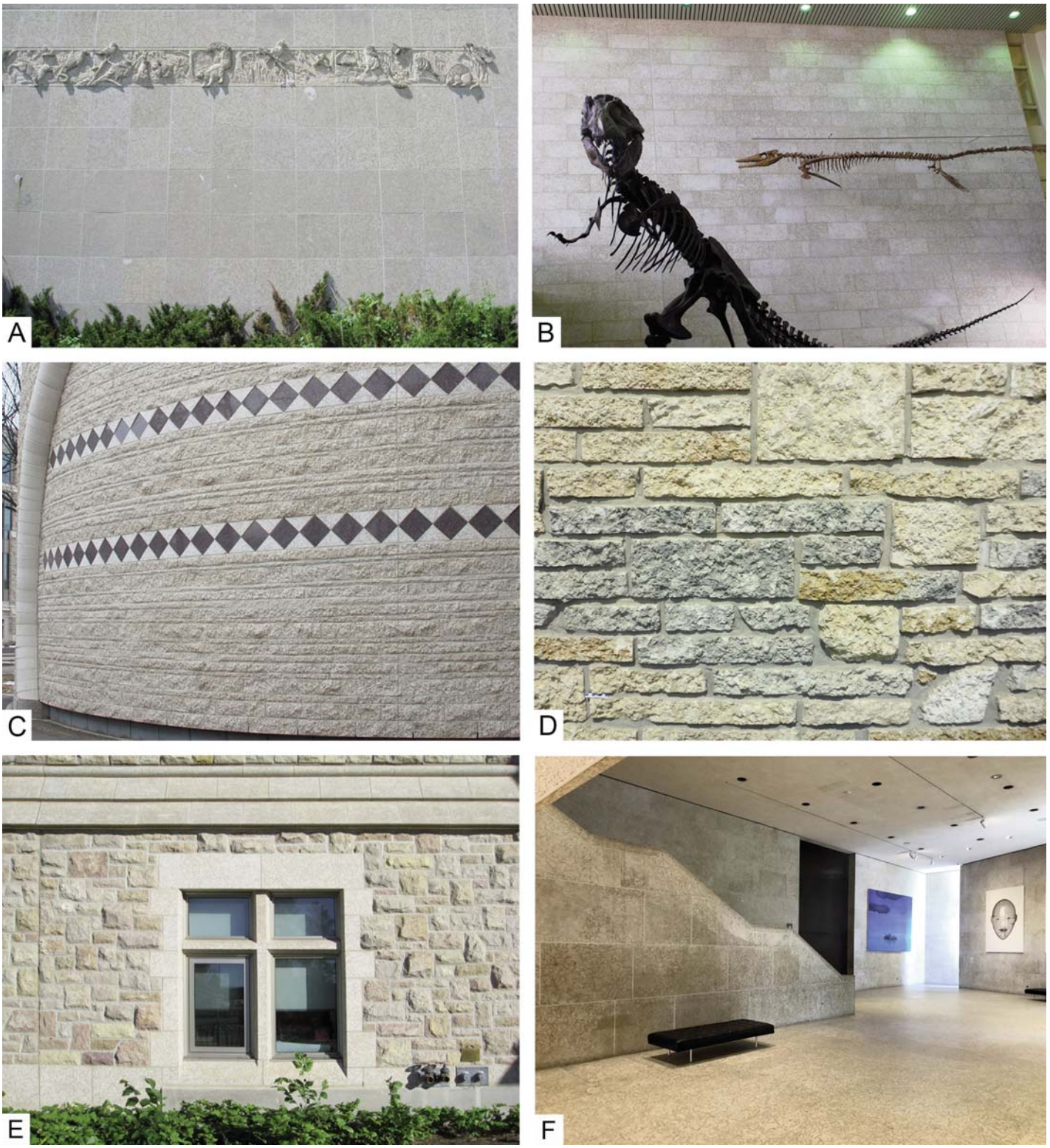

Figure 20. Examples of common Tyndall Stone usages and decorative elements. A. Exterior cladding consisting of coursed ashlar using square slabs with honed finish, with carved animals along top. Royal Saskatchewan Museum, Regina. B. Interior cladding consisting of coursed ashlar with rectangular slabs with honed finish. Natural Sciences Museum, University of Saskatchewan, with replicas of *Tyrannosaurus rex* and *Mosasaurus*. C. Exterior wall with coursed ashlar with split face finish (split perpendicular to bedding), with decorative courses of triangles with honed finish and red-coloured polished granite squares. Gordon Oakes Red Bear Student Centre, University of Saskatchewan. D. Exterior wall with random ashlar with different-coloured rustic ranch rock (rustic finish split along bedding-parallel stylolites). Condominium, Saskatoon. E. Exterior wall of random ashlar with rock-faced dolostone (fieldstone) and Tyndall Stone window surround and mullion, and stringcourses (bands at top and cladding along foundation). Health Sciences Building, University of Saskatchewan. F. Interior walls, floors and staircase faced with Tyndall Stone sawn parallel to bedding, Winnipeg Art Gallery, Winnipeg.

https://doi.org/10.12789/geocanj.2023.50.196

Figure 21. Examples of carved Tyndall stone. A. Fluted column with Ionic capital. Manitoba Legislative Building. B. Façade with pediment, various ornaments and coat of arms of the United Kingdom. Courthouse, Humboldt, Saskatchewan. C. Ornamental element with laurel wreath in honour of the arts and sciences. Carnegie Library, Winnipeg. D. Crest of the University of Saskatchewan. E. Sculpture of farm worker scything with grain elevators and rising sun behind. Bank of Montreal Building, Saskatoon (also Figure 29E). F. Ornament in the shape of tiers of leaves. Manitoba Legislative Building. G. Crest of the Province of Saskatchewan, courthouse, Battleford. H. Ornamental urn. Manitoba Legislative Building.

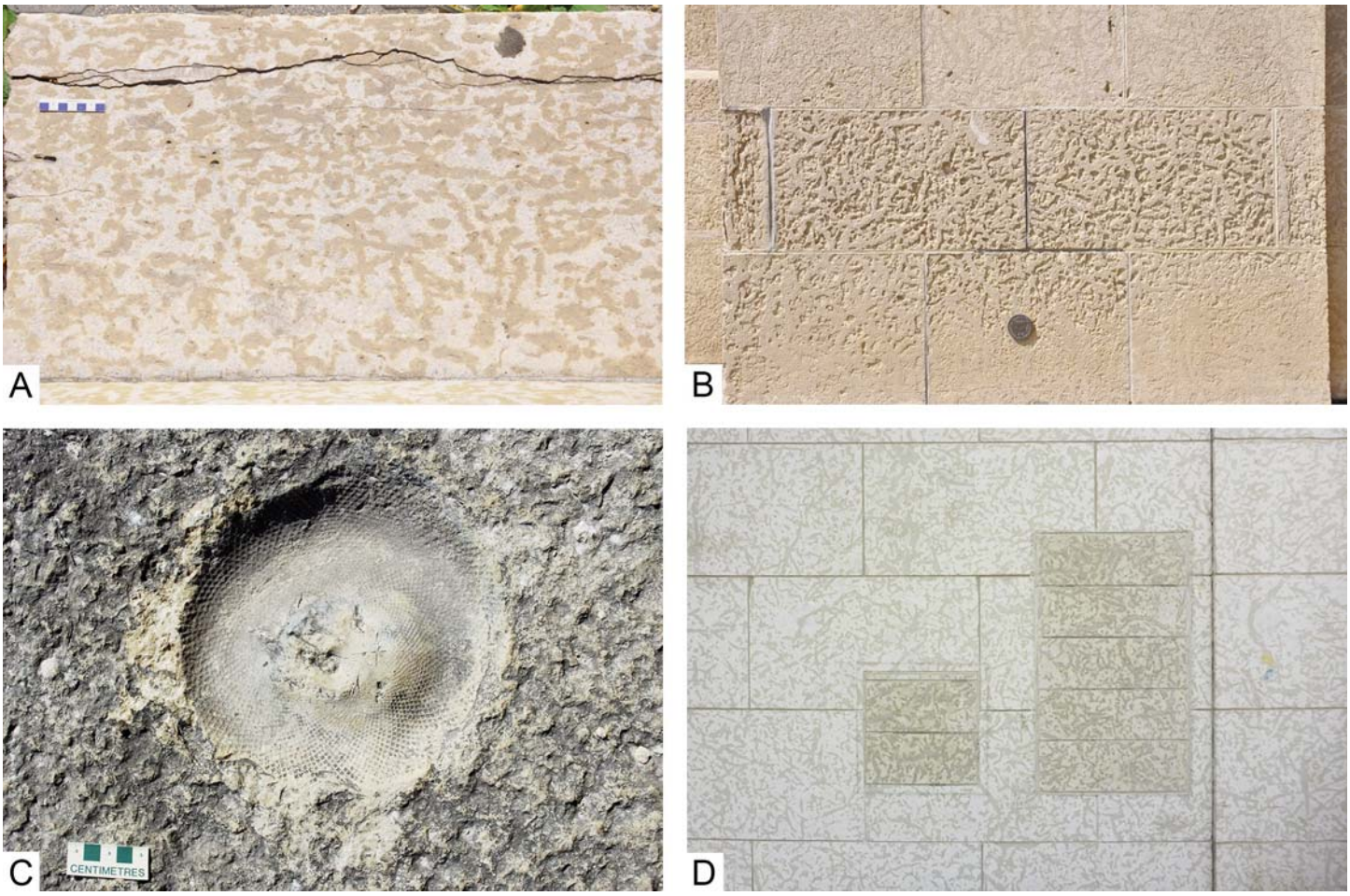

Figure 22. Examples of damage to Tyndall Stone. A. Looking down on plinth with vertically oriented cracks. Winnipeg. Scale in centimetres. B. Weathered bush-hammered foundation slabs, with Canadian Geodetic Survey levelling benchmark tablet (lower centre). Courthouse, Humboldt, Saskatchewan. Width of view approximately 1.5 m. C. Upper surface of stairway retaining wall block with concave mould of receptaculitid, which has popped out. Manitoba Legislative Building. Scale bar in centimetres. D. Cladding of old bank building with night depository drop box portals replaced with stone having different sizes and hue. Prince Albert, Saskatchewan. Width of view approximately 1.5 m.

Table 1. Physical properties of Tyndall Stone, two other limestones and a marble for comparative purposes. ASTM test procedures are noted if recorded.

Property [test procedure]	Tyndall Stone	Indiana Limestone	Tennessee Marble	Georgia Marble
Specific gravity [C97]	2.44	2.1–2.75		
Density (weight) (kg/m^3)	2435 kg/m^3	2307 kg/m^3	2713 kg/m^3	2730 kg/m^3
Compressive strength – dry [ASTM C170]	62.8 MPa	minimum 27.6 MPa	105 MPa	68.1 MPa
Tensile strength		2.1–4.9 MPa		
Shear strength	7.3 MPa	6.2–12.4 MPa		
Transverse strength	9.2 MPa			
Flexural strength [ASTM C880]			17.9 MPa	10.4 MPa
Modulus of rupture – dry [ASTM C99]	9.9 MPa	minimum 4.8 MPa		10.1 MPa
Modulus of rupture – wet [ASTM C99]	5.2 MPa			
Absorption [ASTM C97]	3.49%	maximum 7.5%	0.06%	0.08%
Porosity	average 11.36%	about 5%		
Modulus of elasticity [ASTM C1352]	41.37 GPa	22.75–37.23 GPa		

Sources: Tyndall Stone – gillisquarries.com/about-us/properties (also Gillis Quarries Ltd. n.d., 2012); Indiana Limestone – ILI 2007; Tennessee Marble – tnmarble.com/specifications/; Georgia Marble – polycor.com/stone/marble/georgia-marble-white-georgia/.
Units for US stones changed to metric. ASTM = American Society for Testing and Materials (now ASTM International).

https://doi.org/10.12789/geocanj.2023.50.196

Figure 23. Examples of the range of buildings utilizing Tyndall Stone. A. City Hall (1914), Moose Jaw, Saskatchewan. Beaux Arts style. B. Bessborough Hotel (1932), Saskatoon. Châteauesque style. C. St. Andrew's Church (1912), Moose Jaw. Neo-Gothic style. D. Sturdy Stone Building (1977), Saskatoon. Brutalist style. E. Canadian Museum of History (1989), Gatineau (Ottawa). Expressionist style. Image credit: Wikimedia Commons, remundo (https://en.wikipedia.org/wiki/Canadian_Museum_of_History#/media/File:Canadian_Museum_of_History_(30397442792).jpg).

Examples of Buildings

In the early years, Tyndall Stone was used almost exclusively in the Prairie Provinces of western Canada. Besides the Saskatchewan and Manitoba legislative buildings, it has been used in many other government buildings such as courthouses, post offices, land titles buildings, and city and town halls, as well as banks, department stores, train stations, office buildings, schools, and hotels (Figs. 23–30). It was used to striking effect in the interior of the rotunda of Confederation Hall in the House of Commons, Ottawa (Fig. 2A–D). The stone was used sporadically across the rest of the country prior to the Second World War. In the middle 20th century, its use expanded

Figure 24. Older buildings using Tyndall Stone, Winnipeg. A. Law Courts (1916). Beaux Arts style. B. Land Titles Building (1904). Neo-classical style. C. Hudson's Bay Company Building (1926). Neo-classical style. D. Hamilton Building (1918). Chicago School style. E. Manitoba Power House (1915). F. Union Station (1911). Neo-classical style.

https://doi.org/10.12789/geocanj.2023.50.196

Figure 25. Examples of the range of building styles using Tyndall Stone, Winnipeg. A. Carnegie Library (1905). Neo-classical style. B. Civic Auditorium (1932). Art Deco style. C. Federal Building (1936). Classical Moderne style. D. Castle on the Seine (1986). Contemporary classical style.

to other commercial buildings, museums, art galleries, concert halls, hospitals, universities and churches, as well as residential uses both exterior and interior. Tyndall Stone has been used for several buildings in the USA and for Canada House (Kanada Haus), which is the Embassy of Canada to Germany, in Berlin. It was often used as an accent in buildings mainly constructed with red brick.

Architectural styles have varied over time as taste and construction methods evolved. Before the First World War, the most common were Neo-classical and Beaux Arts styles. A number of Art Deco-inspired buildings were constructed in the 1930s during the Depression. In the 1960s, Modernist style was commonly adopted for public buildings like museums and art galleries, as well as larger banks and other commercial

Figure 26. Newer buildings using Tyndall Stone, Winnipeg. A. Winnipeg City Hall, Susan A. Thompson Building (1963). Modernist style. B. Bank building, Main Street. Modernist style. C. Canada Life Building (1983). Modernist style. D. Canadian Museum for Human Rights (2014). Expressionist style.

buildings. Recent decades have seen a number of forays into Brutalist, Contemporary classical, Postmodern and Expressionist styles.

In addition to the iconic legislative buildings in Regina and Winnipeg, monumental buildings using Tyndall Stone that were constructed in the first decades of the 20th century are distinctive elements in the centres of these and other cities and towns. These buildings, constructed when the Prairie Provinces were growing rapidly in population prior to the Depression, have stood the test of time and are in good condition, lending a sense of permanence. To many they are aesthetically more pleasing compared to more commonplace brick, concrete or glass and steel buildings. In modern times, many of them have been repurposed. Cities and larger towns now have historical or heritage societies and, in collaboration with various levels of government, many of these buildings have been designated as heritage properties and are protected.

CONCLUSIONS

Tyndall Stone is an iconic building stone in Canada. It has been used since the beginning of the 20th century, especially in the Prairie Provinces. It is spectacularly fossiliferous, and slabs sawn parallel to bedding give an unparalleled snapshot of a tropical, shallow seafloor of Late Ordovician age. Conspicuous fossils include receptaculitids, corals, stromatoporoids, nautiloids and gastropods. What makes Tyndall Stone unique is especially the tapestry of brownish mottles composed of dolomite on the light grey to cream limestone background. These mottles represent dolomite replacement of burrows created by infaunal invertebrate animals, along with some of the adjacent matrix. Long thought to have originally been empty galleries and assigned to *Thalassinoides*, they were actually backfilled burrows likely made by large worms, and more reasonably assigned to *Planolites*. They are one component of several bioturbation phenomena, including churning of the bioclastic muddy sediment, and multiple generations of smaller burrows, most of which have linings on their margins and are referable to *Palaeophycus*, also made by worms.

Tyndall Stone is a versatile, durable stone that has been used in a variety of ways for many buildings, especially in the Prairie Provinces, including the legislative buildings of Manitoba and Saskatchewan, courthouses, land titles buildings, city and town halls, banks, stores, office buildings, train stations, hotels, schools, museums, universities and churches, as well as

https://doi.org/10.12789/geocanj.2023.50.196

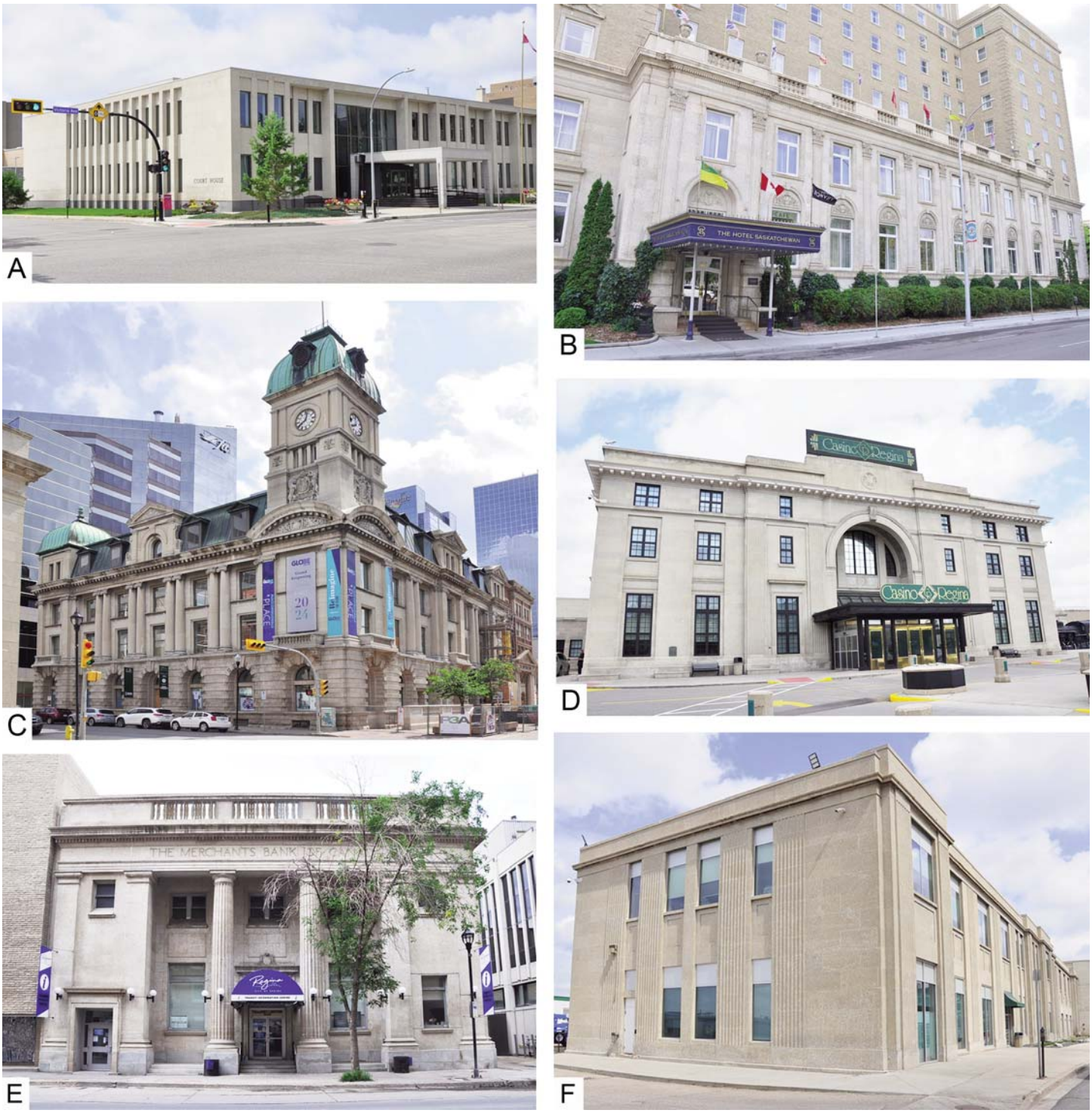

Figure 27. Examples of the range of building styles using Tyndall Stone, Regina. A. Courthouse (1961). Modernist style. B. Hotel Saskatchewan (1927). Neo-classical style. C. Post Office (1909). Beaux Arts style. D. Union Station (1911). Simplified Beaux Arts–Classical style. E. Merchants Bank (1911). Neo-classical style. F. CN/CP Telegraph Building (1932). Art Moderne style.

Figure 28. Examples of the range of building styles using Tyndall Stone, Regina. A. Darke Hall (1929). Neo-Gothic style. B. Imperial Bank of Canada Building (1912). Neo-Georgian style. C. Trust and Loan Company Building (1923). Neo-classical style. D. Motherwell Building (1956). Modernist style. E. Knox–Metropolitan United Church (1913). Norman and Gothic styles. F. Dominion Government Building (1936). Art Deco and Art Moderne styles. G. Use of sawn and split finishes on exterior wall. Commercial building (recent).

https://doi.org/10.12789/geocanj.2023.50.196

Figure 29. Examples of the range of building styles using Tyndall Stone, Saskatoon. A. Land Titles Building (1910). Neo-classical and neo-Romanesque. B. Eaton's Building (1928). Neo-Renaissance style. C. Spinks Addition to Chemistry Building, University of Saskatchewan (2003). Châteauesque style. D. Health Sciences Building (2014). Collegiate Gothic style. E. Bank of Montreal building (1955). Modernist style (also Figure 21E). F. Use of split face, sawn and rustic finishes on exterior wall, in random (lower) and coursed ashlar (upper). Irene and Leslie Dubé Centre for Mental Health, Saskatoon (2010).

Figure 30. Examples of courthouses using Tyndall Stone in combination with red brick. A. Humboldt, Saskatchewan (1916). Edwardian classical style. B. Minnedosa, Manitoba (1910). Queen Anne style. C. Dauphin, Manitoba (1917). Neo-classical style. D. Battleford, Saskatchewan (1909). Neo-Romanesque style.

residential buildings. Many architectural styles have been adopted, ranging from Beaux Arts to Brutalist, Neo-classical to Postmodern. Given its spectacular paleontological content, Tyndall Stone is also a unique educational tool and at hand in most Canadian cities. In October 2022 it was designated a Global Heritage Stone Resource by the International Union of the Geological Sciences Subcommission on Heritage Stones. This was ratified and as of late 2022, Tyndall Stone is an IUGS Heritage Stone, Canada's first (Fig. 31).

Figure 31. Certificate from the International Union of Geological Sciences recognizing Tyndall Stone as a Heritage Stone.

ACKNOWLEDGEMENTS

Our collective fascination for Tyndall Stone goes back decades. We appreciate Ed Dobrzanski for his long interest in the Ordovician of southern Manitoba and Tyndall Stone in particular, and for his help and encouragement. GAY is grateful to Robert Elias for many years of collaborative research on the paleontology of the Tyndall Stone. BRP is grateful to Dolores Pereira for her encouragement of a nomination for recognition by the Heritage Stones Subcommission, and more recently Colin Sproat for collaborative effort on the Upper Ordovician of southern Manitoba. Special thanks to Donna Gillis for quarry access over many years, encouragement in the heritage stone nomination and for comments on quarry operations and products. Abigail Auld commented on historical and architectural aspects. We thank the Manitoba Museum and Stonewall Quarry Park for permission to illustrate dioramas, and Carlton

Brett and Robert Elias for providing many helpful comments as reviewers of the manuscript. We are grateful that Gillis Quarries Ltd. covered the open-access fee and to Jeffrey Dolovich for facilitating that.

REFERENCES

Birse, D.J., 1928, Dolomitization processes in the Palaeozoic horizons of Manitoba: Transactions of the Royal Society of Canada, Sec. IV, v. 22, p. 215–221.

Brisbin, W.C., Young, G., and Young, J., 2005, Geology of the Parliament Buildings 5: Geology of the Manitoba Legislative Building: Geoscience Canada, v. 32, p. 177–193.

Burwash, R.A., Cruden, D.M., and Mussieux, R., 2002, The Geology of Parliament Buildings 2. The geology of the Alberta Legislative Building: Geoscience Canada, v. 29, p. 139–146.

Byerly, D.W., and Knowles, S.W., 2017, Tennessee "Marble": a potential "Global Heritage Stone Resource": Episodes, v. 40, p. 325–331, https://doi.org/10.18814/epiiugs/2017/v40i4/017033.

Cherns, L., Wheeley, J.R., and Karis, L., 2006, Tunneling trilobites: Habitual infaunalism in an Ordovician carbonate seafloor: Geology, v. 34, p. 657–660, https://doi.org/10.1130/G22560.1.

Cocks, L.R.M., and Torsvik, T.H., 2021, Ordovician palaeogeography and climate change: Gondwana Research, v. 100, p. 53–72, https://doi.org/10.1016/j.gr.2020.09.008.

Cowan, J., 1971, Ordovician and Silurian stratigraphy of the Interlake area, Manitoba, *in* Turnock, A.C., *ed.*, Geoscience Studies in Manitoba: Geological Association of Canada, Special Paper 9, p. 235–241.

Dowling, D.B., 1900, Report on the geology of the west shore and islands of Lake Winnipeg: Geological Survey of Canada, Annual Report, v. 11, (1898), Part F, 103 p., https://doi.org/10.4095/296998.

El Taki, H., and Pratt, B.R., 2012, Syndepositional tectonic activity in an epicontinental basin revealed by deformation of subaqueous carbonate laminites and evaporites: Seismites in Red River strata (Upper Ordovician) of southern Saskatchewan, Canada: Bulletin of Canadian Petroleum Geology, v. 60, p. 37–58, https://doi.org/10.2113/gscpgbull.60.1.37.

Elias, R.J., 1980, Borings in solitary rugose corals of the Selkirk Member, Red River Formation (late Middle or Upper Ordovician), southern Manitoba: Canadian Journal of Earth Sciences, v. 17, p. 272–277, https://doi.org/10.1139/e80-023.

Elias, R.J., 1981, Solitary rugose corals of the Selkirk member, Red River formation (late Middle or Upper Ordovician), southern Manitoba: Geological Survey of Canada, Bulletin 344, 61 p., https://doi.org/10.4095/109537.

Elias, R.J., 1991, Environmental cycles and bioevents in the Upper Ordovician Red River-Stony Mountain solitary rugose coral province of North America, *in* Barnes, C.R., and Williams, S.H., *eds.*, Advances in Ordovician Geology: Geological Survey of Canada, Paper 90-9, p. 205–211, https://doi.org/10.4095/132189.

Elias, R.J., Young, G.A., Stewart, L.A., Demski, M.W., Porter, M.J., Luckie, T.D., Nowlan, G.S., and Dobrzanski, E.P., 2013, Ordovician–Silurian boundary interval in the Williston Basin outcrop belt of Manitoba: a record of global and regional environmental and biotic change: Geological Association of Canada-Mineralogical Association of Canada Joint Annual Meeting, Field Trip Guidebook FT-C, Manitoba Innovation, Energy and Mines, Manitoba Geological Survey, Open-File Report OF2013-1, 49 p.

Eltom, H.A., and Goldstein, R.H., 2023, Scale dependence of petrophysical measurements in reservoirs with *Thalassinoides*: Insights from CT scans: Marine and Petroleum Geology, v. 148, article 106036, https://doi.org/10.1016/j.marpetgeo.2022.106036.

Garg, S., Kaur, P., Pandit, M., Fareeduddin, Kaur, G., Kamboj, A., and Thakur, S.N., 2019, Makrana Marble: a popular heritage stone resource from NW India: Geoheritage, v. 11, p. 909–925, https://doi.org/10.1007/s12371-018-00343-0.

Gibert, J.M.de, and Ekdale, A.A., 2010, Paleobiology of the crustacean trace fossil *Spongeliomorpha iberica* in the Miocene of southeastern Spain: Acta Palaeontologica Polonica, v. 55, p. 733–740, https://doi.org/10.4202/app.2010.0010.

Gillis Quarries Ltd., no date, Tyndall Stone, a naturally quarried limestone: 20 p. [technical and commercial brochure].

Gillis Quarries Ltd., 2012, Tyndall Stone, 450 million years of history: 36 p. [residential brochure].

Gingras, M.K., Pemberton, S.G., Muelenbachs, K., and Machel, H., 2004, Conceptual models for burrow-related, selective dolomitization with textural and isotopic evidence from the Tyndall Stone, Canada: Geobiology, v. 2, p. 21–30, https://doi.org/10.1111/j.1472-4677.2004.00022.x.

Goudge, M.F., 1933, Canadian limestone for building purposes: Canada Department of Mines, Mines Branch, Publication no. 733, 196 p.

Goudge, M.F., 1944, Limestones of Canada, Part V: Western Canada: Canada Department of Mines and Resources, Mines and Geology Branch, Report no. 811, 233 p.

Hannibal, J.T., Kramar, S., and Cooper, B.J., 2020, Worldwide examples of global heritage stones: an introduction, *in* Hannibal, J.T., Kramar, S., and Cooper, B.J., *eds.*, Global Heritage Stone: Worldwide Examples of Heritage Stones: Geological Society, London, Special Publications, v. 486, p. 1–6, https://doi.org/10.1144/SP486-2020-84.

Heldal, T., Meyer, G.B., and Dahl, R., 2014, Global stone heritage: Larvikite, Norway, *in* Pereira, D., Marker, B.R., Kramar, S., Cooper, B.J., and Schouenborg, B.E., *eds.*, Global Heritage Stone: Towards International Recognition of Building and Ornamental Stones: Geological Society, London, Special Publications, v. 407, p. 21–34, https://doi.org/10.1144/SP407.14.

Holland, S.M., and Patzkowsky, M.E., 2009, The stratigraphic distribution of fossils in a tropical carbonate succession: Ordovician Bighorn Dolomite, Wyoming, USA: Palaios, v. 24, p. 303–317, https://doi.org/10.2110/palo.2008.p08-095r.

ILI, 2007, Indiana Limestone Handbook (22nd ed.). Indiana Limestone Institute of America, Inc., Bedford, 157 p.

Jin, J., and Zhan, R-b., 2001, Late Ordovician articulate brachiopods from the Red River and Stony Mountain formations, Southern Manitoba: National Research Council Press, Ottawa, 117 p., https://doi.org/10.1139/9780660182834.

Jin, J., Caldwell, W.G.E., and Norford, B.S.,1997, Late Ordovician brachiopods and biostratigraphy of the Hudson Bay Lowlands, northern Manitoba and Ontario: Geological Survey of Canada, Bulletin 513, 122 p., https://doi.org/10.4095/208903.

Jin, J., Harper, D.A.T., Rasmussen, J.A., and Sheehan, P.M., 2012, Late Ordovician massive-bedded *Thalassinoides* ichnofacies along the palaeoequator of Laurentia: Palaeogeography, Palaeoclimatology, Palaeoecology, v. 367–368, p. 73–88, https://doi.org/10.1016/j.palaeo.2011.05.023.

Jin, J., Harper, D.A.T., Cocks, L.R.M., McCausland, P.J.A., Rasmussen, C.M.Ø., and Sheehan, P.M., 2013, Precisely locating the Ordovician equator in Laurentia: Geology, v. 41, p. 107–110, https://doi.org/10.1130/G33688.1.

Kaur, G., 2022, Heritage Stone Subcommission: An IUGS Subcommission of the International Commission on Geoheritage: Journal of the Geological Society of India, v. 98, p. 587–590, https://doi.org/10.1007/s12594-022-2030-1.

Keighley, D.G., and Pickerill, R.K., 1995, The ichnotaxa *Palaeophycus* and *Planolites*: Historical perspectives and recommendations: Ichnos, v. 3, p. 301–309, https://doi.org/10.1080/10420949509386400.

Kendall, A.C., 1976, The Ordovician carbonate succession (Bighorn Group) of southeastern Saskatchewan: Saskatchewan Department of Mineral Resources, Saskatchewan Geological Survey, Report 180, 185 p.

Kendall, A.C., 1977, Origin of dolomite mottling in Ordovician limestones from Saskatchewan and Manitoba: Bulletin of Canadian Petroleum Geology, v. 25, p. 480–504.

Knaust, D., 2020, *Sulcolithos variabilis* igen. et isp. nov.: grooves on firm and hard bedding surfaces: Paläontologische Zeitschrift, v. 94, p. 195–206, https://doi.org/10.1007/s12542-019-00464-z.

Knaust, D., 2021, *Balanoglossites*-burrowed firmgrounds – The most common ichnofabric on earth?: Earth-Science Reviews, v. 220, article 103747, https://doi.org/10.1016/j.earscirev.2021.103747.

Lavoie, D., Pinet, N., Zhang, S., Reyes, J., and 20 others, 2022, Hudson Bay, Hudson Strait, Moose River, and Foxe basins: synthesis of Geo-mapping for Energy and Minerals program. Activities from 2008 to 2018, *in* Lavoie, D., and Dewing, K., *eds.*, Sedimentary Basins of Northern Canada: Contributions to a 1000 Ma Geological Journey and Insight on Resource Potential: Geological Survey of Canada, Bulletin 609, p. 37–76, https://doi.org/10.4095/326074.

Lawrence, D.E., 2001, Building stones of Canada's federal parliament buildings: Geoscience Canada, v. 28, p. 13–30.

Ledoux, R., and Jaco, H.-L., 2003, Geology of the parliament buildings 4. Géologie des édifices du Parlement du Québec: Geoscience Canada, v. 30, p. 145–160.

Myrow, P.M., 1995, *Thalassinoides* and the enigma of early Paleozoic open-framework burrow systems: Palaios, v. 10, p. 58–74, https://doi.org/10.2307/3515007.

Nestor, H., Soesoo, A., Linna, A., Hints, O., and Nõlvak, J., 2007, The Ordovician in Estonia and southern Finland: MTÜ GEOGuide Baltoscandia, Tallinn, 37 p.

Nicolas, M.P.B., Matile, G.L.D., Keller, G.R., and Bamburak, J.D., 2010, Phanerozoic geology of southern Manitoba: Manitoba Innovation, Energy and Mines, Manitoba Geological Survey, Stratigraphic Map SM2010-1, 2 sheets, scale 1:600 000.

Nitecki, M.H., Mutvei, H., and Nitecki, D.V., 1999, Receptaculitids: A Phylogenetic Debate on a Problematic Fossil Taxon: Kluwer/Plenum, New York, 241 p., https://doi.org/10.1007/978-1-4615-4691-7.

Novack-Gottshall, P.M., and Burton, K., 2014, Morphometrics indicates giant Ordovician macluritid gastropods switched life habit during ontogeny: Journal

of Paleontology, v. 88, p. 1050–1055, https://doi.org/10.1666/13-129.
Pak, R., and Pemberton, S.G., 2003, Ichnology of the Yeoman Formation: Saskatchewan Industry Resources, Saskatchewan Geological Survey, Summary of Investigations 2003, Volume 1, Miscellaneous Report 2003-4.1, Paper A-3, 16 p.
Parks, W.A., 1916, Report on the Building and Ornamental Stones of Canada: Volume IV, Provinces of Manitoba, Saskatchewan and Alberta: Canada Department of Mines, Mines Branch, Report 388, 333 p., https://doi.org/10.4095/247657.
Pemberton, S.G., and Frey, R.W., 1982, Trace fossil nomenclature and the *Planolites-Palaeophycus* dilemma: Journal of Paleontology, v. 56, p. 843–881, https://www.jstor.org/stable/1304706.
Pereira, D., and Page, K., 2017, A new IUGS Commission for Geoheritage: The 'ICG': Episodes, v. 40, p. 77–78, https://doi.org/10.18814/epiiugs/2017/v40i1/011.
Pratt, B.R., and Bordonaro, O.L., 2007, Tsunamis in a stormy sea: Middle Cambrian inner-shelf limestones of western Argentina: Journal of Sedimentary Research, v. 77, p. 256–262, https://doi.org/10.2110/jsr.2007.032.
Pratt, B.R., and Haidl, F.M., 2008, Microbial patch reefs in Upper Ordovician Red River strata, Williston Basin, Saskatchewan: signal of heating in a deteriorating epeiric sea, *in* Pratt, B.R., and Holmden, C., *eds.*, The Dynamics of Epeiric Seas: Geological Association of Canada, Special Paper 48, p. 303–340.
Primavori, P., 2015, Carrara Marble: a nomination for 'Global Heritage Stone Resource' from Italy, *in* Pereira, D., Marker, B.R., Kramar, S., Cooper, B.J., and Schouenborg, B.E., *eds.*, Global Heritage Stone: Towards International Recognition of Building and Ornamental Stones: Geological Society, London, Special Publications, v. 407, p. 137–154, https://doi.org/10.1144/SP407.21.
Salad Hersi, O., Lavoie, D., and Nowlan, G.S., 2002, Stratigraphy and sedimentology of the Upper Cambrian Strites Pond Formation, Philipsburg Group, southern Quebec, and implications for the Cambrian platform in eastern Canada: Bulletin of Canadian Petroleum Geology, v. 50, p. 542–565.
Sheehan, P.M., and Schiefelbein, D.R.J., 1984, The trace fossil *Thalassinoides* from the Upper Ordovician of the eastern Great Basin: Deep burrowing in the early Paleozoic: Journal of Paleontology, v. 58, p. 440–447.
Stewart, L.A., Elias, R.J., and Young, G.A., 2010, Stromatoporoids and colonial corals hosting borers and linguloid brachiopods, Ordovician of Manitoba, Canada: Palaeoworld, v. 19, p. 249–255, https://doi.org/10.1016/j.palwor.2010.09.013.
Sweet, W.C., and Bergström, S.M., 1984, Conodont provinces and biofacies of the Late Ordovician, *in* Clark, D.L., *ed.,* Conodont Biofacies and Provincialism: Geological Society of America, Special Papers, v. 196, p. 69–87, https://doi.org/10.1130/SPE196-p69.
Wallace, R.C., 1913, Pseudobrecciation in Ordovician limestones in Manitoba: Journal of Geology, v. 21, p. 402–421, https://doi.org/10.1086/622083.
Westrop, S.R., and Ludvigsen, R., 1983, Systematics and paleoecology of Upper Ordovician trilobites from the Selkirk Member of the Red River Formation, Southern Manitoba: Manitoba Department of Energy and Mines, Mineral Resources Division, Geological Report GR 82-2, 51 p.
Wong, S., 2002, Paleoenvironmental and paleoecological reconstruction of the Tyndall Stone, Selkirk Member, Red River Formation (Late Ordovician), southern Manitoba: Unpublished M.Sc. thesis, University of Manitoba, 343 p.
Young, G.A., Elias, R.J., Wong, S., and Dobrzanski, E.P., 2008, Upper Ordovician rocks and fossils in southern Manitoba: Canadian Paleontology Conference, Field Trip Guidebook No. 13, Geological Association of Canada, St. John's, Newfoundland, 97 p.
Zenger, D.H., 1996a, Dolomitization patterns in widespread "Bighorn Facies" (Upper Ordovician), western craton, USA: Carbonates and Evaporites, v. 11, p. 219–225, https://doi.org/10.1007/BF03175640.
Zenger, D.H., 1996b, Dolomitization of the "C" zone, Red River Formation (Upper Ordovician) in a deep core, Williston basin, Richland County, eastern Montana: Contributions to Geology, University of Wyoming, v. 31, p. 57–75.
Zheng, C.Y.C., Mángano, M.G., and Buatois, L.A., 2018, Ichnology and depositional environments of the Upper Ordovician Stony Mountain Formation in the Williston Basin, Canada: Refining ichnofacies and ichnofabric models for epeiric sea carbonates: Palaeogeography, Palaeoclimatology, Palaeoecology, v. 501, p. 13–29, https://doi.org/10.1016/j.palaeo.2018.04.001.

Received April 2023
Accepted as revised July 2023

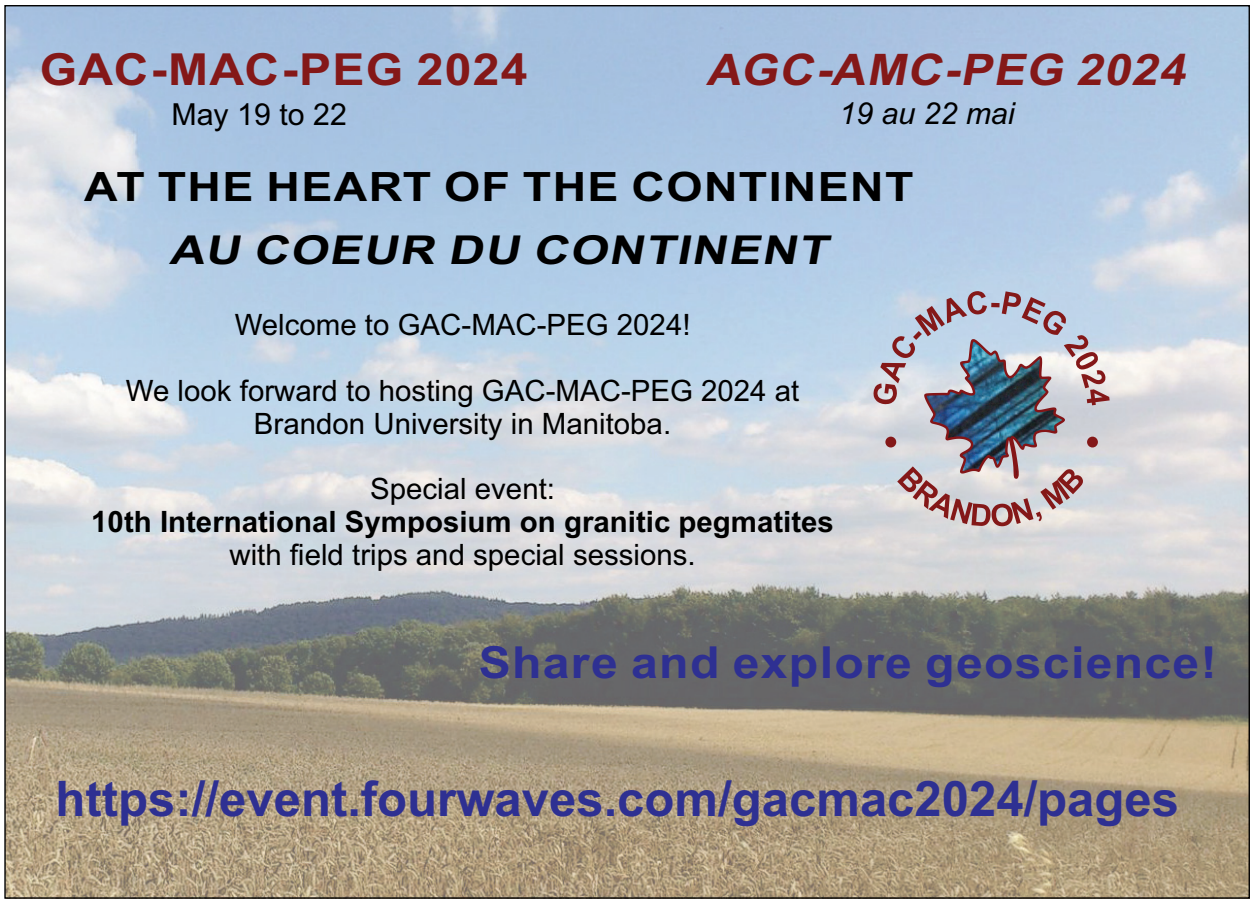

Proposals for symposia, special sessions, field trips, short courses, and workshops are now being accepted at Brandon2024@Brandonu.ca

To submit a proposal email Brandon2024@Brandonu.ca with the name of your session or other event, the contact information for the organizers/convenors, and a short description of the event. This description will be added to the website when it is accepted. Help us build a broad, exciting conference!

The preliminary program will be available in September 2023, and abstract submission will be open from December to March 1, 2024.

Registration will open in February 2024. There will be options to book return or one-way trips with a conference shuttle between the Winnipeg airport and Brandon University.

GEOLOGICAL ASSOCIATION OF CANADA
ASSOCIATION GÉOLOGIQUE DU CANADA

MINERALOGICAL ASSOCIATION OF CANADA
ASSOCIATION MINÉRALOGIQUE DU CANADA

PEG 2024
May 19-22, 2024 Brandon, Manitoba, Canada
10th International Symposium on Granitic Pegmatites

SERIES

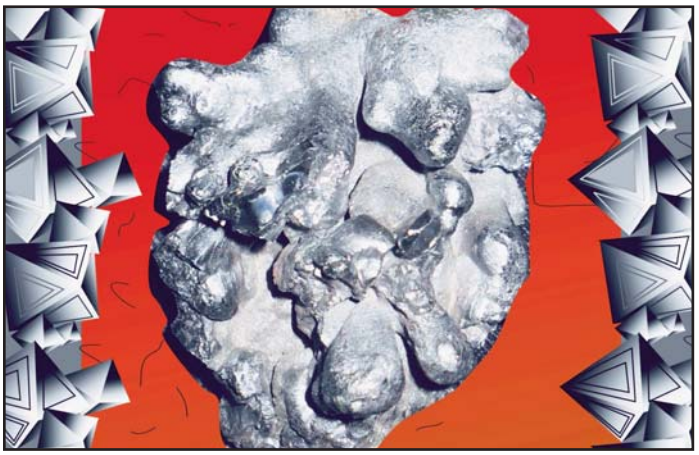

Igneous Rock Associations 29. The Nenana Magnetitite Lava Flow, Alaska Range, Alaska

S.P. Reidel[1], M.E. Ross[2] and J. Kasbohm[3]

[1]Pacific Northwest National Laboratory, Retired,
Present address: 7207 West Old Inland Empire Highway
Benton City, Washington 99320, USA
Email: sreidel105@gmail.com

[2]Professor emeritus, Department of Marine and Environmental Sciences
Northeastern University, Boston, Massachusetts 02115, USA

[3]Department of Earth and Planetary Sciences, Yale University
New Haven, Connecticut 06511, USA

SUMMARY

Magnetitite deposits like El Laco (Chile) are rare and have controversial origins. An unusual magnetitite lava flow overlying a rhyolite unit occurs in the north-central Alaska Range and originally covered ~ 750 km^2 of the Miocene Nenana basin. Dating of the rhyolite and relationships between the magnetitite and sedimentary rocks indicate that both are of Late Miocene age. The magnetitite flow is mainly magnetite with some post-eruptive alteration to hematite. Both the rhyolite flow and the magnetitite flow are vesicular, but the magnetitite flow also has small, millimetre-scale columnar jointing. The vesicular zones in the magnetitite flow grade into massive rock on the scale of a thin section, suggesting a degassing lava origin. Samples of the magnetitite flow contain between 12 and 26 wt.% SiO_2 and between 45 and 75 wt.% FeO. Rare earth elements (REE) and trace elements from the magnetitite and rhyolite have similar patterns but with lesser abundance in the magnetitite. Both the rhyolite and the magnetitite have light-REE-enriched REE profiles with negative Eu anomalies. Electron microscopic analysis shows that most of the silica and trace element content of the magnetitite flow comes from very finely disseminated silicate minerals and glass in the magnetite. This suggests that the magnetitite was derived from a magma that had undergone unmixing into a silica-rich phase and an iron-rich phase prior to its eruption. Fractures and vesicles within the magnetitite flow contain minor rhyolitic glass and minerals suggesting that the rhyolite magma invaded columnar joints in the solidified magnetitite flow, and is a subvolcanic sill-like body at the studied locality. The magnetitite flow erupted prior to the emplacement of the rhyolite, which may be extrusive on a regional scale. The features of the Nenana magnetitite, and its geological relationships, are consistent with genetic models that invoke unmixing of magma into immiscible Fe-rich and Si-rich liquids during ascent.

RÉSUMÉ

Les gisements de magnétitite comme ceux de El Laco (Chili) sont rares et d'origines controversées. Une coulée de lave de magnétitite inhabituelle recouvrant une coulée de rhyolite se trouve dans le centre-nord de la chaîne de l'Alaska et couvrait environ 750 km^2 du bassin miocène de Nénana. La datation de la rhyolite et les relations entre la magnétite et les roches sédimentaires indiquent que les deux sont d'âge Miocène supérieur. La coulée de magnétitite est principalement composée de magnétite avec quelques altérations post-éruptives en hématite. La coulée de rhyolite et la coulée de magnétitite sont toutes les deux vésiculaires, mais la coulée de magnétitite présente également de petits joints colonnaires d'échelle millimétrique. Les zones vésiculaires de la coulée de magnétitite se transforment en roche massive à l'échelle d'une lame mince, suggérant qu'elles proviennent d'une lave en dégazage. Les échantillons de la coulée de magnétitite contiennent entre 12 et 26 % en poids de SiO_2 et entre 45 et 75 % en poids de FeO. Les éléments de terres rares (ETR) et les éléments traces de la magnétitite et de la rhyolite présentent des patrons similaires mais

Geoscience Canada, v. 50, https://doi.org/10.12789/geocanj.2023.50.197 pages 53–71

GC Data Repository: Igneous Rock Associations Series at https://gac.ca/gc-data-repository

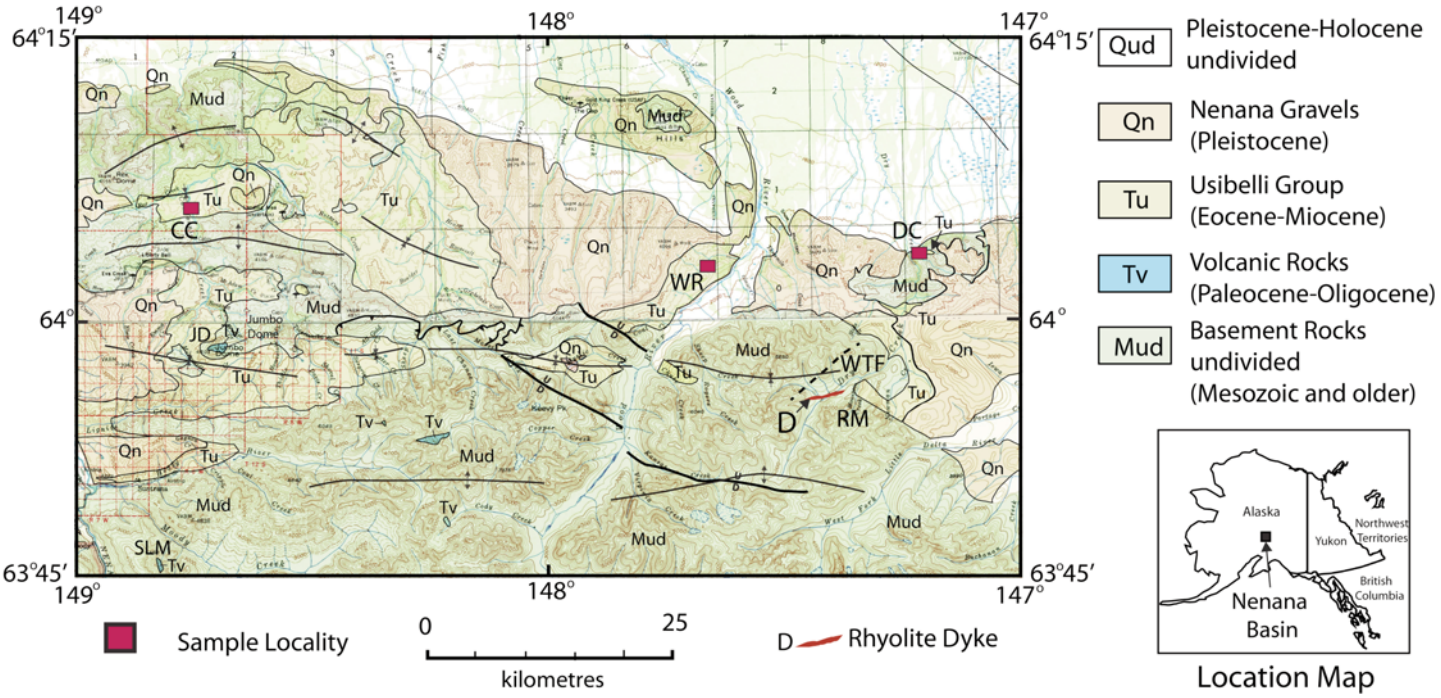

Figure 1. Geologic map of the Nenana Coal Basin, central Alaska Range. Inset map shows the location of the Nenana Coal Basin. Map is based on Wahrhaftig (1970 a,b,c,d,e,f,g,h) and modified from Reidel and Ross (in press). CC, California Creek; DC, Dry Creek; JD, Jumbo Dome; RM, Red Mountain volcanogenic massive sulphide deposit; SLM, Sugar Loaf Mountain; WR, Wood River locality; WTF, volcanogenic massive sulphide prospect. Dyke is that of Freeman et al. 2016.

avec une moindre abondance dans la magnétitite. La rhyolite et de magnétitite présentent toutes deux un patron de terres rares enrichi en éléments de terres rares légers avec une anomalie négative en Eu. L'analyse au microscope électronique montre que la majeure partie de la silice et de la teneur en éléments traces de la coulée de magnétitite provient de minéraux silicatés et de verre finement disséminés dans la magnétite. Ceci suggère que la magnétitite provient d'un magma qui s'était décomposé en une phase riche en silice et une phase riche en fer avant son éruption. Les fractures et les vésicules dans la coulée de magnétitite contiennent du verre et des minéraux rhyolitiques comme constituant mineurs suggérant que le magma de rhyolite a envahi les joints colonnaires dans la coulée de magnétitite solidifiée et est un corps subvolcanique semblable à un filon-couche dans la localité étudiée. La coulée de magnétitite a fait éruption avant la mise en place de la rhyolite, qui peut être extrusive à l'échelle régionale. Les caractéristiques de la magnétitite de Nénana et ses relations géologiques sont cohérentes avec les modèles génétiques qui invoquent la séparation du magma en liquides non miscibles riches en fer et en silicium pendant l'ascension.

Traduit par la Traductrice

INTRODUCTION

Magnetite deposits like El Laco in the Andes Mountains of Chile are rare and have controversial origins. Proposed origins include lava flows (Park 1961; Naslund et al. 2002; Henriquez et al. 2003; Keller et al. 2022; Pietruszka et al. 2023), magmatic assimilation (Bain et al. 2021), replacement (Sillitoe and Burrows 2002, 2003), and as hydrothermal deposits (Dare et al. 2015). Igneous rocks composed of mainly magnetite are called *magnetitite* (Holmes 1928; Johannsen 1938) and can contain apatite as well as a variety of silicate minerals. Similar iron-ore deposits of the Kiruna type occur mainly in Precambrian rocks but also have controversial origins (Frietsch 1978; Parak 1985).

Magnetite deposits are found with a variety of rocks. For example, El Laco typically occurs with andesite; Cerro de Mercado, Mexico, is found with rhyolite (Lyons 1988) and Lakeh Siah in Iran is found in a succession of tuff, rhyolite, limestone and evaporite deposits (Gholipoor et al. 2023).

An unusual magnetitite unit, similar to El Laco, occurs in the glaciated north-central Alaska Range between Healy and Delta Junction and was interpreted as a lava flow (Reidel 1984). The flow occurs in Miocene sedimentary rocks in the Nenana basin. In this paper we describe the occurrence of the lava, here named the Nenana magnetitite flow, present new mineralogical and compositional data, and discuss its possible origin. Numerical geochemical and mineralogical data are not included within this paper but are provided (with other relevant information) as supplementary files in the Geoscience Canada data repository.

Geological Background

The Nenana magnetitite lava flow and an associated rhyolite unit occur within a series of faulted synclines forming the extensional Nenana basin in the north-central Alaska Range (Fig. 1) (e.g. Wahrhaftig 1970a, b, c, d, e, f, g, h). The basin lies north of the Farewell-Denali Fault and within the Tintina Gold Province (not shown in Fig. 1). The north-central Alaska Range consists of an east-west trending eroded complex of Precambrian to Cretaceous greenschist-grade metavolcanic

and metasedimentary rocks that are overlain by Eocene to Holocene sedimentary and volcanic rocks (Wahrhaftig et al. 1969; Kirschner 1994; Dusel-Bacon et al. 2007; Wartes et al. 2013). Associated with the older metavolcanic and metasedimentary rocks are many volcano-plutonic complexes that contain volcanogenic massive sulphide deposits. Two of these deposits occur within the Bonnifield mining district of the Nenana basin (Fig. 1, labels RM and WTF).

Cenozoic sedimentary rocks of the Usibelli Group (Fig. 2) overlie the metavolcanic and metasedimentary rocks and, in turn, are overlain by the Pleistocene Nenana Gravel (Sortor et al. 2021) and glacial deposits. The Usibelli Group ranges in age from Eocene to Miocene and is composed of five formations: Healy Creek, Sanctuary, Suntrana, Lignite Creek and Grubstake (Wahrhaftig 1951, 1987; Wolfe and Tanai 1987; Leopold and Lui 1994; Wilson et al. 1998). Prior to uplift of the Alaska Range in the Miocene, the Usibelli Group was deposited by a southward-flowing drainage that alternated between a coal-forming basin and braided river system. The Usibelli Group sedimentary rocks consist of interbedded poorly consolidated sandstone, conglomerate, claystone and coal.

Two thick ash beds occur in the Grubstake Formation, near the top of the Usibelli Group (Fig. 2). Wahrhaftig et al. (1969) obtained an 8.1 Ma K/Ar radiometric age date on glass in ash from the lower bed. Triplehorn et al. (2000) recalculated the age to be 8.3 Ma using $^{40}Ar/^{39}Ar$ dating of the same glass but considered it to be in error due to excess Ar in the glass. Minerals from the glass were also dated by Triplehorn et al. (2000), who reported a preferred age of 6.7 Ma.

Two volcanic centres are present in the area (Fig. 1): the Jumbo Dome and the Sugar Loaf Mountain rhyolite and andesite. A third, the Buzzard Creek basalt, lies north of the area. Jumbo Dome volcanism is dated at approximately 2.7 ± 0.25 Ma (Wahrhaftig 1970b) but more recently updated to 1.03 ± 0.06 Ma (Athey et al. 2006). Sugar Loaf Mountain is the remnant of a rhyolite flow from which Albanese (1980) obtained a K/Ar age date of 34–32 Ma. The Buzzard Creek basalt is Pleistocene based on it overlying glacial deposits (Péwé et al. 1966). A rhyolite dyke (Fig. 1) of undetermined age lies north of Red Mountain and along Dry Creek (Freeman et al. 2016).

GEOLOGY

The magnetitite flow is exposed as erosional remnants that suggest an original extent estimated at approximately 750 km^2 in the Nenana basin (Fig. 1). The easternmost exposure occurs along a prominent ridge above Dry Creek, and the westernmost locality lies along California Creek in a silty claystone of the Suntrana Formation, as mapped by Wahrhaftig (1970g) but reinterpreted as upper Healy Creek Formation by Wartes et al. (2013). Localities like El Laco and Cerro de Mercado have many separate deposits with associated feeder dykes. In contrast, the Nenana magnetitite flow has no known feeder dyke at any exposure suggesting that the exposures are remnants of a much larger flow.

The magnetitite flow is remarkable in that at every site, the flow has developed small, mm-size columns (Fig. 3) that are typically 4- to 6-sided. The columns can be in contact with other columns or nearly free-standing. Columns are typical in Columbia River Basalt Group (CRBG) basalt flows but not at this small scale. Columns form from slow cooling of the lava (Ross 1989; Reidel et al. 2013) and develop perpendicular and inward from the cooling surfaces. The columns in the Nenana magnetitite flow appear to form inward from its edges.

The Nenana magnetitite lava flow was sampled at three localities (Fig. 1): Dry Creek, California Creek and along the west side of the Wood River opposite Glacier Creek. The Dry Creek locality consists of a 3 m-thick flow along an approximate 100 m east–west exposure. There, the magnetitite overlies a 3 m-thick rhyolite layer that lies upon Mississippian rocks (Beikman 1974) with no exposures of the Usibelli Group nearby. The Dry Creek exposure was mapped as "Pliocene continental deposits" by Beikman (1974) in a compilation map and "Nenana gravels" by Péwé et al. (1966). Due to the remote nature of the outcrops, it is probable that Péwé et al. (1966) never encountered these exposures during their mapping. Any evidence of the Usibelli Group coal-bearing rocks has been removed by erosion, but this exposure has a significant aeromagnetic anomaly (Fig. 4).

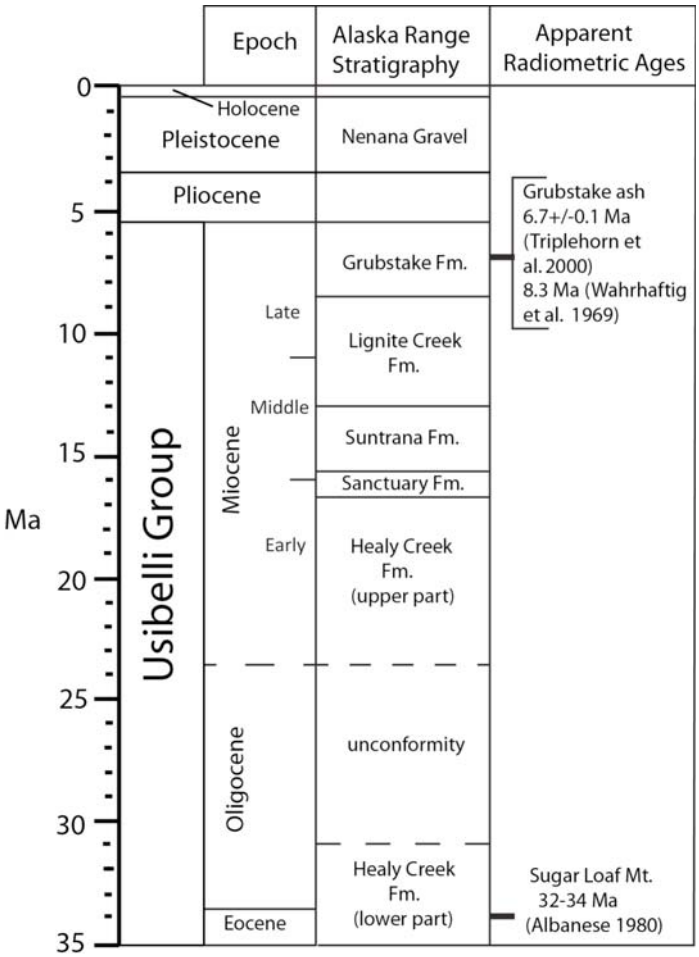

Figure 2. Stratigraphy of the Nenana basin, central Alaska Range. Modified from figure 3 of Triplehorn et al. (2000).

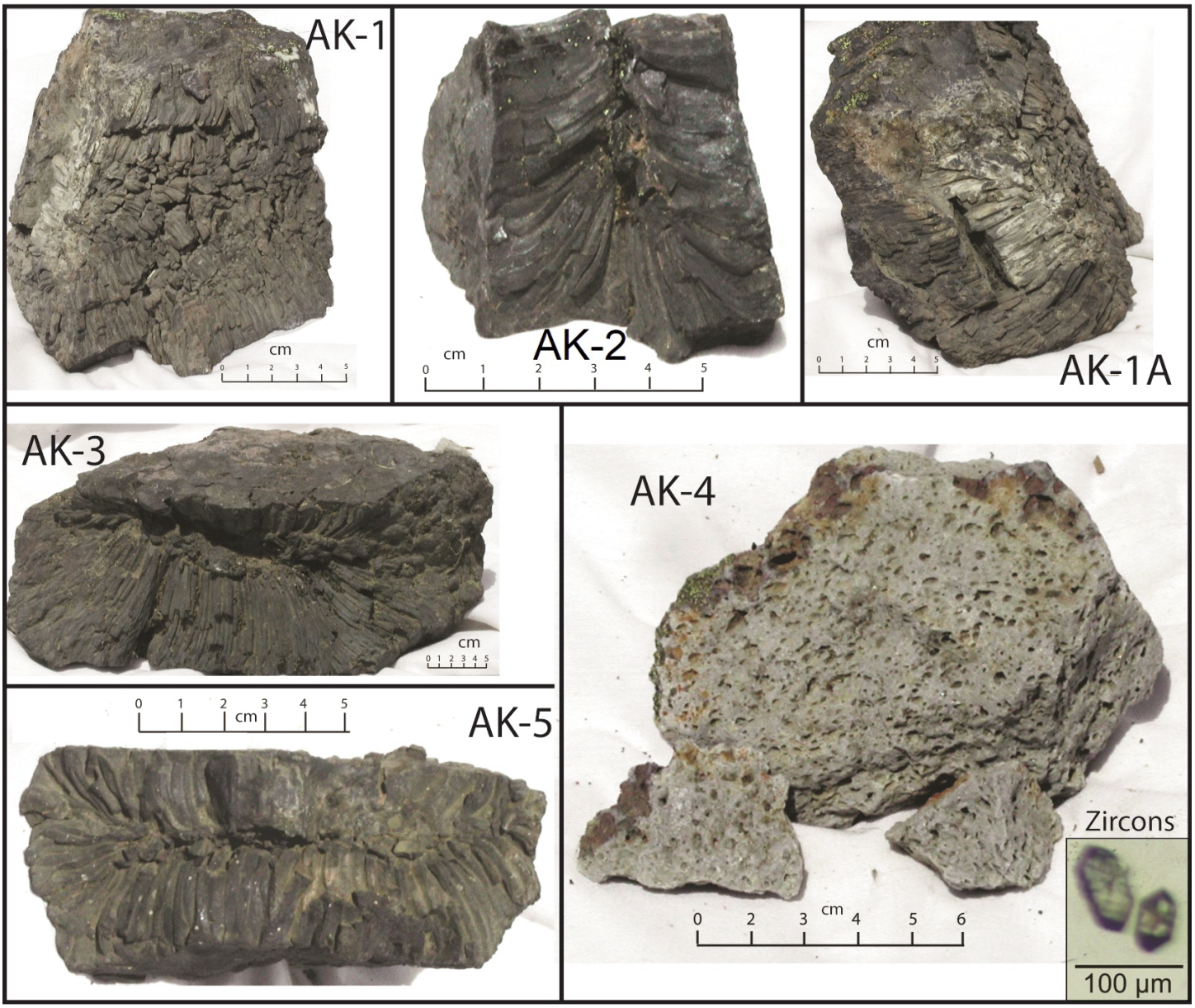

Figure 3. Samples of the magnetitite flow and rhyolite from the Nenana basin, north central Alaska Range. Sample numbers designate analyses and descriptions throughout the paper. Samples AK-3, AK-4, and AK-5 are from the Dry Creek locality (DC, Fig. 1) and samples AK-1 and AK-2 are from the California Creek locality (CC, Fig. 1). Dated zircon grains from the rhyolite are shown in lower right corner of sample AK-4.

The other two magnetitite localities are within the Usibelli Group; however, neither is associated with an underlying rhyolite unit like that seen at the Dry Creek site. At the westernmost locality in California Creek the magnetitite flow appears to have invaded the Miocene sediments, displacing and incorporating them while forming a sill-like layer several centimetres thick. This exposure is like localities in the CRBG where lava flows burrowed into wet sediment producing an 'invasive basalt flow' like that described by Ross (1989) and Reidel et al. (2013). Invasive CRBG flows are common where the basalt erupted onto thick, unconsolidated sediment and are interpreted to represent an extrusive setting. The lava flows burrowed into the sediment and baked the sediment at their mutual contacts. The California Creek site reveals closely similar relationships to these invasive basalt flows, and has a significant aeromagnetic anomaly (Fig. 4) implying that magnetitite is locally extensive.

The third locality is on the west side of Wood River opposite Glacier Creek in either the Suntrana or Lignite Creek Formation as mapped by Wahrhaftig (1970e). This site is poorly exposed and is not marked by an aeromagnetic anomaly.

The rhyolite at the Dry Creek site is primarily a white, massive rock with vesicles throughout (Fig. 3). There are no columnar structures or evidence of obvious flow banding, but it resembles rhyolite flows seen elsewhere in the area. It appears to be an isolated outcrop but mapping by Freeman et al. (2016) identified a rhyolite dyke in Dry Creek about 10 km to the south (Fig. 4). They described the exposure as a "rhyo-

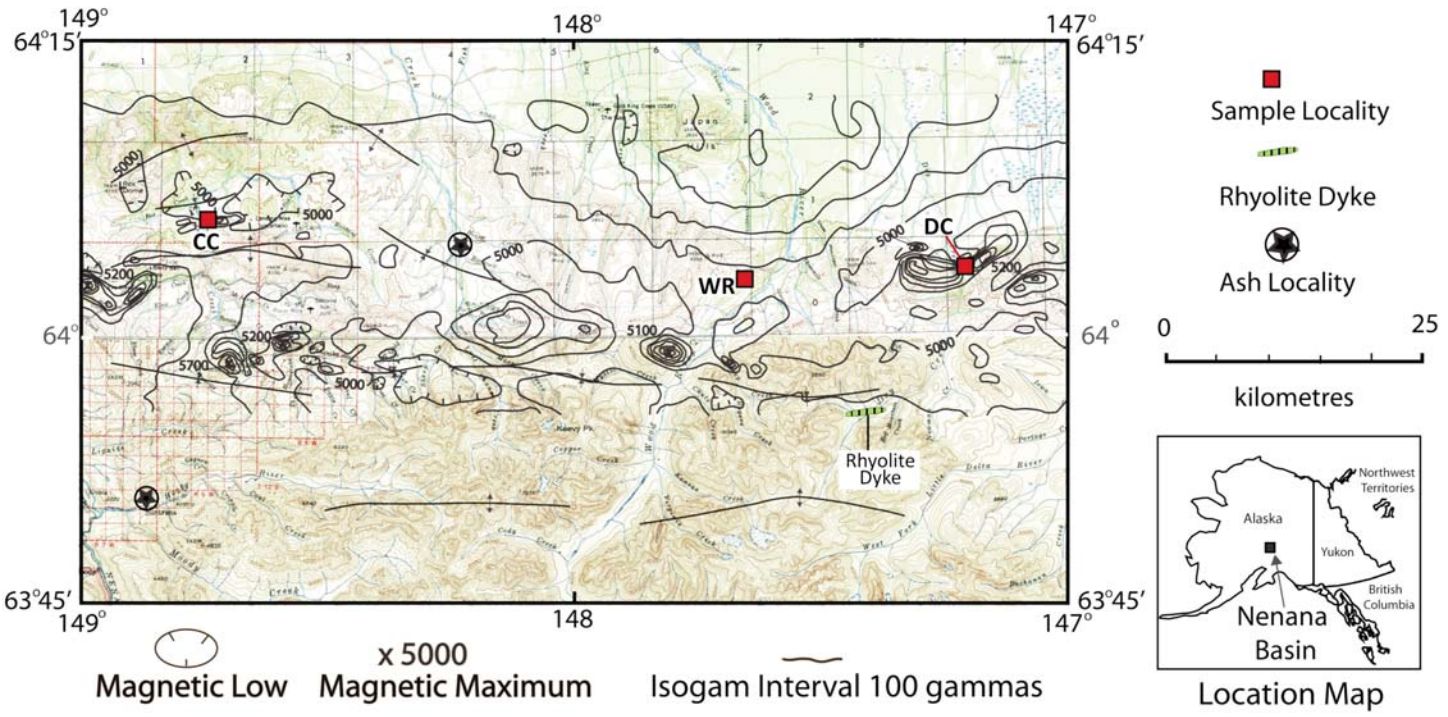

Figure 4. Aeromagnetic map of the Nenana Basin, northern Alaska Range. From Alaska Division of Geology and Geophysical Surveys 1973a, b.

lite breccia dyke". It is white to tan and aphanitic with clasts of schist and pumice; local banding is present along the margins. It forms exposures that cross Dry Creek west of Red Mountain Creek (RM, Fig. 1). No radiometric age was available, but they suggested that it may be equivalent to the Oligocene rhyolite of Sugar Loaf Mountain 48 km to the west (Fig. 1). Its physical similarity and close proximity to the rhyolite underlying the magnetitite flow at Dry Creek indicate that it may be its feeder dyke.

ANALYTICAL METHODS

Mineralogical and Geochemical Analyses

Optical microscopic properties of most minerals identified are listed in the supplementary data for the paper. Percentages of minerals and glass were determined by standard modal analysis. Very few grains were both large enough and oriented correctly for flat-stage measurements.

Microprobe analyses for samples AK-2, AK-3, AK-4, and AK-5 are listed in supplementary data. These were performed by Dr. James Eckart at Earth Materials Characterization Lab, Yale University. Operating conditions: JEOL JXA-8530F; SDD (silicon drift detector) EDS detector: Silicon Drift X-ray detector with 10 mm active area; 133 eV resolution. Analysis beam voltage 15 kV, beam current 10 mA. Microprobe analyses and scanning electron microscopy (SEM) images of sample AK-1 were performed by B. Strope at the Rockwell International Electron Microprobe Laboratory, Richland, Washington on a JEOL electron microprobe. Operating condition: 15 kV. Beam current 10 mA, EDS analysis.

Whole-rock XRF analyses are listed in supplementary data. These were performed by Dr. Rick Conrey at the WSU Peter Hooper GeoAnalytical lab. The methods and procedures are described in Johnson et al. (1999). Inductively coupled plasma–mass spectrometry (ICP–MS) trace-element analyses were performed by Charles Knaack at the WSU Peter Hooper GeoAnalytical lab. Procedures are described on their website.

Geochronology

An attempt was made to determine an age using U–Pb zircon geochronology through chemical abrasion–isotope dilution–thermal ionization mass spectrometry at Princeton University, following methods described in Kasbohm and Schoene (2018).

Zircon grains were separated from their host rock through standard methods of crushing, gravimetric, and magnetic separation techniques using a Bico Braun "Chipmunk" Jawcrusher, disc mill, hand pan, hand magnet, Frantz isodynamic separator, and methylene iodide. Zircon grains from the least magnetic and most dense mineral separate were transferred in bulk to quartz crucibles and annealed in a muffle furnace at 900°C for 48 hours after Mattinson (2005). After annealing, grains were photographed (Fig. 3) and picked in reagent-grade ethanol for analysis. Given the low radiogenic Pb content of the samples, cathodoluminescence images were not obtained. Individual grains were transferred using stainless steel picking tools to separate 3 mL Savillex Hex beakers containing distilled acetone and taken to the clean lab for analysis.

Single zircon grains were loaded into 200 μL Savillex "micro"-capsules with 100 μL 29 M HF + 15 μL 3N HNO_3 for a single leaching step in high-pressure Parr bombs at 185°C for 12 h to remove crystal domains affected by Pb loss (Mattinson 2005). Grains were rinsed post-leaching in 6 N HCl, MQ H_2O, 3N HNO_3, and 29 M HF prior to spiking with EARTHTIME ^{205}Pb–^{233}U–^{235}U tracer and addition of 100 μL

29 M HF + 15 μL 3N HNO_3 (Condon et al. 2015; McLean et al. 2015). Zircon grains were then dissolved to completion in Parr bombs at 210°C for 48 h. Dissolved zircon solutions were subsequently dried down, dissolved in 100 μL 6N HCl, and converted to chlorides in Parr bombs at 185°C for 12 h, after which solutions were dried again and brought up in 50 μL 3N HCl. The U–Pb and trace element aliquots were then separated by anion exchange chromatography using 50 μL columns and AG-1 X8 resin (200–400 mesh, chloride from Eichrom) (Krogh 1973), and dried down with a microdrop of 0.015 M H_3PO_4. The dried U and Pb aliquot was loaded in a silica gel emitter (Gerstenberger and Haase 1997) to an outgassed zone-refined Re filament.

Isotopic determinations were performed using an IsotopX PhoeniX-62 thermal ionization mass spectrometer (TIMS) at Princeton University, with Pb analysis performed in peak-hopping mode on a Daly-photomultiplier ion-counting detector. Analyses are listed in supplementary data. A correction for mass-dependent Pb fractionation was applied using a Pb fractionation of 0.182 ± 0.041%/amu, as determined by repeat measurements of NBS982 at Princeton. A Daly-photomultiplier deadtime of 28.8 ns was used, as determined by repeat measurements of NBS standards. Corrections for interfering isotopes under masses 204 and 205 were made cycle-by-cycle by measuring masses 201 and 203 and assuming they represent $^{201}BaPO_2$ and ^{203}Tl and using natural isotopic abundances to correct for $^{204}BaPO_2$, $^{205}BaPO_2$, and ^{205}Tl.

UO_2 measurements were performed in static mode on Faraday cups with a bulk U fractionation correction calculated from the deviation of measured $^{233}U/^{235}U$ from the known tracer $^{233}U/^{235}U$ (0.995062 ± 0.000054 (1σ)), and an oxide composition of $^{18}O/^{16}O$ of 0.00205 was used (Nier 1950). Data reduction was performed using the programs Tripoli and U–Pb Redux (Bowring et al. 2011; McLean et al. 2011) and the decay constants of Jaffey et al. (1971). All common Pb was attributed to laboratory blank with a mean isotopic composition determined by total procedural blank measurements. Uncertainties in reported U–Pb zircon dates are at the 95% confidence level and exclude tracer calibration and decay constant uncertainties.

RESULTS

Age of Formation

Although we have no means of dating the magnetitite flow, we attempted to obtain a U–Pb zircon age for the associated rhyolite (sample AK-4; Fig. 3). From a small hand sample, six zircon grains smaller than 100 μm were separated through standard methods, and of these, two were dated (the rest were lost at some stage of zircon chemistry prior to dating). Both grains were low in uranium and yielded very imprecise Th-corrected $^{206}Pb/^{238}U$ ages of 15.31 ± 0.52 Ma and 11.12 ± 0.65 Ma, with low ratios of radiogenic to common Pb (0.331 pg Pb*/1.08 pg Pbc = 0.31, and 0.0637 pg Pb* / 0.36 pg Pbc = 0.17, respectively). Because of the imprecision of these dates, their dispersion, and the protracted crystallization of zircon in a magma chamber prior to eruption (Miller et al. 2007; Simon et al. 2008) we do not consider either of these dates to be the actual age of the rhyolite. Nonetheless, the data do suggest a maximum Tortonian (Late Miocene) age for the rhyolite at Dry Creek. It is possible that processing a larger volume of this sample for zircon geochronology would yield a greater number of larger zircon grains from which more precise U–Pb dates could be obtained, which we would suggest for future work.

Empirical field evidence suggests that both the magnetitite flow and associated rhyolite are of Miocene age, consistent with our rhyolite zircon dates. The magnetitite flow is invasive into the Miocene Usibelli Group at California Creek. In addition, we suggest that the rhyolite may also be the source for the two ash beds (Figs. 1, 2) that occur in the Usibelli Group, as indicated in Fig. 4. The age of 6.7 Ma for glass minerals from the lower ash obtained by Triplehorn et al. (2000) may thus be consistent with our imprecise upper age boundary suggested by zircon geochronology. Thus, we conclude that the rhyolite and the closely associated magnetitite flows are of Late Miocene age.

Mineralogy and Petrology

Selected minerals and/or glasses were identified optically in the magnetitite samples (AK-1, AK-2, AK-3 and AK-5) and the rhyolite sample (AK-4) and were analyzed by electron microprobe to determine their compositions. Minerals identified in the magnetitite and rhyolite samples are shown in figures 5 through 13.

Magnetitite Petrography

The minerals identified in the magnetitite flow include magnetite, augite, chlorite, olivine, biotite, quartz, apatite, rutile, sanidine, and muscovite. The magnetitite consists predominately of magnetite (Figs. 5a, 6b, 7, and 8a) with minor silicate minerals occurring as tiny (< 0.1 mm) anhedral to subhedral grains confined to vein-like ragged vesicles, cooling joints (Figs. 5b and 6b), and a few, irregular, partly rounded, more open vesicles (Figs. 5c and 7b). Most of the vesicles and joints are barren, containing small amounts of silicate minerals and magnetite (Fig. 6b) in clusters or as discrete grains scattered along their lengths. These minerals most often line the walls of the vesicles and joints. Highly vesicular zones (Fig. 5d) in the magnetitite consist of small, equant to irregular, barren vesicles locally, suggesting vesiculation in an extrusive environment.

Estimating the 2V or sign of a mineral was only possible on a few small grains of quartz, plagioclase, hornblende, and sanidine. Sanidine grains were verified in magnetitite samples AK-2 and AK-5 by microprobe analyses (Figs. 8c and 9a). A few tiny, moderately birefringent grains are probably augite with one grain in sample AK-1 (Fig. 9c) providing a biaxial, optically positive interference figure. Brown, weakly pleochroic anhedral grains were identified as chlorite by microprobe analyses. Colourless rhyolite glass was observed only in a small lens-shaped vesicle and along cleavage partings in a sanidine grain in sample AK-5 (Figs. 8a, 8c and 9a). Microprobe analysis identified olivine and augite in sample AK-1. Acicular, dark red needles of rutile occur in a tiny, lens-shaped vesicle in sample

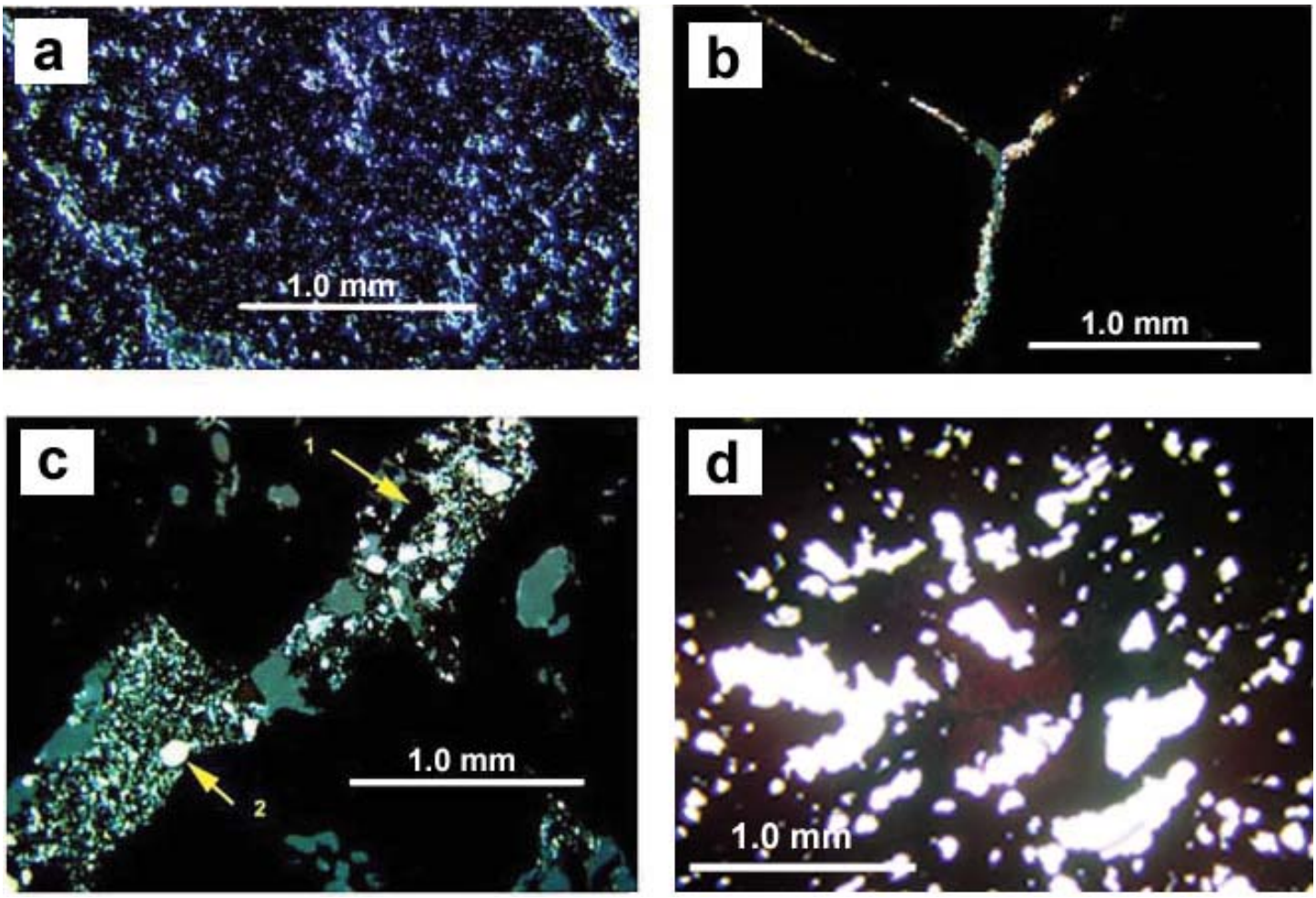

Figure 5. Photomicrographs of the magnetitite flow. (a) Magnetite in sample AK-1 in reflected light. Non-reflective areas are hematite alteration. (b) Cooling joints in AK-2 are partially filled with silicate phases. The brownish grains are chlorite. The angles of intersection of the joints are produced by small-scale columnar jointing (see Figure 3). (c) An elongate, partially rounded vesicle in AK-3 filled with quartz, magnetite (1), and alkali feldspar (2) viewed under crossed polars. (d) A highly vesicular zone in AK-2 resulting from degassing of the magnetitite flow.

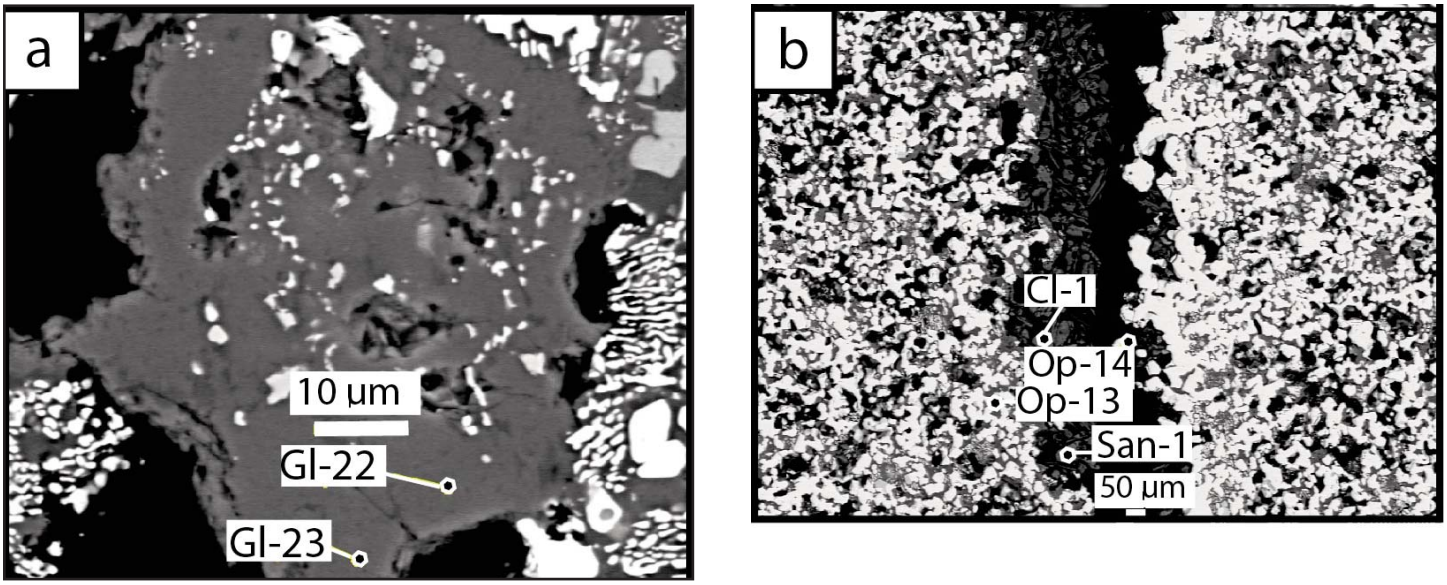

Figure 6. Scanning electron microscope photomicrographs showing sites analyzed in AK-2. (a) Gl-22 and Gl-23 are rhyolite glass adjacent to a sanidine grain. Myrmekite is visible along the right and left margins of the image. (b) Cl-1 is chlorite, Op-13 and Op-14 are magnetite, and San-1 is sanidine.

https://doi.org/10.12789/geocanj.2023.50.197

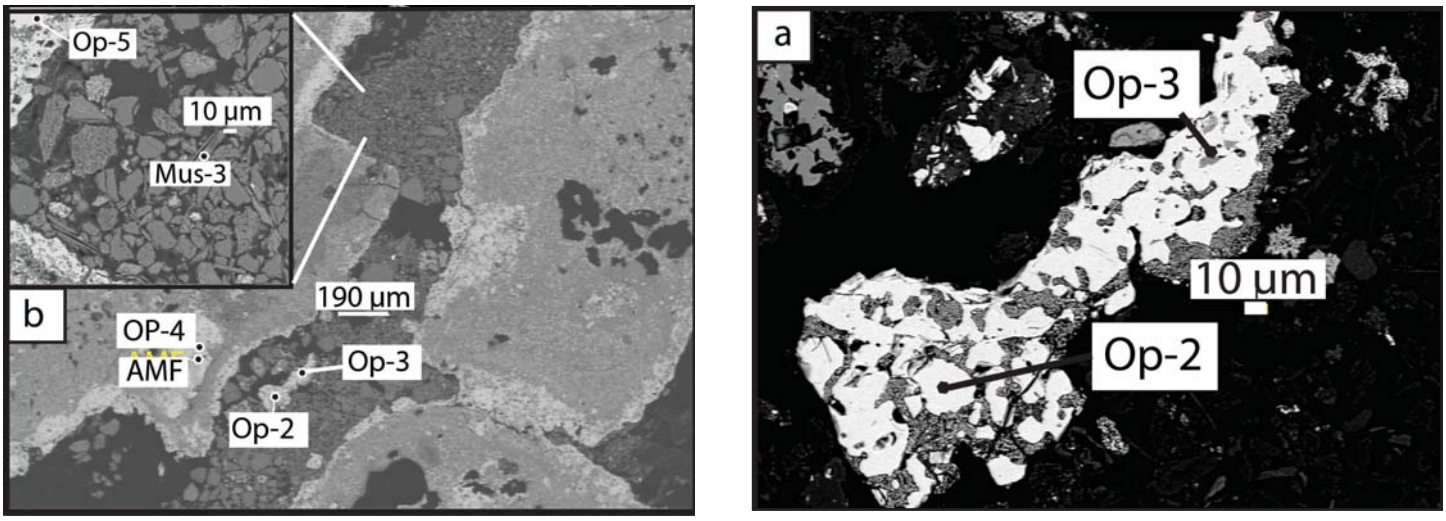

Figure 7. Scanning electron microscope photomicrograph showing sites analyzed in AK-3. (a) Op-2 and Op-3 are magnetite grains within glass with tiny inclusions. (b) Analyzed site in AK-3 in same vesicle shown in Figure 5c. Op-4 and Op-5 are magnetite, Mus-3 is muscovite, and AMF is unknown opaque mineral.

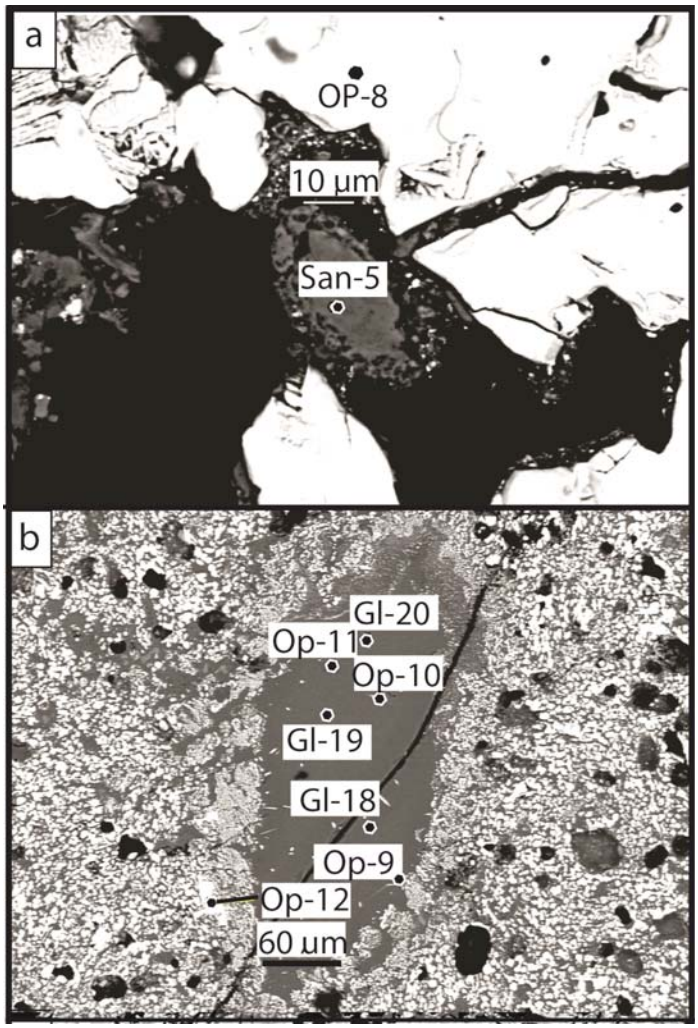

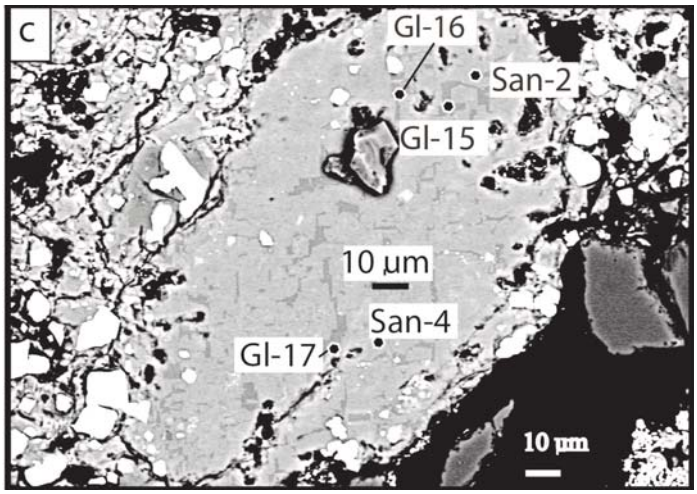

Figure 8. Scanning electron microscope photomicrograph showing sites microprobed in the magnetitite flow (AK-5). San = sanidine; other symbols as in Figure 7. Darker, thin, linear areas in the sanidine in 8c are glass-filled cleavage fractures.

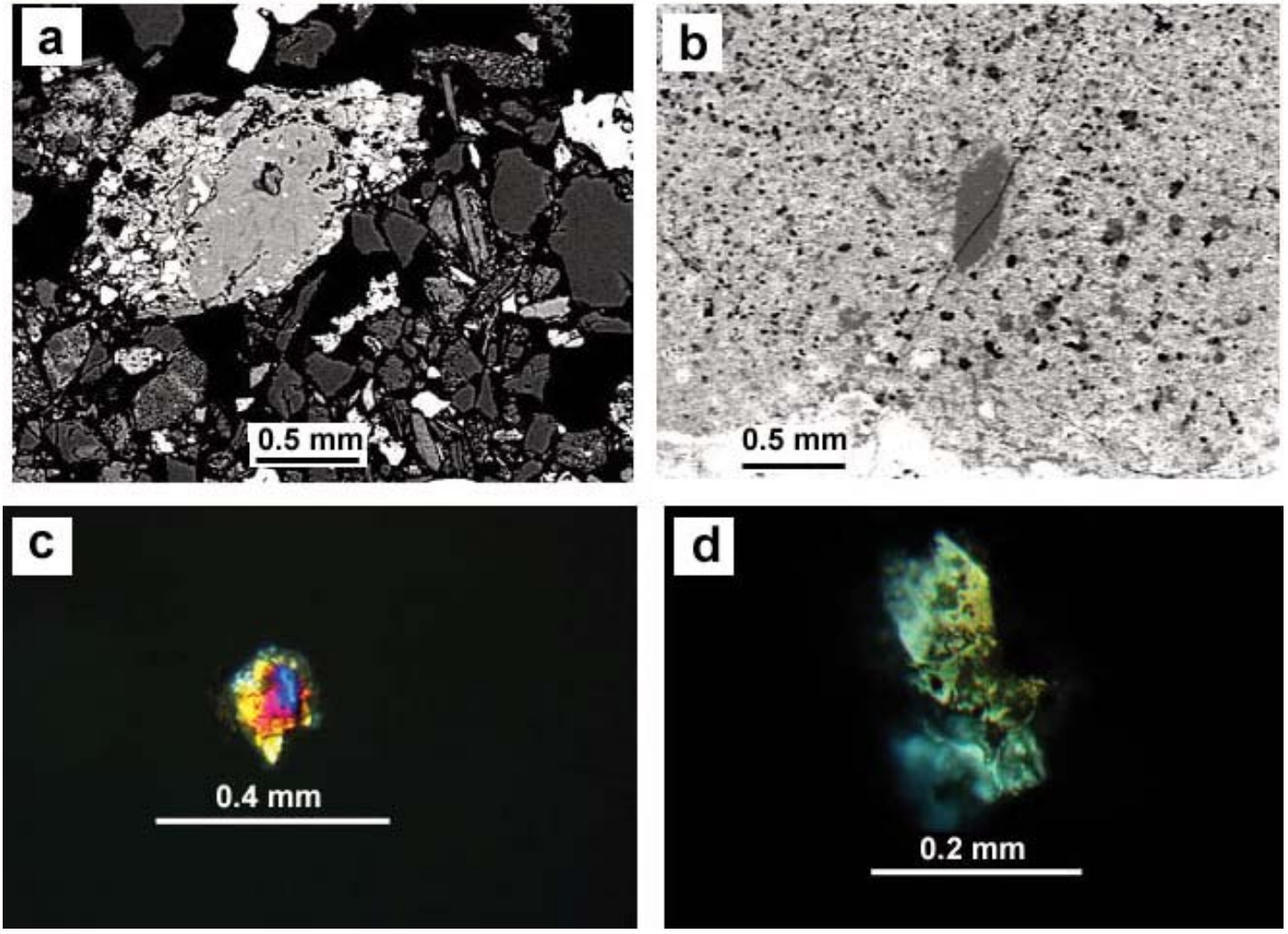

Figure 9. Photomicrographs. (a). Sanidine shown in Figure 8c in reflected light. (b). Rhyolite glass in lens-shaped vesicle in AK-5 (plane-polarized light). See Figure 8c for sites analyzed. An augite grain (c) and quartz grain (d) sampled by scraping from a joint surface in hand specimen AK-1 (Figure 3). Crossed polars.

AK-5 (Fig. 10a). A uniaxial negative, low birefringent, anhedral grain in a vesicle in AK-5 may be apatite (Fig. 10b).

Rhyolite Petrography

The minerals identified in the rhyolite include magnetite, ilmenite, augite, chlorite, hornblende, plagioclase, alkali feldspar/sanidine, muscovite, quartz, and apatite (Fig. 11). Overall, the silicate minerals in the rhyolite resemble those observed in the magnetitite flow.

The rhyolite is vesicular, but vesicles are rounded and smooth-walled in contrast to those in the magnetitite flow (Fig. 12). Colourless rhyolite glass makes up over 92 vol.% of the rock (Fig. 12). Silicate phases identified in the rhyolite glass itself are plagioclase, augite, alkali feldspar/sanidine, and quartz (Fig. 13). Only a trace of augite and 1.6 vol.% feldspar were recognized in the rhyolite whereas magnetite and ilmenite make up a combined 2.5 vol.%. Magnetite in the rhyolite is generally equant but locally is dendritic adjacent to vesicles (Fig. 12c). Ilmenite forms as more elongate grains in the glass (Fig. 12d). Only one tiny plagioclase grain was identifiable in the glass itself and exhibited albite twinning providing an estimated (Michel-Levy method) anorthite content of 36% (andesine). Microprobe data indicate that the plagioclase ranges from andesine to labradorite. Abundant, small, irregular fragments of pumice are present in the rhyolite glass. Small, dark, irregular to tabular bodies are also present in the glass and are interpreted to be metasedimentary and/or sedimentary fragments that were derived from the basement rock. Minerals are present within a few vesicles as scattered clusters or discrete grains of sufficient size for tentative identification optically. They include quartz, feldspar, magnetite, ilmenite, biotite, muscovite, augite, chlorite, and hornblende (Figs. 12 and 13). The presence of muscovite, augite, hornblende, and chlorite was also verified by microprobe analyses. A single, uniaxial (sign indeterminate), anhedral, tiny grain with extreme birefringence is present in a vesicle and may be calcite or zircon. Trace amounts of an unidentified, deep blue mineral of unknown composition occurs in vesicles in AK-4 (Fig. 10 c and d). It is tabular, nonpleochroic, and has parallel extinction.

https://doi.org/10.12789/geocanj.2023.50.197

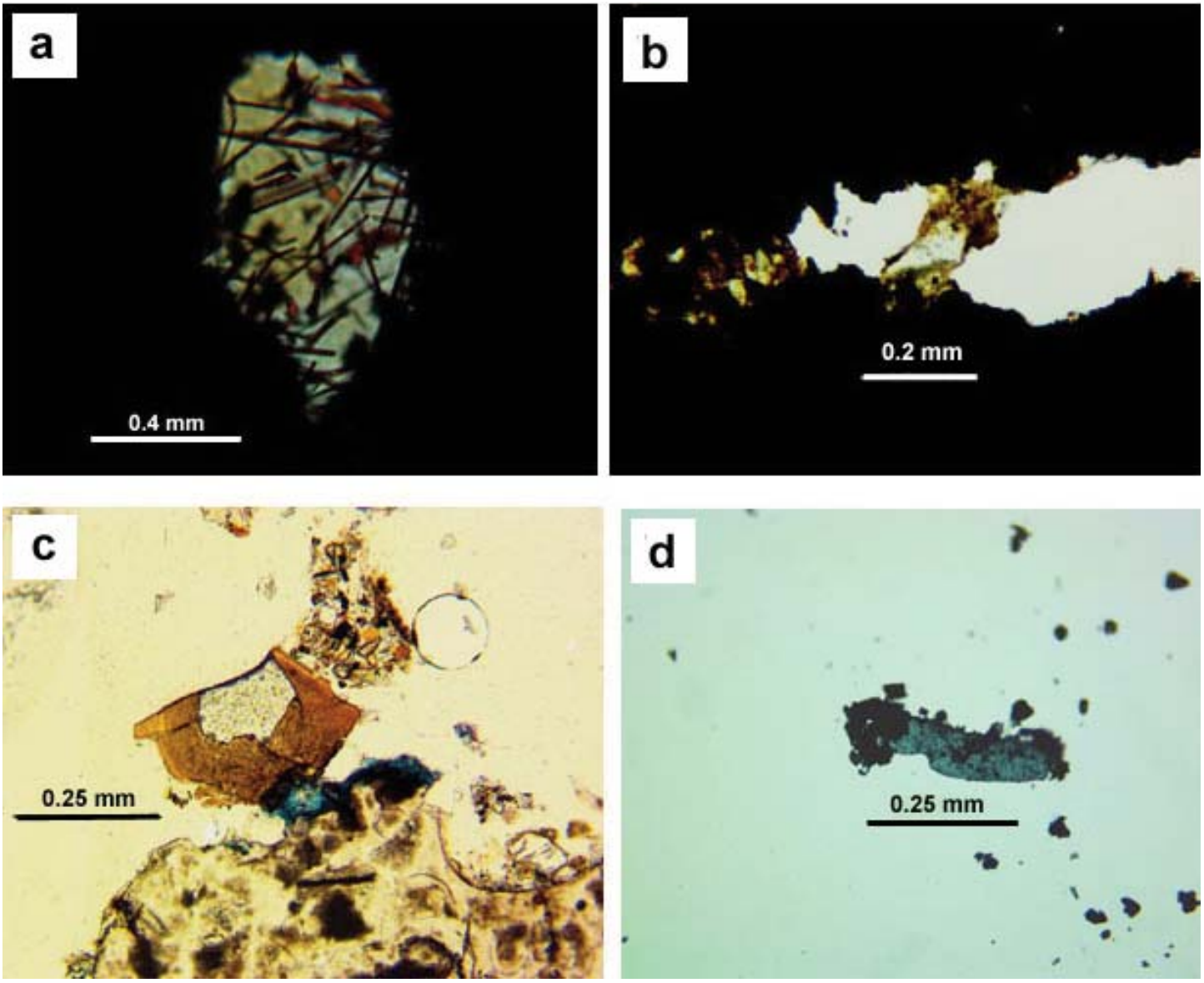

Figure 10. Photomicrographs of unusual grains in AK-5 and AK-4 (all in plane-polarized light). (a) Needles of rutile in a vesicle in AK-5. (b) Probable apatite (uniaxial negative, low birefringence) grain in fracture in AK-5. (c) Unidentified blue mineral in a vesicle with a brown glass fragment in the rhyolite (AK-4). (d) Unidentified blue mineral sampled by scraping from a vesicle in hand specimen AK-4 (Figure 3).

Opaque Mineral Compositions

Three opaque minerals were identified in magnetitite and rhyolite: magnetite, ilmenite and an unknown iron–magnesium–aluminum opaque mineral. The latter was found only in the magnetitite flow. The magnetite compositions in magnetitite and rhyolite are similar. They have 95–99 wt.% FeO with typically < 1 wt.% SiO_2, MnO, MgO and V_2O_5. Al_2O_3 ranges from detection limits to 3.2 wt.%. Ilmenite was identified only in the rhyolite (Figs. 11c, 12d); it has ~ 50 wt.% FeO and TiO_2 and detectable CaO, MgO and SiO_2. The third opaque mineral, termed AMF, occurs in magnetitite flow samples AK-1 and AK-3 (AMF, Fig. 7b). It has 50–70 wt.% FeO, 20 wt.% MgO and ~17 wt.% Al_2O_3. SiO_2 is typically < 1 wt.%. We have been unable to make a positive identification of this mineral, although it may be some type of spinel.

Glass Compositions

Glass occurs in all samples of the magnetitite flow (AK-1, AK-2, AK-3 and AK-5) and in the rhyolite (AK-4). Five glass analyses were obtained from magnetitite sample AK-1; three lie within the dacite field and have high iron contents (~ 9–9.7 wt.%), whereas two lie within the rhyolite field (Fig. 14). One of these latter analyses was obtained from a glass inclusion in a plagioclase grain, and one is groundmass material. The three analyses that plot in the dacite field have lower Na_2O, and K_2O but higher FeO contents (9.0–9.7 wt.%) compared to those plotting in the rhyolite field. Three andesite analyses from AK-4 are from a single glass clast in a vesicle (Fig. 12b, grain 1) that was distinguished optically from other glass analyzed by its occurrence and brown colour. Two other analyses from AK-4 lie in the rhyolite field.

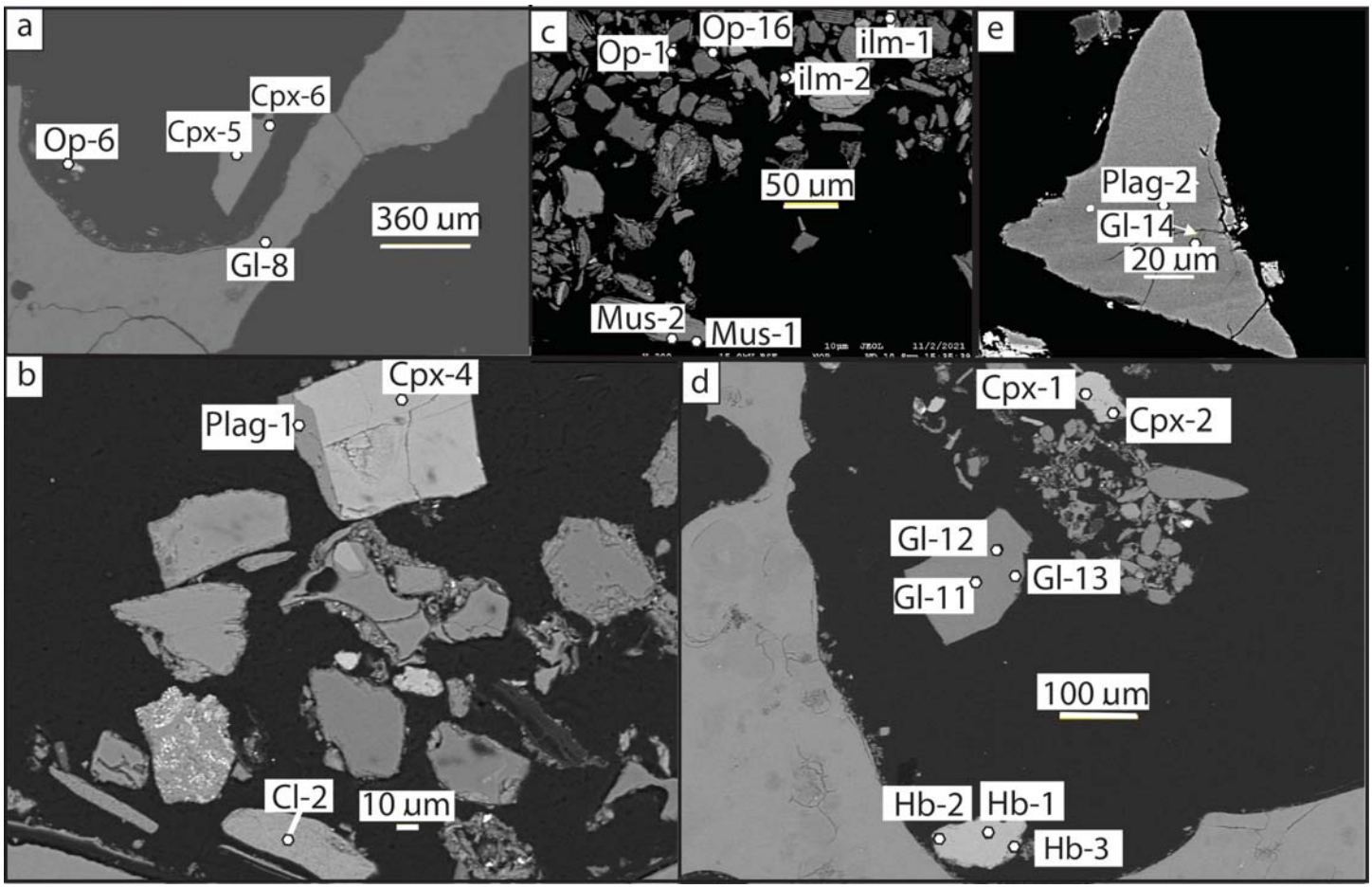

Figure 11. Scanning electron microscope photomicrographs of grains in vesicles microprobed in the rhyolite (AK-4). Symbols as follows: Cl = chlorite, Cpx = clinopyroxene, Gl = glass, Hb = hornblende, ilm = ilmenite, Mus = muscovite, Op = magnetite, Plag = plagioclase.

Four glass occurrences were analyzed by electron microprobe in magnetitite sample AK-2. Two lie within the rhyolite field and two lie within the trachyte–andesite field (Fig. 14). However, the latter two analyses were at the edge of a feldspar grain and may not be pure glass as they have higher Al_2O_3 and K_2O suggesting the analysis may have included feldspar. Six glasses were analyzed in a vesicle in magnetitite sample AK-5 and all lie within the rhyolite field (Fig. 14).

Rock Compositions

The magnetitite and rhyolite compositions are listed in supplementary data and illustrated in Figure 15. The SiO_2 and Al_2O_3 contents of the rhyolite are typical of most such rocks and it contains only minor Na_2O and K_2O. All other oxides are less than 1% by weight.

The four magnetitite samples have varying amounts of FeO (as total Fe) and SiO_2 with FeO ranging between 79.1 and 56.9 wt.% and SiO_2 ranging between 28.1 and 12.3 wt.%. Al_2O_3 is typically between 8.3 and 4.7 wt.% whereas all other oxides are less than 1 wt.% except for MgO which is between 1.5 and 3.5 wt.%. On Figure 15, there is a strong correlation between FeO and SiO_2, Al_2O_3, CaO, Th and Zr in both rhyolite and magnetitite whereas a correlation is present only in magnetitite for MgO, TiO_2 and P_2O_5.

Rare earth elements (REE) are plotted in Figure 16a following Sun and McDonough (1989). The REE patterns for the magnetitite samples and the rhyolite are similar with magnetitite generally showing lower REE contents than rhyolite. All analyses show enrichment in light REE and a depletion of Eu, especially for the rhyolite. The magnetitite and rhyolite samples are also plotted with respect to Bulk Earth abundance (Fig. 16b) following Hickey et al. (1986). Patterns for both are similar with significant depletions in Nb, Sr and TiO_2 suggesting that the magnetitite flow and the rhyolite may come from the same source. However, the relatively high SiO_2 content of the magnetitite flow is problematic as silica and other major, minor and trace elements do not enter magnetite and the Nenana magnetitite flow contains only minor amounts of optically visible silicate minerals. Figure 17 shows a 2000x magnification of a scanning electron microscope image and 'backscatter X-ray' images for a magnetite grain in sample AK-1. These show that silica glass and silicate minerals are finely disseminated throughout the magnetite but would not be visible under an optical microscope even at the highest magnification (400x). Silica and other major and trace elements revealed by the whole rock analyses of the magnetitite appear to have been incorporated into magnetite as it formed from the magma.

https://doi.org/10.12789/geocanj.2023.50.197

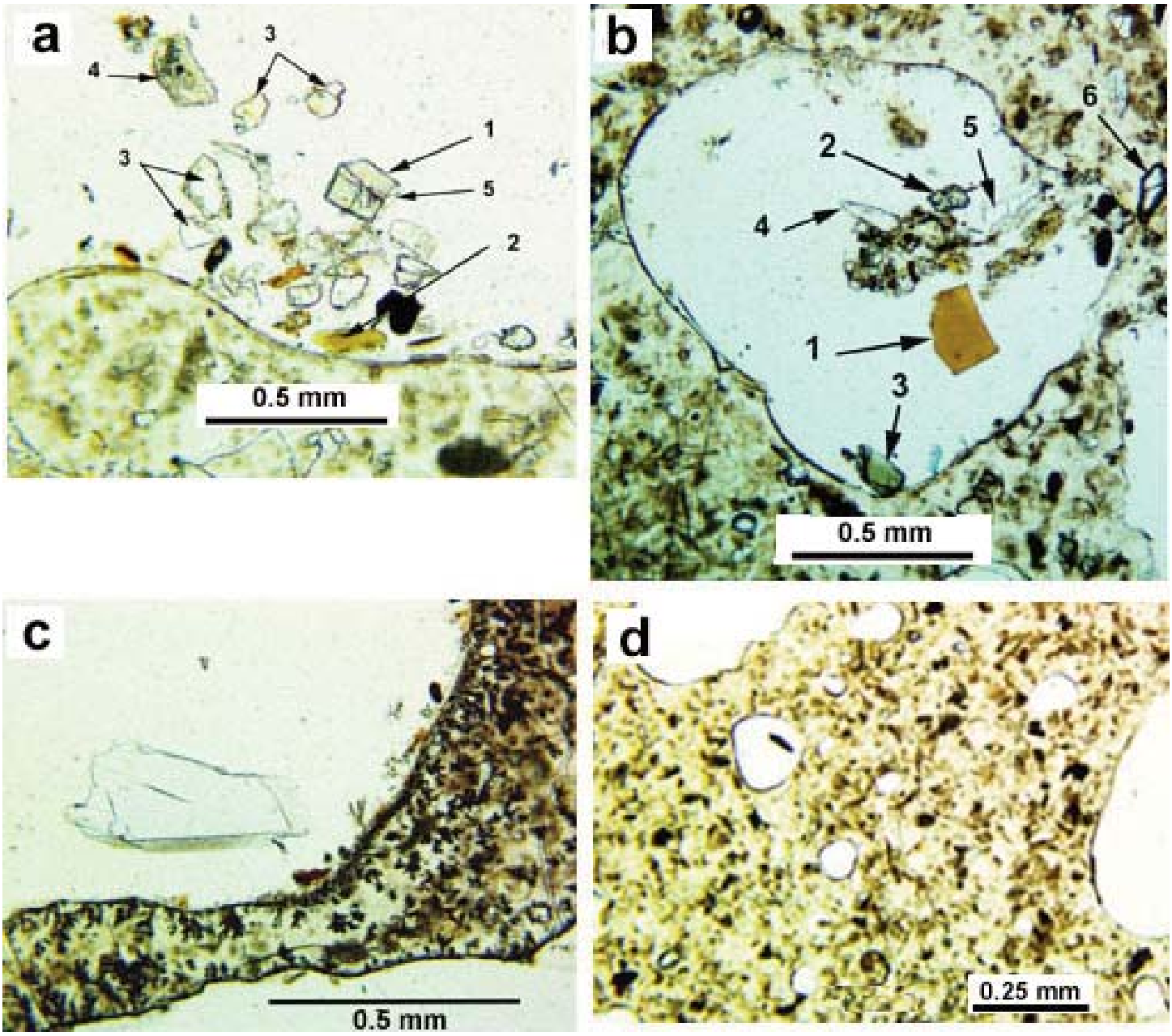

Figure 12. Photomicrographs of the rhyolite (AK-4), all in plane-polarized light. (a) A vesicle containing augite (1), chlorite (2), quartz (3), a fragment of the rhyolite (4), and a remnant of plagioclase attached to the margin of the augite grain (5). Some of the dark, fuzzy bodies in the rhyolite are thought to be sedimentary rock fragments. (b) A vesicle in the rhyolite containing a brown glass fragment (1), augite (2), hornblende (3), quartz (4), and possible plagioclase (biaxial positive, moderate 2V) grain (5). Grain 6 just outside the vesicle is probably an alkali feldspar (biaxial negative with a 2V > 50). (c) Hornblende grain in vesicle in the rhyolite. Dendritic magnetite fringes the vesicle. (d) Typical appearance of the rhyolite glass. The opaque, equant grains are magnetite, and the opaque, elongate grains are ilmenite.

DISCUSSION

Petrogenesis

Two of the most persuasive pieces of evidence for the Nenana magnetitite deposit being a lava flow are the vesicles and small-scale columnar jointing (Figs. 3 and 5). Cooling columns are characteristic of contraction as lava solidifies. They are present in lavas of the Columbia River Basalt Group, Icelandic lavas, the Giant's Causeway, Ireland, and Devil's Post Pile National Monument in California and numerous other localities. The columnar structures in the Nenana magnetitite are unusual because of their small scale. The highly vesicular zones in the magnetitite consist of small, equant to irregular vesicular zones that grade into massive rock on the scale of a thin section, suggesting a degassing lava origin. Another point supporting an extrusive magmatic origin for the magnetitite flow is its extent. Although only isolated outcrops remain (Fig. 1), the magnetitite flow occurs over a wide area, which is inconsistent with an origin from more local replacement processes, magmatic assimilation, or hydrothermal activity.

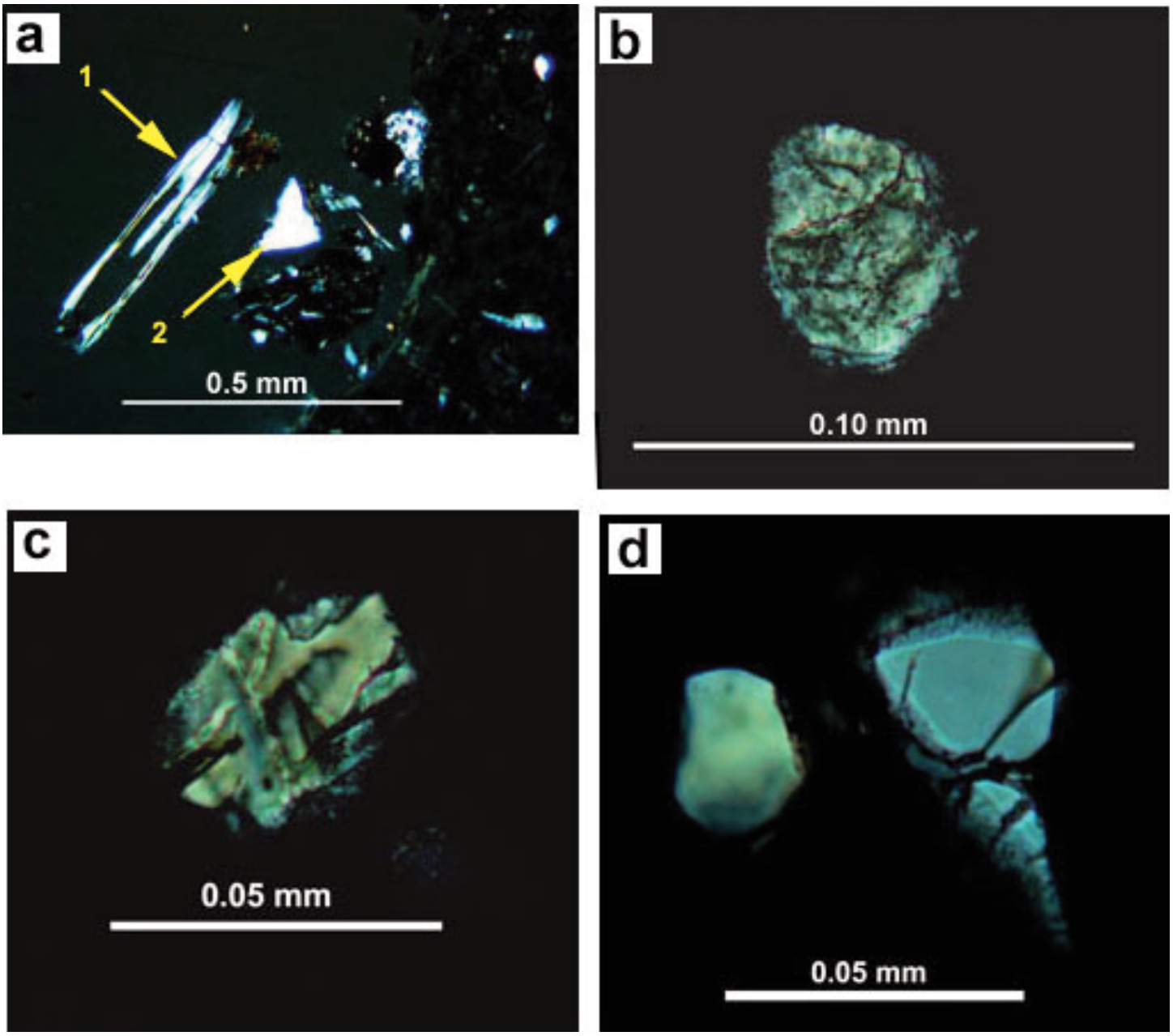

Figure 13. Photomicrographs of minerals in the rhyolite (AK-4) (all under crossed polars). (a) Muscovite (1) and plagioclase (2) in a vesicle. (b) Clinopyroxene in rhyolite glass. (c) Alkali feldspar in rhyolite glass. (d) Quartz in rhyolite glass.

We originally assumed that the magnetitite flow and the associated rhyolite had separate origins, but we now believe that their histories are intertwined. Although the magnetitite flow sits atop the rhyolite, it is clear that the magnetitite flow erupted first, and rhyolite magma was subsequently injected into the magnetitite flow along cooling joints and fractures as they were forming. However, whole rock compositions and detailed backscatter X-ray images (Fig. 17) show that the magnetitite magma also had considerable silica-rich liquid as part of it and that some of that silica-rich liquid was incorporated in magnetite as it crystallized.

We postulate that the rhyolite was injected beneath the solidified magnetitite flow as a sill-like body where it invaded the magnetitite along joints and fractures while moving or rafting all or parts of the flow. The rhyolite magma may have breached the magnetitite to form truly extrusive zones, but these cannot be demonstrated with confidence. The Dry Creek exposure has been extensively eroded by glaciation and all that remains is a remnant. All of the Usibelli Formation has been removed locally but based on the surrounding area and the California Creek exposure, Usibelli Formation sedimentary rocks were once more abundant. The California Creek expo-

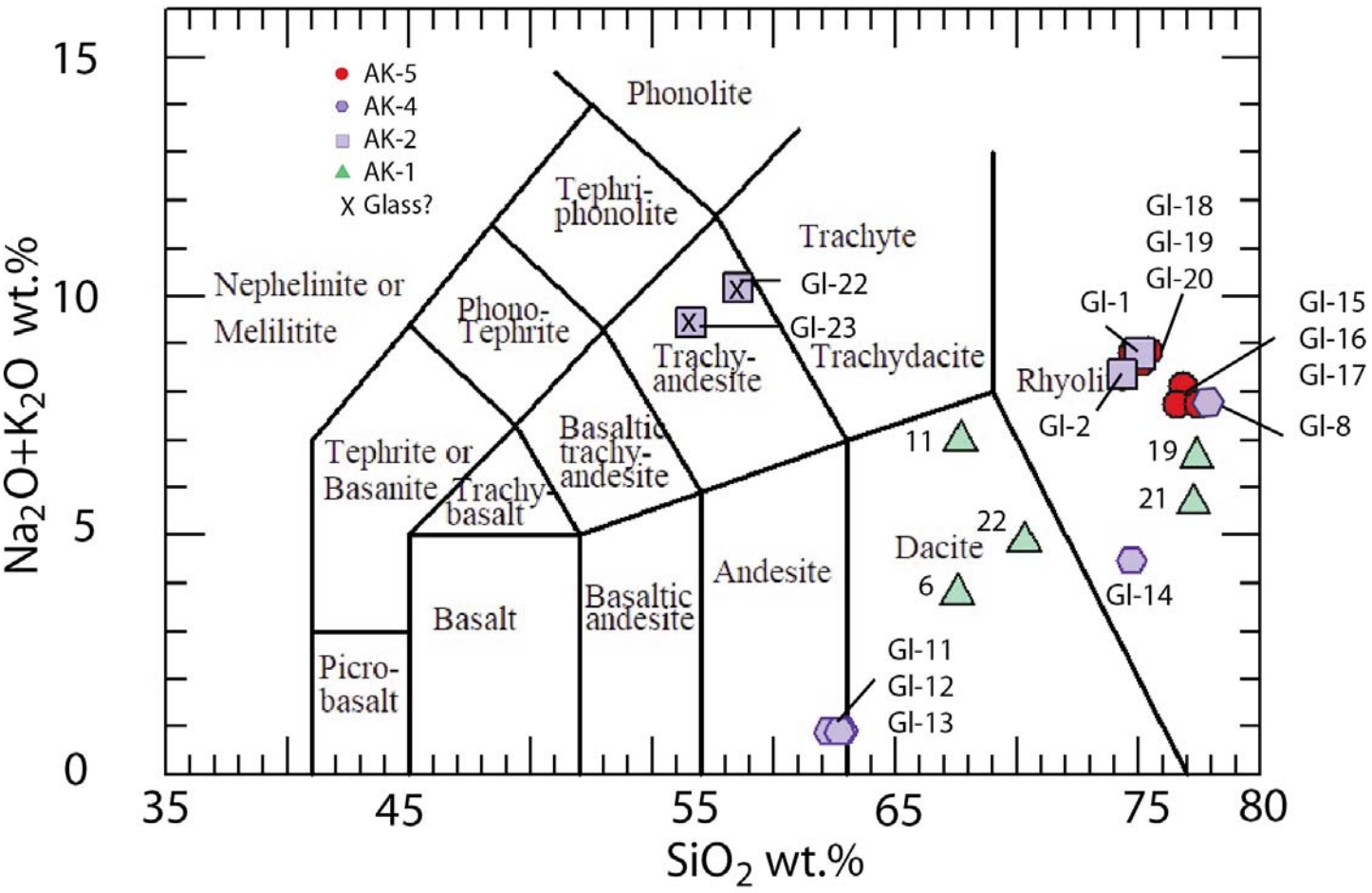

Figure 14. Diagram showing glass analyzed by microprobe for the magnetitite flow and rhyolite (AK-4). Numbers are the microprobe analysis; 'x' is for the glass analyses that might include a mineral (see text).

sure suggests that the magnetitite penetrated into unconsolidated wet sediments, but this behaviour is seen in other extrusive environments such as the Columbia River basalts (e.g. Reidel et al. 2013).

Origin of the Magnetitite Flow

Where the magnetitite flow originated is unclear. Although a possible dyke-like feeder has been identified for the rhyolite, no magnetitite dyke has been recognized and aeromagnetic anomalies provide little help due to extensive erosion.

An alternative hypothesis is that the magnetitite flow is not truly magmatic in origin, but resulted from an ancient coal-seam fire. The Nenana basin is a coal basin and coal-seam fires are known to have occurred (Wahrhaftig 1951). We can reject this hypothesis, however, by comparing the magnetitite flow to the nearby Mystic Creek coal-seam fire-induced paralava described by Reidel and Ross (in press). The Mystic Creek paralava superficially resembles a lava flow but its mode of occurrence, the presence of the unusual mineral sekaninaite, and its andesitic composition argue against such an interpretation for the Nenana magnetitite. The coal-seam fire interpretation is also inconsistent with the relationships of the Nenana magnetitite to the Usibelli Group sedimentary rocks at California Creek, and also inconsistent with the magnetitite-rhyolite relationships at the Dry Creek locality.

Our preferred hypothesis is that the magnetitite flow erupted through the same conduit as the associated rhyolite, but prior to emplacement and/or eruption of the rhyolite. Keller et al. (2022) proposed a genetic magmatic model for the El Laco magnetite–apatite deposit in Chile which bears many similarities to the Nenana magnetitite flow. The Keller et al. (2022) model is based on iron-rich (iron- oxide?) melt being derived from liquid immiscibility developed within an iron-enriched silicate magma. Although the Nenana magnetitite flow does not have the significant amount of apatite common in many other magnetitite deposits, apatite is present as microscopic grains and phosphorus comprises about 0.1 wt.% of the flow. More importantly, the physical features of the Nenana magnetitite and El Laco are similar. They resemble a basalt flow with small columns and vesicles embedded in the magnetite. One key difference between El Laco and Nenana magnetitite is that El Laco is associated with an andesite whereas the Nenana flow is closely associated with rhyolite flow. However, other magnetitite flows are associated with rhyolite (e.g. Cerro de Mercado, Lakeh Siah) so this is not unknown.

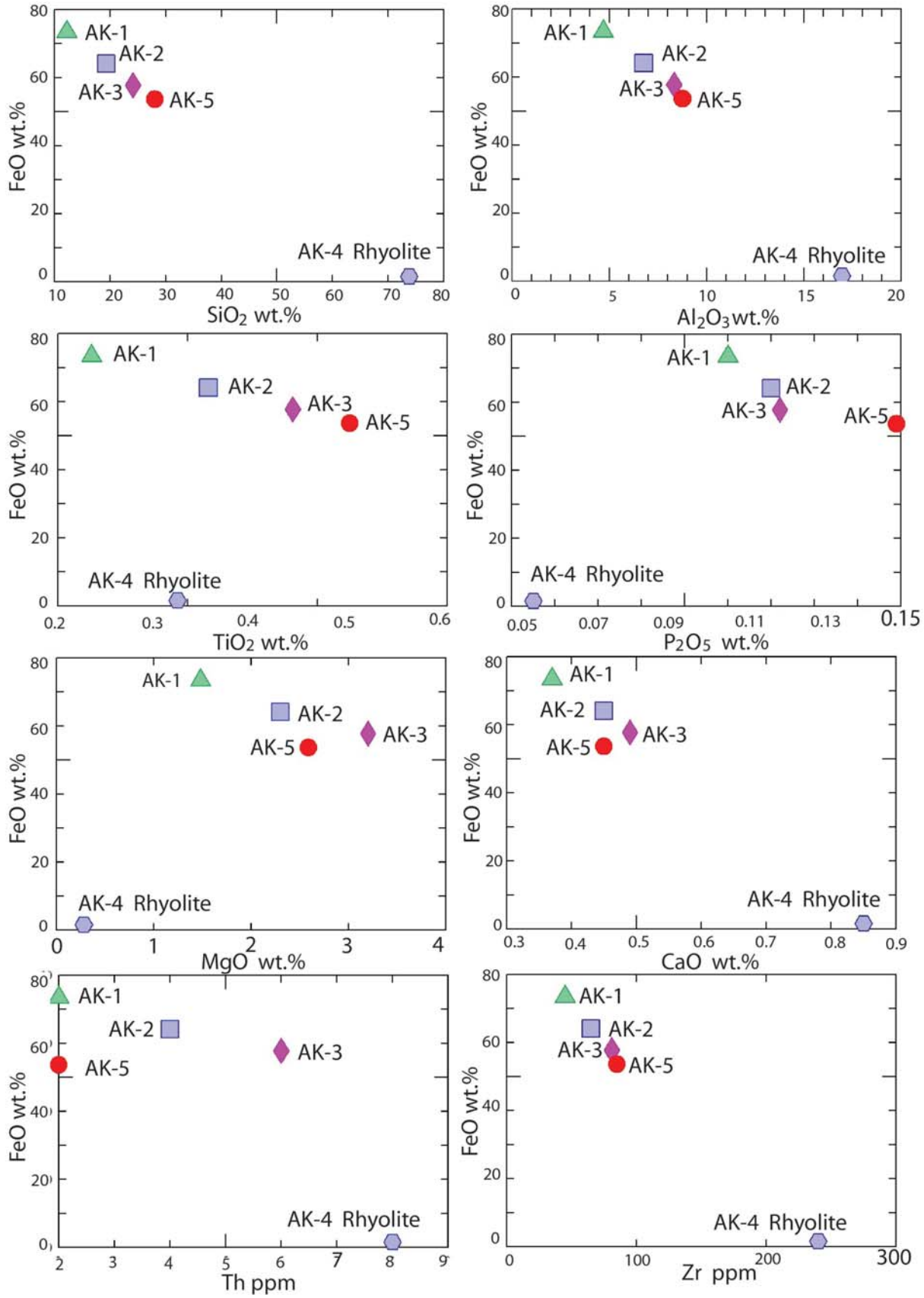

Figure 15. Geochemical variation diagrams for samples from the magnetitite flow and rhyolite (AK-4).

https://doi.org/10.12789/geocanj.2023.50.197

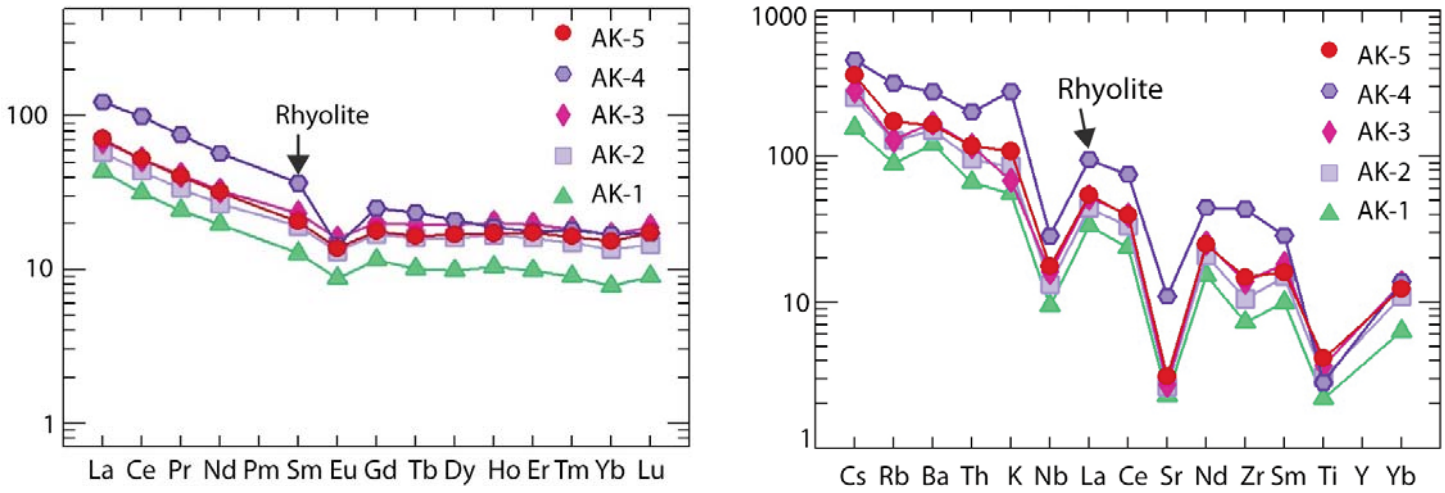

Figure 16. Trace element patterns from the magnetitite flow and rhyolite, Nenana basin, Alaska. (a) Rare earth element profiles normalized to chondrites following Sun and McDonough (1989). (b) Trace element patterns normalized to the Bulk Earth of Hickey et al. (1986).

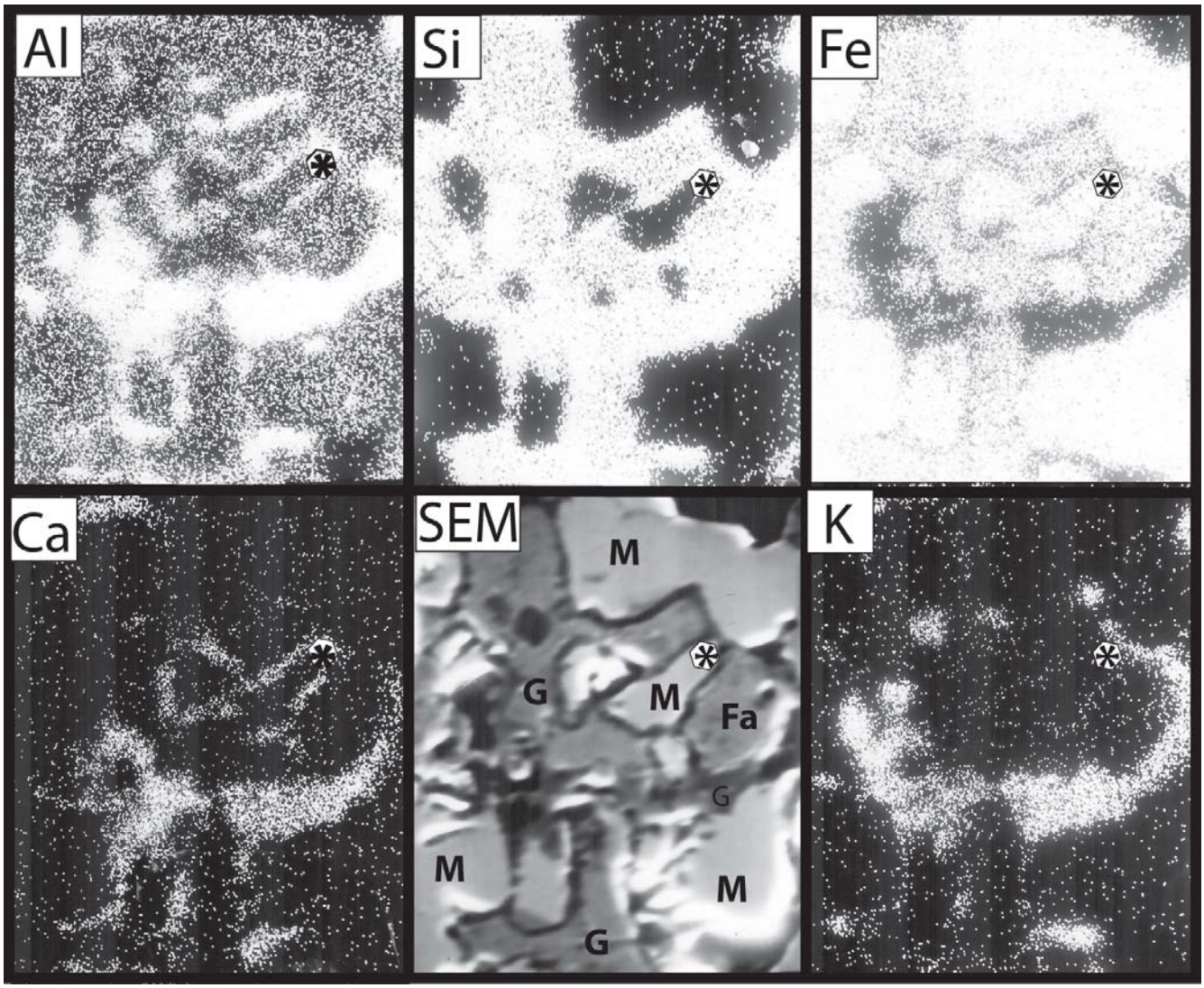

Figure 17. Scanning electron microscope (SEM) image and backscatter X-ray images from a magnetite grain in sample AK-1. Backscatter images are of the same area as in the SEM image. Magnification is 2000x. Al, aluminum; Ca, calcium; Fa, fayalite olivine; Fe, iron; G, glass; K, potassium; M-Magnetite; Si, silicon. *- reference point for each image.

The Keller et al. (2022) model envisages the 'unmixing' of andesite parent magma into a Fe-rich melt and Si-rich melt, followed by vapour-driven ascent of the magmas to the surface. With cooling, the silica-rich magma tends toward a dacite–rhyolite melt and the Fe-rich magma to magnetitite. Once the Fe-rich melt forms, it develops as micro-droplets which collect at the bottom of the magma chamber on a very short time scale. The model suggests that once the Fe-rich melt collects in this way, fracturing of rock caused by either an inflating magma chamber and/or tectonic extension provides pathways to the surface. Due to the very large contrast between the viscosity of the silica-rich melt and the Fe-rich melt (~ 6 orders of magnitude), the Fe-rich melt will ascend much faster than the silica-rich melt. However, the Fe-rich magma is unlikely to continue to ascend at the initial rate. If the volatile solubility decreases upon decompression in silica magmas, the model predicts that a magmatic volatile phase exsolves into bubbles as the Fe-rich liquid ascends. Crystallization of magnetitite upon cooling may further facilitate volatile saturation and exsolution. The volume expansion caused by this will move the liquid with an increasing speed and allow it to erupt as a lava flow.

Observations of the Nenana magnetitite flow appear to support a model like that proposed by Keller et al. (2022). The temporal relationships in which formation of the magnetitite flow eruption is followed by arrival of the rhyolite fit the Keller et al. (2022) model. The high silica content of the magnetitite flow along with the finely disseminated silica glass, silicate minerals and trace elements in magnetite grains suggest that they are remnants of an unmixing process of the same magma. Vesicles in the magnetite of the Nenana magnetitite flow indicate exsolving of volatiles into bubbles as the Fe-rich liquid ascended as proposed by Keller et al. (2022). The highly vesicular nature of the associated rhyolite also supports a vapour-driven eruption.

CONCLUSIONS

Although magnetitite flows studied from around the world are controversial, the Nenana magnetitite flow is of extrusive volcanic origin. Data supporting this interpretation include the following.

1. The extent of the magnetitite flow. Although only isolated outcrops remain in the heavily glaciated Alaska Range, the magnetitite flow occurs over a wide area suggesting that it originated as a sheet-like lava. Although localities like El Laco have multiple dykes that fed multiple localities, the Nenana magnetitite flow exposures lack obvious feeder dykes. However, one possible rhyolite feeder dyke occurs near the Dry Creek site and might also have facilitated eruption of the earlier magnetitite.
2. The high silica content of the magnetitite samples and presence of finely disseminated silica glass and minerals in the magnetite appear to be records of the magma unmixing process. This is further supported by trace element patterns (e.g. REE, trace element profiles) of the magnetitite flow and the associated rhyolite, which indicate a close relationship.
3. The magnetitite flow has vesicles and small-scale columnar jointing typical of a mafic lava flow. The highly vesicular zones in the magnetitite consist of vesicular zones that grade into massive rock on the scale of a thin section, suggesting a lava that degassed upon eruption.
4. Fractures and vesicles within the magnetitite flow contain glass and minerals typical of the associated rhyolite suggesting that the rhyolite magma invaded the magnetitite flow as a sill after the magnetitite flow had cooled and solidified. This is consistent with the timing relationships suggested by Keller et al. (2022) for the El Laco flow in Chile.

ACKNLOWLEDGEMENTS

We thank three anonymous reviewers for their review and comments that greatly improved the manuscript. In addition, we thank Andrew Kerr, Cindy Murphy and Robert Raeside for comments on the final draft that improved it and helped tie the manuscript together. We also thank B. Schoene and the Princeton University TIMS Lab for supporting our geochronology efforts. This material is based upon work funded by the National Science Foundation under Award No. 1952753.

Dr. Rick Conrey at the Peter Hooper GeoAnalytical lab at WSU provided XRF analyses. Dr. James Eckert at the Earth Materials Characterization Lab, Yale University, provided microprobe analyses of samples AK-2, AK-3, AK-4 and AK-5. B. Strope at the Rockwell International Electron Microprobe Laboratory, Richland, Washington, analyzed sample AK-1 and contributed the SEM work.

REFERENCES

Alaska Division of Geological and Geophysical Surveys, 1973a, Aeromagnetic survey, east Alaska Range, Fairbanks Quadrangle, Alaska, scale 1:250,000,1 sheet.

Alaska Division of Geological and Geophysical Surveys, 1973b, Aeromagnetic survey, east Alaska Range, Healy Quadrangle, Alaska, scale 1:250,000, 1 sheet.

Albanese, M.D., 1980, The geology of three extrusive bodies in the central Alaska Range: Unpublished MSc thesis, University of Alaska Fairbanks, 104 p., http://hdl.handle.net/11122/5943.

Athey, J.E., Newberry, R.J., Werdon, M.B., Freeman, L.K., Smith, R.L., and Szimugala, D.J., 2006, Bedrock geological map of the Liberty Bell area, Fairbanks A-4 Quadrangle, Bonnifield Mining District, Alaska: Alaska Division of Geological and Geophysical Surveys Report of Investigation 2006-2, scale 1:50,000, 98 p.

Bain, W.M., Steele-MacInnis, M., Tornos, F., Hanchar, J.M., Creaser, E.C., and Pietruszka, D.K., 2021, Evidence for iron-rich sulfate melt during magnetite (-apatite) mineralization at El Laco, Chile: Geology, v. 49, p. 1044–1048, https://doi.org/10.1130/G48861.1.

Beikman, H.M., *compiler*, 1974, Preliminary geologic map of the southeast quadrant of Alaska: U.S. Geological Survey Miscellaneous Field Studies Map 612, 2 sheets, scale 1:1,000,000.

Bowring, J.F., McLean, N.M., and Bowring, S.A., 2011, Engineering cyber infrastructure for U–Pb geochronology: Tripoli and U–Pb_Redux: Geochemistry, Geophysics, Geosystems, v. 12, Q0AA19, https://doi.org/10.1029/2010GC003479.

Condon, D.J., Schoene, B., McLean, N.M., Bowring, S.A., and Parrish, R.R., 2015, Metrology and traceability of U–Pb isotope dilution geochronology (EARTHTIME Tracer Calibration Part I): Geochimica et Cosmochimica Acta, v. 164, p. 464–480, https://doi.org/10.1016/j.gca.2015.05.026.

Dare, S.A.S., Barnes, S.-J., and Beaudoin, G., 2015, Did the massive magnetite "lava flows" of El Laco (Chile) form by magmatic or hydrothermal processes? New

constraints from magnetite composition by LA-ICP-MS: Mineralium Deposita, v. 50, p. 607–617, https://doi.org/10.1007/s00126-014-0560-1.

Dusel-Bacon, C., Aleinikoff, J.N., Premo, W.R., Paradis, S., and Lohr-Schmidt, I., 2007, Tectonic setting and metallogenesis of volcanogenic massive sulfide deposits in the Bonnifield Mining District, Northern Alaska Range, *in* Gough, L.P., and Day, W.C., *eds.*, Recent U.S. Geological Survey Studies in the Tintina Gold Province, Alaska, United States, and Yukon, Canada—Results of a 5-Year Project: U.S. Geological Survey Scientific Investigations Report 2007–5289-B, p. B1–B7, https://doi.org/10.3133/sir20075289B.

Freeman, L.K., Newberry, R.J., Werdon, M.B., Szumigala, D.J., Andrew, J.E., and Athey, J.E., 2016, Preliminary bedrock geologic map data for the eastern Bonnifield mining district, Fairbanks and Healy quadrangles, Alaska: Alaska Division of Geological and Geophysical Surveys Preliminary Interpretive Report 2016-3, 6 p., https://doi.org/10.14509/29661.

Frietsch, R., 1978, On the magmatic origin of iron ores of the Kiruna type: Economic Geology, v. 73, p. 478–485, https://doi.org/10.2113/gsecongeo.73.4.478.

Gerstenberger, H., and Haase, G., 1997, A highly effective emitter substance for mass spectrometric Pb isotope ratio determinations: Chemical Geology, v. 136, p. 309–312, https://doi.org/10.1016/S0009-2541(96)00033-2.

Gholipoor, M., Barati, M., Tale Fazel, E., and Hurai, V., 2023, Textural and compositional constraints on the origin, thermal history, and REE mobility in the Lakeh Siah iron oxide-apatite deposit—NE Bafq, Iran: Mineralium Deposita, v. 58, p. 963–986, https://doi.org/10.1007/s00126-023-01163-1.

Henriquez, F., Naslund, H.R., Nyström, J.O., Vivallo, W., Aguirre, R., Dobbs, F.M., and Lledó, H., 2003, New field evidence bearing on the origin of the El Laco magnetite deposit, northern Chile - A Discussion: Economic Geology, v. 98, p. 1497–1500, https://doi.org/10.2113/gsecongeo.98.7.1497.

Hickey, R.L., Frey, F.A., Gerlach, D.C., and Lopez-Escobar, L., 1986, Multiple sources for basaltic arc rocks from the southern volcanic zone of the Andes (34°–41°S): Trace element and isotopic evidence for contributions from subducted oceanic crust, mantle, and continental crust: Journal of Geophysical Research, v. 91, p. 5963–5983, https://doi.org/10.1029/JB091iB06p05963.

Holmes, A., 1928, The Nomenclature of Petrology, second edition: Thomas Murby and Co., London, 248 p.

Jaffey, A.H., Flynn, K.F., Glendenin, L.E., Bentley, W.C., and Essling, A.M., 1971, Precision measurement of half-lives and specific activities of ^{235}U and ^{238}U: Physical Review C, v. 4, p. 1889–1906, https://doi.org/10.1103/PhysRevC.4.1889.

Johannsen, A., 1931–1938, A Descriptive Petrology of Igneous Rocks, Volumes 1–4: University of Chicago Press.

Johnson, D.M., Hooper, P.R., and Conrey, R.M., 1999, XRF Analysis of rocks and minerals for major and trace elements on a single low dilution Li-tetraborate fused bead: Advances in X-Ray Analysis, v. 41, p. 843–867.

Kasbohm, J., and Schoene, K., 2018, Rapid eruption of the Columbia River flood basalt and correlation with the mid-Miocene climate optimum: Science Advances, v. 4, eaat8223, https://doi.org/10.1126/sciadv.aat8223.

Keller, T., Tornos, F., Hanchar, J.M., Pietruszka, D.K., Soldati, A., Dingwell, D.B., and Suckale, J., 2022, Genetic model of the El Laco magnetite-apatite deposits by extrusion of iron-rich melt: Nature Communications, v. 13, 6114, https://doi.org/10.1038/s41467-022-33302-z.

Kirschner, C.E., 1994, Interior basins of Alaska, *in* Plafker, G., and Berg, H.C., *eds.*, The Geology of Alaska, The Geology of North America, Decade of North American Geology: Geological Society of America, v. G-1, p. 469–493, https://doi.org/10.1130/DNAG-GNA-G1.469.

Krogh, T.E., 1973, A low-contamination method for hydrothermal decomposition of zircon and extraction of U and Pb for isotopic age determinations: Geochimica et Cosmochimica Acta, v. 37, p. 485–494, https://doi.org/10.1016/0016-7037(73)90213-5.

Leopold, E.B., and Liu, G., 1994, A long pollen sequence of Neogene age, Alaska Range: Quaternary International, v. 22–23, p. 103–140, https://doi.org/10.1016/1040-6182(94)90009-4.

Lyons, J.I.,1988, Volcanogenic iron oxide deposits, Cerro de Mercado and vicinity, Durango: Economic Geology, v. 83, p. 1886–1906, https://doi.org/10.2113/gsecongeo.83.8.1886.

Mattinson, J.M., 2005, Zircon U–Pb chemical abrasion ("CA-TIMS") method: Combined annealing and multi-step partial dissolution analysis for improved precision and accuracy of zircon ages: Chemical Geology, v. 220, p. 47–66, https://doi.org/10.1016/j.chemgeo.2005.03.011.

McLean, N.M., Bowring, J.F., and Bowring, S.A., 2011, An algorithm for U–Pb isotope dilution data reduction and uncertainty propagation: Geochemistry, Geophysics, Geosystems, v. 12, Q0AA18, https://doi.org/10.1029/2010GC003478.

McLean, N.M., Condon, D.J., Schoene, B., and Bowring, S.A., 2015, Evaluating uncertainties in the calibration of isotopic reference materials and multi-element isotopic tracers (EARTHTIME Tracer Calibration Part II): Geochimica et Cosmochimica Acta, v. 164, p. 481–501, https://doi.org/10.1016/j.gca.2015.02.040.

Miller, J.S., Matzel, J.E.P., Miller, C.F., Burgess, S.D., and Miller, R.B., 2007, Zircon growth and recycling during the assembly of large, composite arc plutons: Journal of Volcanology and Geothermal Research, v. 167, p. 282–299, https://doi.org/10.1016/j.jvolgeores.2007.04.019.

Naslund, H.R., Henriquez, F., Nyström, J.O., Vivallo, W., and Dobbs, F.M., 2002, Magmatic iron ores and associated mineralisation: Examples from the Chilean High Andes and Coastal Cordillera, *in* Porter, T.M., *ed.*, Hydrothermal iron oxide copper-gold and related deposits: A global perspective: Porter Geoscience Consultancy Publishing, Adelaide, v. 2, p. 207–226.

Nier, A.O., 1950, A redetermination of the relative abundances of the isotopes of carbon, nitrogen, oxygen, argon, and potassium: Physical Review, v. 77, p. 789–793, https://doi.org/10.1103/PhysRev.77.789.

Parak, T., 1985, Phosphorus in different types of ore sulfides in the iron deposits, and the type and origin of ores at Kiruna: Economic Geology, v. 80, p. 646–665, https://doi.org/10.2113/gsecongeo.80.3.646.

Park, C.F., 1961, A magnetite "flow" in northern Chile: Economic Geology, v. 56, p. 431–441, https://doi.org/10.2113/gsecongeo.56.2.431.

Péwé, T.L., Wahrhaftig, C., and Webber, F., 1966, Geologic map of the Fairbanks quadrangle, Alaska: U.S. Geological Survey Miscellaneous Geologic Investigations Map 455, scale 1:250,000.

Pietruszka, D.K., Hanchar, J.M., Tornos, F., Whitehouse, M.J., and Velasco, F., 2023, Tracking isotopic sources of immiscible melts at the enigmatic magnetite-(apatite) deposit at El Laco, Chile, using Pb isotopes: Geological Society of America Bulletin, https://doi.org/10.1130/B36506.1.

Reidel, S.P., 1984, An iron-rich lava flow from the Nenana coal field, central Alaska: *in* Short Notes on Alaskan Geology 1982–1983: Alaska Division of Geology and Geophysical Surveys, Professional Report 86B, p. 5–8, https://doi.org/10.14509/2261.

Reidel, S.P., and Ross, M.E., *in press*, A rare sekaninaite occurrence in the Nenana Coal Basin, Alaska Range, Alaska: American Mineralogist, https://doi.org/10.2138/am-2022-8698.

Reidel, S.P., Camp, V.E., Tolan, T.L., and Martin, B.S., 2013, The Columbia River flood basalt province, Stratigraphy, areal extent, volume, and physical volcanology, *in* Reidel, S.P., Camp, V.E., Ross, M.E., Wolff, J.A., Martin, B.S., Tolan, T.L, and Wells, R.E., *eds.*, The Columbia River Flood Basalt Province: Geological Society of America Special Papers, v. 497, p. 1–43, https://doi.org/10.1130/2013.2497(01).

Ross, M.E., 1989, Stratigraphic relationships of subaerial, invasive, and intracanyon flows of Saddle Mountains Basalt in the Troy basin, Oregon and Washington, *in* Reidel, S.P., and Hooper, P.R., *eds.*, Volcanism and Tectonism in the Columbia River Flood-Basalt Province: Geological Society of America Special Papers, v. 237, p. 131–142, https://doi.org/10.1130/SPE239-p131.

Sillitoe, R.H., and Burrows, D.B., 2002, New field evidence bearing on the origin of the El Laco magnetite deposit, northern Chile: Economic Geology, v. 97, p. 1101–1109, https://doi.org/10.2113/gsecongeo.97.5.1101.

Sillitoe, R.H., and Burrows, D.B., 2003, New field evidence bearing on the origin of the El Laco magnetite deposit, northern Chile - A Reply: Economic Geology, v. 98, p. 1501–1502, https://doi.org/10.2113/gsecongeo.98.7.1501.

Simon, J.I., Renne, P.R., and Mundil, R., 2008, Implications of pre-eruptive magmatic histories of zircons for U–Pb geochronology of silicic extrusions: Earth and Planetary Science Letters, v. 266, p. 182–194, https://doi.org/10.1016/j.epsl.2007.11.014.

Sortor, R.N., Goehring, B.M., Bemis, S.P., Ruleman, C.A., Caffee, M.W., and Ward, D.J., 2021, Early Pleistocene climate-induced erosion of the Alaska Range formed the Nenana Gravel: Geology, v. 49, p. 1473–1477, https://doi.org/10.1130/G49094.1.

Sun, S.-s., and McDonough, W.F., 1989, Chemical and isotopic systematics of oceanic basalts: Implications for mantle composition and processes, *in* Saunders, A.D., and Norry, M.J., *eds.*, Magmatism in the Ocean Basins: Geological Society Special Publications, v. 42, p. 313–345, https://doi.org/10.1144/GSL.SP.1989.042.01.19.

Triplehorn, D.M., Drake, J., and Layer, P.W., 2000, Preliminary $^{40}Ar/^{39}Ar$ ages from two units in the Usibelli Group, Healy, Alaska: New light on some old problems, *in* Pinney, D.S., and Davis, P.K., *eds.,* Short Notes on Alaska Geology 1999: Alaska Division of Geological and Geophysical Surveys Professional Report 119I, p. 117–127, https://doi.org/10.14509/2691.

Wahrhaftig, C., 1951, Geology and coal deposits of the western part of the Nenana coal field, Alaska, *in* Barnes, F.F., *ed.*, Coal investigations in south-central Alaska,

1944–46: U.S. Geological Survey Bulletin 963-E, p. 169–186.
Wahrhaftig, C., 1970a, Geologic map of the Healy D-2 quadrangle, Alaska: U.S. Geological Survey Geologic Quadrangle Map GQ-804, scale 1:63,360, 1 sheet.
Wahrhaftig, C.,1970b, Geologic map of the Healy D-3 quadrangle, Alaska: U.S. Geological Survey Geologic Quadrangle Map GQ-805, scale 1:63,360, 1 sheet.
Wahrhaftig, C., 1970c, Geologic map of the Healy D-4 quadrangle, Alaska: U.S. Geological Survey Geologic Quadrangle Map GQ-806, scale 1:63,360, 1 sheet.
Wahrhaftig, C., 1970d, Geologic map of the Healy D-5quadrangle, Alaska: U.S. Geological Survey Geologic Quadrangle Map GQ-807, scale 1:63,360, 1 sheet.
Wahrhaftig, C., 1970e, Geologic map of the Fairbanks A-2 quadrangle, Alaska: U.S. Geological Survey Geologic Quadrangle Map GQ-808, scale 1:63,360, 1 sheet.
Wahrhaftig, C., 1970f, Geologic map of the Fairbanks A-3 quadrangle, Alaska: U.S. Geological Survey Geologic Quadrangle Map GQ-809, scale 1:63,360, 1 sheet.
Wahrhaftig, C., 1970g, Geologic Map of the Fairbanks A-4 Quadrangle, Alaska: U.S. Geological Survey Geologic Quadrangle Map 810, scale 1:63,360, 1 sheet, https://dggs.alaska.gov/webpubs/usgs/gq/oversized/gq-0810sht01.pdf.
Wahrhaftig, C., 1970h, Geologic map of the Fairbanks A-5 quadrangle, Alaska: U.S. Geological Survey Geologic Quadrangle Map GQ-811, scale 1:63,360, 1 sheet.
Wahrhaftig, C., 1987, The Cenozoic section at Suntrana, Alaska, *in* Hill, M.L., *ed.*, Cordilleran Section of the Geological Society of America: Geological Society of America, The Decade of North American Geology (DNAG), Centennial Field Guide 1, p. 445–450, https://doi.org/10.1130/0-8137-5401-1.445.
Wahrhaftig, C., Wolfe, J.A., Leopold, E.B., and Lanphere, M.A., 1969, The coal-bearing group in the Nenana coal field, Alaska: Contributions to Stratigraphy: U.S. Geological Survey Bulletin 1274-D, p. D1–D30, https://doi.org/10.3133/b1274D.
Wartes, M.A, Gillis, R.J., Herriott, T.M., Stanley, R.G., Helmold, K.P., Peterson, C.S., and Benowitz, J.A., 2013, Summary of the 2012 reconnaissance field studies related to petroleum geology of the Nenana basin, interior Alaska: Division of Geological and Geophysical Surveys, Alaska Geological Survey, Preliminary Interpretive Report 2013-2, 13 p., https://doi.org/10.14509/24880.
Wilson, F.H., Dover, J.H., Bradley, D.C., Weber, F.R., Bundtzen, T.K., and Haeussler, P.J., 1998, Geologic map of central (interior) Alaska: U.S. Geological Survey Open-File Report OF 98-133-A, version 1.2, https://pubs.usgs.gov/of/1998/of98-133-a/.
Wolfe, J.A., and Tanai, T., 1987, Systematics, phylogeny, and distribution of Acer (Maples) in the Cenozoic of western North America: Journal of the Faculty of Science, Hokkaido University, v. 22, p. 1–246, http://hdl.handle.net/2115/36747.

Received February 2023
Accepted as revised April 2023

For access to the Reidel et al. (2023) Supplementary Material, Appendix A: Petrographic Data, Appendix B: Microprobe Analyses, Appendix C: Chemical Analyses, and Appendix D: U–Pb Geochronological Data, please visit the GAC's open source GC Data Repository for the Igneous Rock Associations Series at: https://gac.ca/gc-data-repository/.

GEOLOGICAL ASSOCIATION OF CANADA
(2023–2024)

Corporate Members

PLATINUM

MEMORIAL UNIVERSITY

GOLD

AngloAmerican

NORTHWEST TERRITORIES GEOLOGICAL SURVEY

SILVER

ROYAL TYRRELL MUSEUM

YUKON GEOLOGICAL SURVEY

BRITISH COLUMBIA GEOLOGICAL SURVEY

NICKEL

UNIVERSITY OF WATERLOO — CONCORDIA CUM VERITATE

GEOSCIENCE CANADA AND THE GEOLOGICAL ASSOCIATION OF CANADA ARE GRATEFUL TO THE CANADIAN GEOLOGICAL FOUNDATION FOR THEIR FINANCIAL SUPPORT OF THIS JOURNAL

Canadian Geological Foundation — Fondation Géologique du Canada — 1968

Officers

President
Alwynne Beaudoin
Vice-President
Nikole Bingham-Koslowski
Treasurer
Deanne van Rooyen
Secretary
Tim Fedak

Councillors

Alwynne Beaudoin
Nikole Bingham-Koslowski
Kirstin Brink
Tim Fedak
David Lowe
Nadia Mohammadi
David Moynihan
Deanne van Rooyen
Rajeev Sasidharan Nair
Ricardo Silva
Diane Skipton
Colin Sproat

GAC Editors

GAC Books
Vacant
Geolog
Roger Paulen
Geoscience Canada
Andy Kerr

Standing Committees

Communications
Kirstin Brink
Finance
Deanne van Rooyen
GAC Lecture Tours
Nadia Mohammadi
Publications
David Lowe
Science Program
Rajeev Sasidharan Nair

GEOSCIENCE CANADA

JOURNAL OF THE GEOLOGICAL ASSOCIATION OF CANADA
JOURNAL DE L'ASSOCIATION GÉOLOGIQUE DU CANADA

SERIES

2023 VOLUME 50 GSCNA7 50 17-72
PRINT EDITION ISSN 0315-0941
ONLINE EDITION ISSN 1911-4850